Earliest Vallesian suid remains from Creu de Conill 20 (Vallès-Penedès Basin, NE Iberian Peninsula)

Sharrah McKenzie[1] · Leonardo Sorbelli[1] · Marco Cherin[2] · Sergio Almécija[3,4,1] · Marta Pina[5,1] · Juan Abella[1,6,7] · Àngel H. Luján[1,8] · Daniel DeMiguel[9,10,1] · David M. Alba[1,*]

[1] Institut Català de Paleontologia Miquel Crusafont, Universitat Autònoma de Barcelona, Edifici ICTA-ICP, c/ Columnes s/n, Campus de la UAB, 08193 Cerdanyola del Vallès, Barcelona, Spain

[2] Dipartimento di Fisica e Geologia, Università degli Studi di Perugia, Via A. Pascoli, 06123, Perugia, Italy

[3] Division of Anthropology, American Museum of Natural History, Central Park West at 79th Street, New York, NY 10024, USA

[4] New York Consortium in Evolutionary Primatology, New York, NY, USA

[5] South Bank Applied BioEngineering Research, Division of Mechanical Engineering and Design, London South Bank University, UK

[6] Grup d'Investigació en Paleontologia de Vertebrats del Cenozoic (PVC-GIUV), Departament de Botànica i Geologia, Universitat de València, 46100, Burjassot, València, Spain

[7] Instituto Nacional de Biodiversidad (INABIO), Pje. Rumipamba N. 341 y Av. de los Shyris (Parque La Carolina), Quito, Ecuador

[8] Masaryk University, Faculty of Sciences, Department of Geological Sciences, Kotlářská 2, 611 37 Brno, Czech Republic

[9] ARAID foundation, Zaragoza, Spain

[10] Universidad de Zaragoza, Departamento de Ciencias de la Tierra, and Instituto Universitario de Investigación en Ciencias Ambientales de Aragón (IUCA), Pedro Cerbuna 12, 50009 Zaragoza, Spain

***Corresponding author:**

David M. Alba

david.alba@icp.cat

ORCIDs:

Sharrah McKenzie: 0000-0002-8259-3756

Leonardo Sorbelli: 0000-0002-3246-5887

Marco Cherin: 0000-0003-4291-4372

Sergio Almécija: 0000-0003-1373-1497

Marta Pina: 0000-0001-9762-6402

Juan Abella: 0000-0002-3433-6093

Àngel H. Luján: 0000-0003-1844-0453

Daniel DeMiguel: 0000-0001-6138-7227

David M. Alba: 0000-0002-8886-5580

Abstract

Although the suid assemblages from the Miocene of the Vallès-Penedès Basin (NE Iberian Peninsula) are reasonably well known, taxonomic studies devoted to them have lagged behind during the last decades. We describe the unpublished suid dentognathic remains from the earliest Vallesian (MN9) of Creu de Conill 20 (CCN20; 11.18 Ma), which represents the First Appearance Datum of hipparionin equids in western Europe. The sample includes 118 specimens, mostly isolated teeth, and a few maxillary and mandibular fragments. More than three-quarters of the specimens are assigned to the suine *Propotamochoerus palaeochoerus*, which is characteristic of MN9, albeit the described remains are slightly larger than average for the species. The rest of the sample belongs to a large tetraconodontine that is assigned to *Parachleuastochoerus valentini*, recorded elsewhere from MN7+8 to MN9, except for two specimens attributed to the small suid cf. *Albanohyus* sp. Our results support a synchronous dispersal of *Hippotherium* and *P. palaeochoerus* into Western Europe at ~11.2 Ma, suggesting that the latter is a suitable biochronological marker of the Vallesian. In turn, the remains of *Pa. valentini* refine our knowledge on the dental morphology of this species and strengthen the view that this species (unlike *Conohyus doati* and *Conohyus melendezi*) is not a junior synonym of *Conohyus simorrensis*. The lack of *Listriodon splendens* and *Versoporcus* sp. from CCN20, together with the scarcity of *Albanohyus*, contrasts with their abundance in the roughly coeval site of Castell de Barberà, hinting at local paleoenvironmental differences.

Keywords Suidae · *Propotamochoerus* · *Parachleuastochoerus* · Late Miocene · Taxonomy · Spain.

Introduction

Suoids from the Vallès-Penedès Basin

For many decades, the study of the Miocene suoids from the Vallès-Penedès Basin (NE Iberian Peninsula) proceeded in parallel with that of the rest of the large mammal assemblages, with species occurrences being frequently included in faunal lists without being accompanied by detailed descriptions. Only a few studies (Crusafont and Lavocat 1954; Crusafont et al. 1955) were devoted to the fossil remains of this group from the Vallès-Penedès Basin until Golpe Posse (1971) published her PhD dissertation on Iberian suiforms. This unpublished work gave rise to a short summary (Golpe Posse 1972a) and a longer published account (Golpe Posse 1972b). Additional works by the same author, devoted to particular suids from the Vallès-Penedès Basin, followed in subsequent years (e.g., Golpe-Posse 1975 1977, 1978, 1980, 1981). Since the 1980s and until about a decade ago, Vallès-Penedès suoid remains figured more or less prominently in several publications by other authors concerned with specific taxa (Pickford 1981; Van der Made and Moyà-Solà 1989; Pickford and Moyà Solà 1994, 1995; Van der Made 1996a, 1996b, 1999, 2010; Van der Made et al. 1998, 2014; Van der Made and Morales 1999; Orliac 2006; Orliac et al. 2006). Van der Made (1990b, 1997a) further refined and updated the taxonomic attribution of the Vallès-Penedès suoids within the framework of the Iberian Miocene. However, the fact that Van der Made (1990b, 1997a) did not describe the remains in detail, coupled with the poor iconography of Golpe Posse's (1971, 1972b) dissertation, has made it difficult to critically revise and update the taxonomic attributions of the Vallès-Penedès material not described in the aforementioned papers without directly inspecting the fossils.

Most recently, some suoid remains from the Vallès-Penedès Basin were further discussed in several additional monographs on various taxa (Pickford 2015, 2016b, 2017) as well as within the framework of a revision of the European Tetraconodontidae (Pickford and Laurent 2014; Pickford 2016a), including the description of *Parachleuastochoerus* remains from several Vallès-Penedès sites (Pickford 2014). Together with the preliminary study by Tomàs et al. (2011) on *Albanohyus* from Abocador de Can Mata and the redescription of the Ca l'Almirall tetaconodont remains (McKenzie et al. 2022), these are the few papers specifically devoted to the description of suoid remains from the Vallès-Penedès Basin during the last decade. This contrasts with the wealth of new suoid material that has been recovered during the multiple fieldwork campaigns performed in this basin, particularly from the late Aragonian and the early Vallesian. Given the fast but frantic progress made in suoid systematics during the past couple of decades, and the never-ending disagreements regarding the taxonomy of European suoids (e.g., see differences between Pickford 2014 and Van der Made et al. 2020 regarding the Tetraconodontinae), the largely unpublished and understudied collection of suoid remains from the Vallès-Penedès Basin calls for an in-depth revision. With this aim in mind, here we describe all the currently available dentognathic suid remains from the earliest Vallesian locality of Creu de Conill 20 (CCN20), in order to substantiate their taxonomic attribution as well as to discuss their paleoenvironmental and biochronological implications. All these remains are unpublished and were mostly recovered during successive campaigns performed since 2016, when excavations of this locality were resumed after its initial discovery 25 years ago (Agustí and Galobart 1998).

The locality of Creu de Conill 20

The multiple fossiliferous localities of Creu de Conill (CCN) were discovered in 1995 during the restoration of a homonymous gravel quarry, which subsequently became the controlled debris deposit of Can Guitard (Fig. 1a–b), within the municipality of Terrassa (Catalonia, Spain), SW of the city urban nucleus. Previous finds at the nearby site of les Martines during the 1950s (Crusafont Pairó 1952; Crusafont and Truyols 1954) hinted at the fossiliferous potential of the area. In 1995, coinciding with the restoration of the gravel quarry, personnel from the former Institut de Paleontologia Miquel Crusafont in Sabadell (currently, ICP) prospected the area and found multiple fossiliferous horizons. Paleomagnetic samplings were performed there during the 1990s (Garcés 1995; Garcés et al. 1996; Agustí et al. 1997). A rescue excavation was also undertaken in late 1995 and 1996 at CCN20—the locality that showed a greater accumulation of large vertebrate remains—leading to the recovery of some fossil vertebrate remains, including the equid *Hippotherium*, carnivorans, and artiodactyls (Agustí and Galobart 1998). Among the latter, there was a suid maxilla that was attributed by the authors to *Korynochoerus palaeochoerus*—currently *Propotamochoerus palaeochoerus* (Kaup, 1833)—but which remained unpublished until now. Although CCN20 could not be systematically excavated at the time, given the presence of abundant fossil remains and the biochronological importance of the site (see next section below), it was agreed with the landowner that the fossiliferous outcrop would not be covered by debris during the restoration of the quarry, so as to be excavated sometime in the future.

In subsequent years, preliminary faunal lists of CCN20 were reported (Agustí and Galobart 1998; Agustí et al. 1997; Casanovas-Vilar et al. 2006), and the micromammal remains from CCN20 and the nearby locality of CCN22 were described in detail (Casanovas-Vilar et al. 2006). However, only a single large mammal fossil from the 1995–1996 excavations at CCN20 (a mandibular fragment of the barbourofelid *Albanosmilus jourdani*) was described in detail (Robles et al. 2013). In the meantime, the fossil-bearing horizon of CCN20 was progressively covered due to the natural erosion of sediments and vegetation growth as time went by, until the locality was finally reopened in 2016 with the aid of an excavator machine, being systematically excavated during the following years (2017–2019 and 2021–2022; Fig. 1c–e). These successive fieldwork campaigns led to the recovery of more than 3,000 macrovertebrate remains, with the large mammal fossil assemblage being dominated by particularly abundant remains of bovids and hyaenids, and to a lesser extent suids and hipparionins. The suid remains recovered between 2016 and 2022 are more fragmentary than the above-mentioned maxilla, but have led to the recognition that a large tetraconodontine and a small suoid are also recorded therein. The description and identification of the suid remains recovered to date from CCN20 will thus contribute to a better characterization of the earliest Vallesian suid assemblages from western Europe generally, and more specifically from the Vallès-Penedès Basin, where they are otherwise well known only from the roughly coeval site of Castell de Barberà (Golpe-Posse 1971, 1972b, 1975, 1977; Van der Made 1990b, 1996a, 1996b, 1997; Fortelius et al. 1996; Pickford 2016a).

Age and geological background

The locality of CCN20 is located in the uppermost part of the former gravel quarry, on the eastern slope of the Creu de Conill hill, close to the crossroads between Carrer de Sant Muç and Camí de les Martines (Fig. 1a–b).

From a geological viewpoint, all Creu de Conill localities belong to the Upper Continental Units of the Vallès-Penedès Basin (Fig. 1f), which are Middle to Late Miocene (Aragonian to Turolian) in age (Casanovas-Vilar et al. 2016a and references therein). Both CCN20 and CCN22 are located within a short stratigraphic section of less than 50 m, constituted by conglomeratic levels interbedded with brownish and grayish to greenish mudstones (Agustí and Galobart 1998), known as the Can Guitard 1 section (Garcés 1995; Garcés et al. 1996; Agustí et al. 1997). The fossiliferous layer exposed in 2016 was provisionally labeled CCN2016, given the impossibility to confirm at the time that it corresponded to the exact stratum excavated in the 1990s as CCN20. However, subsequent excavation works have shown that the fossiliferous layer, which is more than 1 m deep, has considerable horizontal continuity and corresponds, in all probability, to CCN20—as further confirmed by M. Llenas (pers. comm.), an ICP technician that participated in the original excavation.

From a stratigraphic viewpoint, CCN20 is located below CCN22 in the lowermost portion of the aforementioned Can Guitard 1 section, within the Montagut composite sequence (Garcés 1995; Garcés et al. 1996; Agustí et al. 1997; Casanovas-Vilar et al. 2006). Based on magnetostratigraphic data, CCN20 correlates to the base of C5r.1n (Garcés et al. 1996), with an interpolated age of 11.18 Ma (Casanovas-Vilar et al. 2016b; recalculated after Garcés et al. 1996, 1997 based on Ogg 2012). CCN20 represents the First Appearance Datum of the equid *Hippotherium* in the Vallès-Penedès Basin (Garcés et al. 1996; Agustí et al. 1997), which by definition marks the beginning of the Vallesian European land mammal age (Crusafont Pairó 1950, 1951, 1953; Crusafont Pairó and Truyols Santonja 1960). It is thus correlated to the *Hippotherium–Cricetulodon hartenbergeri* inteval subzone of the Vallès-Penedès Basin on biostratigraphic grounds (Casanovas-Vilar et al. 2016a, 2016b)—equivalent to Agustí et al.'s (1997) *Megacricetodon ibericus* + *Hipparion* zone—whose base is defined by the first local occurrence of *Hippotherium*. CCN20 is thus roughly coeval with the site of Castell de Barberà, which is now conclusively correlated to the earliest Vallesian (~11.2 Ma) based on magnetostratigraphic data (Alba et al. 2019).

Materials and Methods

Studied and Comparative Samples

Studied Sample The described material includes 118 dentognathic specimens (Table 1), mostly comprising isolated teeth as well as a few maxillary and mandibular fragments. All the specimens are housed in the ICP and their catalog numbers are preceded by the acronym IPS. Mandibular and maxillary fragments have been illustrated in various views, and socketed teeth have been further depicted in greater detail together with isolated specimens. Cheek teeth (both permanent and deciduous) have been illustrated at least in occlusal view (mesial on top), while anterior premolars have been also depicted in buccal and lingual views, and incisors and canines in lingual, mesial, labial, and distal views.

Comparative Sample Measurements for the comparative sample were taken from the literature. The size and proportions of the CCN20 dental specimens were compared with those of the suines *P. palaeochoerus*, *Propotamochoerus hysudricus* (Stehlin, 1899), *Propotamochoerus provincialis* (Blainville, 1847), *Propotamochoerus hyotherioides* (Schlosser, 1903), *Propotamochoerus aegaeus* Lazaridis et al., 2022, and

Hippopotamodon major (Gervais, 1850), as well as the tetraconodontine *Parachleuastochoerus valentini* (Filhol, 1822). *Propotamochoerus wui* Van der Made and Han, 1994 was not considered in the quantitative comparisons because it is clearly smaller than the described remains.

Measurements of *P. palaeochoerus* correspond to specimens from France, Germany, Austria, Hungary, and Ukraine (Mottl 1966, after Depéret 1887; Hellmund 1995; Van der Made et al. 1999; Fortelius et al. 2005; Pickford 2013a, 2015; Iannucci and Begun 2022). Measurements of the roughly coeval species *P. hysudricus* from Asia correspond to fossils from multiple sites of the Siwaliks from Indo-Pakistan and, to a lesser extent, Myanmar (Colbert 1935; Pickford 1988; Thaung-Htike et al. 2006; Sein et al. 2009; Khan et al. 2010; Batool et al. 2015; Sarwar et al. 2016; Dar et al. 2019; Aslam et al. 2021). In turn, measurements of the Late Miocene and Early Pliocene species *P. provincialis* correspond to fossils from France, Italy, Spain, and Turkey (Morales 1984; Van der Made 2003; Gallai 2006; Gallai and Rook 2006, 2011; Pickford 2013c; Iannuci et al. 2021), whereas those of *P. hyotherioides* are from the Late Miocene of China (Van der Made and Han 1994; Hou et al. 2019) and those of *P. aegaeus* from the Turolian of Greece, North Macedonia, and Burgaria (Hellmund 1995; de Bonis and Bouvrain 1996; Geraads et al. 2008; Sylvestrou and Kostopoulos 2009; Lazaridis 2015; Kostopoulos and Sylvestrou 2022; Lazaridis et al. 2022) but not Italy (Gallai 2006; Gallai and Rook 2006, 2011; Iannucci et al., 2021), as the latter were kept in *P. provincialis* following Iannucci et al. (2021). Measurements of *H. major* (for species attribution, see Pickford 2015) correspond to more abundant specimens from Austria, Azerbaijan, Bulgaria, France, Georgia, Germany, Greece, Hungary, Italy, Moldova, Turkey, Spain, and the Siwaliks (Ginsburg 1988; Van der Made and Hussain 1989; Van der Made et al. 1992, 2013; Kostopoulos 1994; de Bonis and Bouvrain 1996; Van der Made 1997; Kostopoulos et al. 2001; Sylvestrou and Kostopoulos 2006, 2009; Pickford 2013a, 2015). Finally, the measurements of *Pa. valentini* correspond to specimens from Spain, France, Germany, and Austria (Pickford 2014, 2016a). The comparative sample for multivariate statistical analyses is described later in this section in greater detail.

Note that the comparative sample of *P. palaeochoerus* does not include material from other localities in the Vallès-Penedès Basin because it is currently under study and will be described in further detail elsewhere in the future. The same applies to the material of *Pa. valentini* from the same basin, except for the sample from the site of Sant Quirze, which was originally described by Golpe-Posse (1971, 1972b) and subsequently redescribed by Pickford (2014). We take this approach because, given the recent developments in tetraconodontine taxonomy (see the Introduction), the former attributions by Golpe-Posse (1971, 1972b) are not reliable and cannot be revised without studying the material because most of the remains were not described in detail or even figured. Some of the sites with *P. palaeochoerus* (Eppelsheim), *H. major* (Melchingen), or both (Gau-Weinheim, Esselborn) included in the comparative sample correspond to mixed assemblages that have yielded older and younger remains (Pickford 2013a, 2015, 2016a). However, there seems to be a consensus that *P. palaeochoerus* is restricted to the Vallesian, with most localities being correlated to MN9 and a few to MN10 (Pickford 2013a, 2016a). In contrast, *H. major* is mostly recorded from the late Vallesian and the Turolian (i.e., MN10–MN13; Pickford 2015), with the possible exception of Plakias in Greece (Pickford 2015), which has been tentatively correlated to early MN9 (de Bruijn et al. 2012). In the case of *Pa. valentini*, even if the dating of some sites is uncertain, some of them are conclusively correlated to MN7+8 (e.g., Saint-Gaudens, Sant Quirze), whereas others are correlated to MN9 (Pickford 2016a). The only exception is the site of Mira in Spain, which was correlated to MN9 by Pickford (2014, 2016b) but which is in fact MN5 in age and, in our opinion, does not

record *Pa. valentini* but a *Conohyus* (contra Pickford 2014, 2016b; see Discussion and Conclusions for further details).

Data availability All data generated during this study are included in this published article or in the supplementary information file. The dataset of published measurements analyzed during the current study is available from the corresponding author on request.

Terminology, Measurements, and Statistical Analyses

Dental Terminology Tooth loci are denoted by an uppercase or lowercase letter (for upper and lower teeth, respectively) denoting tooth type (I/i = incisors, C/c = canine, P/p = premolar, M/m = molar) followed by a letter indicating tooth position and preceded by D/d in the case of deciduous teeth. Male and female canines are denoted by m and f, respectively, following tooth position. Terminology for the orientation of tooth and dental arcade axes follow the recommendations by Smith and Dodson (2003: fig. 7), except that 'labial' has only been applied to the anterior dention (so that 'buccal' instead of 'labial' has been used for cheek teeth). Occlusal features are generally termed after Van der Made (1996b: figs. 1–15) with modifications for accessory cusplets (e.g., see Fujita et al. 2000: fig. 2), except that the 'paraconid' of lower premolars is termed 'prestylid' and that the 'tetracone' and 'tetrapreconule' of upper molars are referred to as 'hypocone' and 'hypopreconule', respectively (Thaung-Htike et al. 2006: fig. 2; McKenzie et al. 2022).

Dental Measurements They were taken with a digital caliper to the nearest 0.1 mm. Maximum mesiodistal length (MD) and labiolingual/buccolingual breadth (BL) were taken for all tooth loci except male lower canines, where maximum breadths of the labial (La), lingual (Li), and distal (Di) faces were measured instead. For DP4s and permanent molars, buccolingual breadth was taken separately at the mesial lobe (BLm) and the distal (or central, in third molars) lobe (BLd), and then the greatest value was selected as BL. Tooth crown proportions were assessed by means of a breadth/length index (BLI = BL / MD × 100).

Comparisons and Statistical Analyses Dental size and proportions of the studied sample were compared with species included in the comparative sample (see next subsection) by means of bivariate plots of BL vs. MD for deciduous and permanent cheek teeth. Differences in dental measurements among the postcanine teeth were compared with those of other species by means of principal components analyses (PCAs), based on the variance-covariance matrix, separately for upper (P2–M3) and lower (p2–M3) cheek teeth; first premolars (P1 and p1) were excluded from the analyses due to the scarcity of maxillae and mandibles preserving the whole postcanine dentition. For each individual included in the PCAs, the linear measurements of L and W were converted into shape indices (Mosimann shape ratios; e.g., see Mosimann and James 1979; Jungers 1995; Cuccu et al. 2022) by dividing them by the geometric mean of the measurements of each specimen. Besides the species included in the bivariate comparisons, individuals of *Versoporcus steinheimensis* (Fraas, 1870) from Steinheim (Pickford 2016a), *Conohyus simorrensis* (Lartet, 1851) from Käpfnach and Carpetana (Pickford, 2013b), *Parachleuastochoerus huenermanni* (Heissig, 1989) from Lučane, and *Parachleuastochoerus kretzoii* Fortelius et al., 2005 from Rudabánya were included in the PCAs (see Online Resource 1). Only principal components

(PCs) explaining more than 5% variance each were interpreted. The PCAs were computed with PAST v. 4.04 for Mac (Hammer et al. 2001), while bivariate dental plots were constructed with Microsoft® Excel v. 16.65 for Mac.

Systematic remarks

With regard to European tetraconodontine alpha-taxonomy, for the reasons exposed in greater detail in the Discussion and Conclusions, we follow Pickford (2016a; see also Pickford 2014; Pickford and Laurent 2014) to a large extent, although we also concur with Van der Made et al. (2020) regarding the taxonomic validity of certain species of *Conohyus*. Additional clarification is required here regarding some of the tetraconodontines included in the comparative sample for the PCAs. Thus, the material from Käpfnach attributed to *C simorrensis* corresponds to the holotype of *Sus abnormis* Kaup, 1859, which was considered by Pickford (2016a) a junior subjective synonym of the former. The attribution of the material from Lučane to *Pa. huenermanni* similarly follows Pickford (2016a), being alternatively considered by Van der Made (2020) to represent a distinct subspecies, *Parachleuastochoerus steinheimensis olujici* (Bernor et al., 2004), which is not recognized as taxonomically valid here. Finally, *Pa. kretzoii* is considered a distinct species following Pickford (2016a), whereas Van der Made (2020) considered it a junior subjective synonym of *Pa. huenermanni*.

Regarding suines, the genus *Propotamochoerus* is included in the tribe Dicoryphochoerini Schmidt-Kittler, 1971 following Van der Made et al. (2020), with Propotamochoerini Pickford, 1993 being considered its junior synonym. It is noteworthy that the systematics of Late Miocene and Early Pliocene suines requires further clarification as it is subject to ongoing debates that are outside the scope of this paper but deserve to be briefly mentioned here. Thus, Pickford (2013c) considered that the inclusion of *P. provincialis* in *Propotamochoerus* is debatable and left the species without a formal generic ascription (i.e., "*Sus*" *provincialis*), while we prefer to follow common practice by most recent authors (e.g., Iannucci et al. 2021; Iannucci and Begun 2022; Lazaridis et al. 2022) and provisionally refer this species to *Propotamochoerus*. In turn, Pickford (2015, 2016c) favored an inclusion of *P. hyotherioides* in genus *Hippopotamodon*, but we similarly follow more recent authors (Hou et al. 2019; Iannucci et al. 2021; Iannucci and Begun 2022; Lazaridis et al. 2022) in including this species in *Propotamochoerus*. Finally, the distinctiveness of *P. aegaeus* was questioned by Iannucci et al. (2021), who considered it a junior synonym of *P. provincialis*, before the species was formally erected by Lazaridis et al. (2022). The purported diagnostic features of *P. aegaeus* relative to *P. provincialis* should be thus subjected to further scrutiny in the light of the variation displayed by other species of the genus to discern whether they warrant a distinct species status or rather reflect intraspecific variability. However, until an in-depth revision of the genus *Propotamochoerus* is accomplished, we prefer to tentatively keep the species distinct.

Abbreviations

Locality and institutional abbreviations: **CCN20**, Creu de Conill 20; **ICP**, Institut Català de Paleontologia Miquel Crusafont, Sabadell, Barcelona, Spain; **IPS**, acronym of the ICP collections (for the former 'Institut de Paleontologia de Sabadell').

Measurement abbreviations: **BL**, buccolingual breadth; **BLI**, breadth/length index; **L**, left; **MD**. mesiodistal length; **R**, right.

Systematic Paleontology

Order Artiodactyla Owen, 1848
Superfamily Suoidea Gray, 1821
Family Suidae Gray, 1821
Subfamily Suinae Gray, 1821
Tribe Dicoryphochoerini Schmidt-Kittler, 1971
Genus *Propotamochoerus* Pilgrim, 1925
Propotamochoerus palaeochoerus (Kaup, 1833)
Figs. 2a, 3a–c, 4a–d, f–g, i–l, n–t, v–w, y–a', c'–h', 5a–b, 6a–d, 7a–l, p–t, 8a–c, f–h, 9a–d, f–p, r–h', 10a–d, f–q, u–x, 11a–e, h–o, q–b'

Referred Material

See Table 1 for a list of referred material and Appendix Table 1 for measurements.

Description

Maxilla and Upper Permanent Teeth There is a single maxillary fragment (IPS28739; Fig. 2a) from CCN20, which corresponds to an adult individual preserving the R and L P2–M3 series as well as the R P1 (although the crown is detached from the socketed portion of the roots; Fig. 4a). The bone is not very well preserved, with abundant cracks and fissures, as well as missing chips. The premaxilla is missing, and the palate is preserved from the mesial (R side) and the distal (L side) aspects of the P1 to slightly distally from the M3s, being about 184 mm in length and 19 mm in breadth at the mesial level of the P3s. The L zygomatic arch is badly damaged, but the zygomatic process of the maxilla is preserved on the R, being ~80 mm long in craniocaudal direction and ~30 mm dorsoventrally, and anteriorly originating from the distal M1 level. The nasals are preserved up to the distal level of the P2. The postcanine toothrows are parallel except for the P1, which is oriented somewhat obliquely relative to the mesiodistal axis of the P2–M3. There is a diastema of ~1 cm between the distal root of the R P1 and the mesial end of the P2 crown.

The upper incisors are only represented by a very worn L I2 (IPS107919; Fig. 3a) that preserves most of the root (except for a small apical fragment). The crown is labiolingually compressed and quite elongate mesiodistally, tapering both mesially and distally and protruding from the cervix both at its mesial and distal ends. The labial occlusal contour is moderately convex, whereas the lingual is straighter. Most of the occlusal details cannot be ascertained due to wear, with dentine exposed throughout a flat wear surface that occupies most of the crown but tapers in distolabial direction. Nevertheless, a narrow basal fossa flanked by a poorly defined lingual cingulum can still be discerned in the distolingual aspect of the crown. The cervix forms a marked postanticline and a subtle endoanticline, but no preanticline. The root is labiolingually compressed, markedly tilted distally relative to the cervix, and slightly curved lingually from cervix to apex. It is quite robust at its base,

progressively tapering toward the apex due to the more distally inclined mesial aspect compared with the distal one.

The C1 is represented by two female specimens: IPS124843 (Fig. 3b), which is essentially unworn; and the slightly larger IPS113643 (Fig. 3c), which displays a large wear facet on the mesiolingual aspect of the crown that extends beyond the cervix and is also worn out at its apex. Both specimens display a similar crown morphology and only differ slightly in root shape, which is stouter and slightly less curved in IPS113643. The crown is moderately high and bluntly pointed, with its apex tilted distalward in labial/lingual views, due to the gently convex mesial profile (which appears continuous with that of the root) and the straighter distal profile (which at its basalmost portion slightly bulges distally from the root). The occlusal contour is labiolingually compressed in both specimens (BLI = 67–70%). The mesiolabial crown wall is convex, whereas the lingual aspect is much flatter, shaping a slightly curved and subtle vertical precrista that runs from the crown apex across about two-thirds of crown height. In turn, the distalmost aspect of the crown is markedly concave, defining a vertical, narrow and triangular fossa that extends apically from the cervix, progressively tapering until terminating close to the crown tip. This fossa, whose concavity extends beyond the cervix onto the basal portion of the root (more marked in IPS113643), is limited by a poorly-defined distolingual vertical endocrisita and a much more marked (sharper in IPS124843 and thicker but blunter in IPS113643) vertical postcrista on the distolabial side. The latter is somewhat thickened on its basalmost portion, at the level of the postsyncline, distally bulging slightly from the cervix level. The cervix extends somewhat further onto the root lingually than labially, and it shows a marked mesiolingual preanticline and a somewhat shallower and smaller postanticline distally; the ectoanticline is more concave in IPS113643 than in IPS124843. The root is tilted distally, with a convex mesial margin and a straighter to mildly concave distal margin in labial/lingual views; it more markedly tapers from the cervix to its apex in IPS124843 than in IPS113643, the latter displaying a blunter and more abrupt apex. To a lesser extent, the root is also curved labially, especially in IPS124843, although in both specimens the apicalmost portion of the root is tilted labially and separated from the rest of the root by a marked labial constriction (further accompanied by a lingual constriction in IPS124843).

The P1 is represented by an isolated unworn crown (IPS114242; Fig. 4b) and the crown detached from the IPS28739 maxilla (Fig. 4a). The crown displays an elongate occlusal contour much longer than broad, slightly more buccolingually compressed in IPS114242 (BLI = 38%) than in IPS28739 (42%), and broader distally than mesially in both specimens. The mesial and distal contours are markedly convex, whereas the buccal one is rather straight and the lingual one displays a convexity at the level of the main cusp. The crown relief is low. There are two main cusps: the paracone, which is located toward the mesial half of the crown; and the similarly-developed but much lower metacone. The paracone precrista is straight and connects the apex of this cusp with a well-developed prestyle, which is lower than the metacone and located at the mesialmost end of the crown; in IPS114242, the paracone precrista shows a mild swelling along its midway, probably not discernible in IPS28739 due to wear. The paracone postcrista is also straight but shorter than the precrista and IPS114242 displays yet another swelling (not discernible in IPS28739), separated from the metacone, which is located slightly more buccally than the paracone, by a slightly marked cleft. There is a very short metacone postcrista that terminates at the distal marginal ridge before reaching the distalmost end of the crown. There is no buccal cingulum except for some remnants at the level of the prestyle and the metacone. In contrast, a narrow cingulum can be discerned on the lingual side (more marked IPS114242), extending from the prestyle to the distal end of

the metacone postcrista, albeit being interrupted at the level of the paracone. In IPS114242, the distobuccal cingulum and the distal marginal ridge delimit a narrow fovea surrounding the metacone and metacone postcrista. IPS28739 clearly evinces the presence of two distinct roots, the distal one slightly stouter than the mesial.

The P2 and P3 are represented by the R and L antimeres of the IPS28739 maxilla (Fig. 4a). These teeth display several cracks filled with sediment, although their morphology is not severely distorted. Like the P1, the P2 is a biradiculate premolar with a low and elongate crown, although somewhat larger and broader relative to length (BLI = 53–55%) than the preceding premolar. The occlusal contour of the P2 displays a vaguely figure-eight occlusal contour, which is markedly convex mesially, rather straight mesiolingually and mesiobuccally, and markedly expanded distolingually and distobuccally, terminating in a straight and narrow distal contour. The paracone is more centrally located along the mesiodistal axis than in the P1. The paracone precrista of the P2, like that of the P1, ends in a prestyle that is located at the mesialmost end of the crown and surrounded by mild cingular developments restricted to the mesial margin. Also, as in the P1, the paracone postcrista is short and terminates in a moderately developed (and partly worn) metacone, which is located before the distal end of the crown; however, the postcrista is more obliquely oriented in the P2 than in the P1, due to the more buccal location of the metacone relative to the protocone. The distobuccal expansion of the crown is also more marked than the distolingual one and displays a sharp cingulum that encloses a very narrow and comma-shaped fossa around the buccal aspect of the metacone and its very short postcrista. In contrast, the distolingual expansion of the crown consists of a flatter and more ledge-like cingulum, which is continuous (i.e., not interrupted at the paracone level) with the less developed mesiolingual cingulum.

Unlike the P1 and P2, the P3 is triradiculate and possesses a higher, larger, and relatively broader (only slightly longer than broad: BLI = 92–94%) crown. Its occlusal contour is asymmetrically suboval: markedly convex mesially, moderately and irregularly convex buccally, straight distally, and sinuous lingually (i.e., a mesiolingual concavity is followed by a very convex distolingual protrusion). Wear is more marked than in the preceding premolars, with a long dentine exposure extending from the paracone apex until the crown distal margin. However, even taking wear into account, the crown is not very high relative to its basal dimensions. Despite wear, it can still be ascertained that, distally from the paracone, there was a well-developed but lower metacone. The prestyle is well developed but more lingually located than in the preceding premolars, being continuous with the mesial marginal ridge, which constitutes a cuspule-like enamel thickening on its mesiobuccal end. A small and buccally-open mesial fovea is delimited by the mesial ridge, the prestyle, and the mesiobuccal aspect of the protocone. The prestyle is separated from the mesial end of the protocone precrista by a curved groove. There is no buccal cingulum except for a short and narrow style distobuccally to the metacone. In contrast, there is a wide and continuous lingual cingulum that extends from the prestyle until the distolingual corner of the crown, where it constitutes a buccolingually compressed but distinct protocone, separated from the paracone and metacone by a deep, narrow, and obliquely oriented fossa.

The P4 is represented by the two antimeres of the IPS28739 maxilla (Fig. 4a), along with an isolated specimen (IPS107194; Fig. 4k) and a buccal crown fragment (IPS124437; Fig. 4l). The specimens from the maxilla are somewhat damaged (particularly the R one) and display moderate wear (with dentine exposure at the apices of the three main cusps). The isolated complete specimen is similarly worn but well preserved, whereas the buccal fragment is slightly less worn. This premolar has three cusps and the crown that is broader than long

(BLI = 119–136%). All the specimens display a similar occlusal morphology, although the contour of IPS28739 is subsquare (almost as long lingually than buccally) and broader relative to length, whereas in IPS107194 the crown tapers lingually due to the oblique mesial and distal sides. Nevertheless, in both individuals the mesial and distal contours are straight, the lingual contour is bluntly convex, and the buccal one is moderately convex with a slight constriction between the two buccal cusps. The protocone is centrally located along the mesiodistal axis of the tooth in IPS107194 and slightly more mesially positioned in IPS28739, and its dentine exposure is roughly semicircular. The two buccal cusps are subequal in size and smaller than the protocone, displaying more rounded (albeit irregular) dentine exposures. They are located close to one another more peripherally than the protocone; the paracone is almost aligned with the protocone, whereas the metacone is closer to the distobuccal corner of the crown. The protocone is separated from the buccal cusps by a deep and narrow protofossa that is partially obliterated in both individuals by the paracone endocrista, the protocone precrista, and a distal sagittal cuspule (particularly well developed in IPS28739) located next to the end of the protocone postcrista. The mesial and distal cingula are well developed, and there is a distinct prestyle close to the mesiobuccal crown corner at the end of the paracone ectocrista, albeit slightly less developed than the preconule. In IPS107194 there is a moderately developed cingulum along the buccal crown margin that bears two (mesial and distal) tiny secondary cuspules, whereas in IPS28739 the cingulum is more restricted to the distolingual aspect of the protocone.

The upper molars are represented by the R and L antimeres of the IPS28739 maxilla (Figs. 2a and 4n–o, y–z, f'–g'); two M1 germs (IPS113741 and IPS114191; Fig. 4q, s) associated with deciduous premolars (Fig. 10i–k, n–o, u–w, see below); an almost unworn M1 (IPS114098; Fig. 4t); three M1 germ fragments (IPS107114, IPS95729, and IPS125680; Fig. 4r, v–w); three mesial fragments of M2 germs (IPS114227, IPS114241, and IPS107901; Fig. 4c'–e'); and R M1 (IPS128040; Fig. 4p), M2 (IPS128039; Fig. 4a'), and M3 (IPS128038; Fig. 4h') that were found in the same area and stratigraphic horizon but not in close spatial association. Based on size and degre of wear, the three latter specimens likely belong to the same individual, but this cannot be confidently asserted because the M3 was found about 1 m away from the M1 and M2. The molars from the IPS28739 maxilla show that the M2 is larger but similar in overall morphology to the M1, whereas the M3 is similarly broad to the M2 but more elongate. The L M1 of the IPS28739 maxilla is only partly preserved and somewhat distorted, whereas the R antimere is better preserved, displaying a subrectangular occlusal contour that is approximately as broad mesially than distally, and slightly longer than broad (BLI = 95%). However, it should be taken into account that this tooth does not adequately preserve the original occlusal contour of the tooth, as its concave mesial contour and straight distal margin are due to interproximal wear. Furthermore, the occlusal surface of this specimen displays moderately advanced wear, with dentine exposure in the four main cusps (most extensive in the hypocone, where the dentine lacuna becomes confluent with that of the hypopreconule). The details that can be observed are in agreement with those displayed by the remaining specimens, in which occlusal morphology can be ascertained in greater detail. The crown of these specimens displays a subrectangular contour that is somewhat longer in relative terms (BLI = 81–88%) than in the specimens from the maxilla. The crown displays only moderate lingual flare and two (mesial and distal) distinct lobes that are subequal in size and delimited by a slightly oblique transverse valley as well as marked lingual and especially buccal constrictions. Both lobes display convex contours, the distal one being mesiodistally more elongate. The mesial contour is only slightly convex (almost straight), whereas the distal one is very convex and distally protruding. There are four main cusps, the lingual ones slightly more distally located than the corresponding

buccal cusps. The cusps are conical and similar in size, although the hypocone is somewhat smaller and less distinct than the trigon cusps in some specimens. The cusps display distinct Fürchen, although the pattern of crests and Fürchen is partly disrupted by secondary enamel grooves and folds, and both the crests emerging from the cusps and the cingula display abundant enamel wrinkling. The hypopreconule is lower and smaller than the four main cusps, but similarly displays variously developed crests separated by distinct Fürchen as well as profuse wrinkling. The hypopreconule does not block the transverse valley (except perhaps in the specimens from the IPS28739 maxilla; Fig. 4n–o), which in most specimens is buccally closed by a single or double ectoconule, and sometimes even interrupted by additional secondary cuspules located between the hypopreconule and the buccal ectoconule. In most specimens there is also a more or less distinct ectoconule at the end of the hypocone ectocrista (distally from the lingual end of the transverse valley). The mesial cingulum is well developed, being constituted by two mesially convex arched portions that converge toward the mesial end of the protocone protocrista, forming a poorly-defined and moderately-developed protoconule. The distal cingulum is also well developed, but more restricted lingually, originating distally from the hypocone and extending along the distobuccal aspect of the crown around the metacone, terminating at the buccal ectoconule. Like the mesial cingulum, the distal one is decorated by abundant radial enamel folds, which in some specimens constitute a distinct centrally located cuspule at the distalmost end of the crown.

The M2s of the IPS28739 maxilla (Fig. 4y–z) and the isolated specimen IPS128039 (Fig. 4a') display comparable lingual flare and the same occlusal morphology as the M1s from CCN20 at a larger size, except perhaps by a greater difference in the relative elongation between the distal and the mesial lobes (which is more marked in the M2s). The two antimers from IPS28739 display slightly broader proportions (BLI = 90%) than IPS128939 (BLI = 84%). The buccal ectoconule is moderately developed, whereas the lingual one merely appears as a continuation of the hypocone ectocrista in IPS28739 and better developed in IPS128039, probably being variable as in the M1s. In the M2s of IPS28739 the distobuccal extension of the distal cingulum around the metacone appears less defined than in most M1s, but this is probably attributable to wear, as IPS128039 shows a more distinct cingulum. The three mesial M2 germ fragments (Fig. 4c'–e') show a relatively well-developed protoconule and the presence of marked Fürchen with profuse enamel wrinkling, as in the unworn M1s.

Finally, the M3s are represented by the two antimeres from the IPS28739 maxilla (Fig. 4f'–g'), which are only moderately worn (with very limited dentine exposure at the apices of the two mesial cusps, and remnants of the Fürchen and enamel wrinkling still visible) and the almost unoworn specimen IPS128038 (Fig. 4h'), which is missing the distalmost end of the crown. The M3 displays an elongate subtriangular contour that is much longer than broad (BLI = 63–67%) and tapers distally from the mesial lobe, being longer lingually than buccally (despite the fact that the mesial margin is slightly more protruding buccally). The crown displays a moderate lingual flare and is not basally bulging. There are five main cusps, with the mesial ones being more extensive and less peripheral than the hypocone and the paracone, which are more buccolingually compressed. The protocone and hypocone are clearly more distally located than the corresponding buccal cusps, whereas the pentacone is located closer to the crown midline than the hypocone but clearly tilted toward the lingual side. The three lobes of the crown are separated from one another by relatively marked buccal and lingual constrictions, which the buccal portions of the crown wall being more convex than the lingual ones. The distolingually protruding third lobe is markedly convex. The mesial cingulum is very well developed and centrally interrupted by a large protopreconule. The centrally located hypopreconule displays a triangular outline and is larger than

the protopreconule. The lingual end of the transverse valley is distally flanked by a distinct ectoconule located at the end of the hypocone ectocrista. In contrast, the buccal ectoconule is poorly developed, consisting of two small thickenings of the enamel at the end of the transverse valley. The latter is however interrupted by the distal end of the external endocrista of the protocone, which contact the mesiobuccal aspect of the hypopreconule base. Distally from the latter cuspule, there is a smaller pentapreconule, of similar size to the protopreconule. The pentacone is well developed but somewhat smaller than the remaining main cusps. It is lingually flanked by a distinct ectoconule, closely packed between the hypocone postcrista and the mesiolingual aspect of the hypocone base. A thick but short cingulum with profuse enamel wrinkling originates from the mesiobuccal aspect of the pentacone and surrounds the buccal aspect of the pentapreconule until terminating at the level of the metacone postcrista (IPS28739) or running all along the buccal side of the crown and merging with the mesial cingulum (IPS128038).

Mandible and Lower Permanent Teeth Among the CCN20 sample, there are two relatively complete adult mandibles preserving the symphysis and mandibular corpora but lacking the rami (IPS107069 and IPS114386; Fig. 5a–b), as well as additional mandibular fragments from four additional individuals, one adult (IPS95623; Fig. 6b) and three juveniles (IPS114003, IPS124336a–b, and IPS124841; Fig. 6a, c–d). IPS107069 (Fig. 5a) preserves the R p2–m3 and the L p3–m3 series but no anterior teeth and the symphysis is very damaged, such that the two corpora are severely crushed against each other (to such an extent that the overlapping L corpus hinders taking reliable measurements in the posterior premolars and anterior molars). The cheek teeth of this specimen are only lightly worn and the m3s are erupted but not in full occlusion, indicating that the mandible belongs to a subadult or young adult individual. IPS114386 (Fig. 5b) similarly preserves the R and L p3–m3 series and the p2 alveoli, but despite multiple cracks and some damage (with some missing bone portions) this specimen more reliably preserves the shape of the mandibular corpora and symphysis. It displays a more advanced degree of wear (with dentine exposure in the cheek teeth), being most severe in the m1s, where only the crown walls barely remain. The L p3 of this specimen is artifactually tilted upward and buccally on its mesial portion due to damage. Neither IPS107069 nor IPS114386 allow us to ascertain whether a p1 was originally present, as both mandibles are damaged mesially from the p2 level, and they cannot either be sexed due to the lack of canines. The other adult specimen (IPS95623; Fig. 6b) is a R mandibular fragment severely distorted by multiple cracks filled with matrix. It preserves the lightly worn m2–m3, the mesial roots and the basalmost portion of the distal crown of the m1, the distal alveolus of the p4, and the partial c1; only a transverse section of the canine can be observed, indicating that the specimen belong to a male individual. Based on IPS114386, the mandible displays a V-shaped morphology with moderately converging tooth rows in mesial direction and a mesially more protruding symphysis. The posteriormost end of the symphysis is located at about mid-p2 level. From mesial to distal, the corpora only moderately increase in depth, further increasing in breadth buccally from the m2 and especially the m3, where the mesial end of the ramus originates. The remaining (juvenile) specimens do not show many details about mandibular morphology, other than displaying shallower and slenderer corpora than adult specimens. The most complete juvenile specimen is IPS114003, which preserves the whole R corpus from the symphysis and most of the ramus. The bone is however very damaged, and both the incisors and the dp2 are missing, merely preserving the dp3–m1 series (with the dp3 being unaligned relative to the dp4–m1 due to damage) and a mesiolingual fragment of the unerupted m2 germ (which is exposed due to damage). The

deciduous canine might have been originally shed, as the permanent c1 was about to emerge, being observable thanks to damage on the surrounding bone. It is only a germ lacking most of the root, but both its morphology (see below) and the presence of enamel on the distal side of the crown indicate that the specimen belongs to a female individual. The other juvenile mandibular fragments are not informative regarding mandibular shape. IPS124841 only preserves a partial dp4 (Fig. 6d) as well as the detached dp3 crown, whereas IPS124336 includes L (IPS124336a) and R (IPS124336b) fragments with dp3–m1 (Fig. 6c; albeit the L dp3 is detached) plus the isolated partial L dp2 crown. In IPS124336a–b, the m1s are only partially erupted and thus unworn, whereas the dp4s are also essentially unworn except for a flat wear surface on the mesial lobe of the L dp4. Mesially from the dp2, the R fragment further preserves the tip of the c1f germ inside the crypt (observable due to damage, but less so than in IPS114003, although similarly assigned to a female individual based on the presence of enamel on the distal aspect of the crown). The teeth from all these mandibular specimens will be described below together with that of isolated specimens.

As explained above, none of the mandibular specimens preserves incisors. Nevertheless, in contrast to the scarce sample of upper incisors, the lower ones are abundantly represented in the sample, even if not sufficiently preserved to adequately ascertain their morphology in most cases. The six i1s available from CCN20 are attributed to *P. palaeochoerus*. IPS107181 and IPS107801 correspond to apical crown portions (Fig. 7a–b) that display the same morphology and degree of wear, suggesting that they might be antimeres of the same specimen. IPS114264, in contrast, preserves most of the labial crown wall from the unworn apical ridge to almost the cervix (Fig. 7c), but is missing most of the lingual portion of the crown, whereas IPS107212 preserves most of the root but is broken just above the labial cervix level (Fig. 7d) and IPS114496 only consists of a mesial crown fragment (Fig. 7f). Finally, IPS124324 is the most completely preserved i1, including the whole crown and the basal portion of the root (Fig. 7e). However, this specimen is very worn, so that most of the crown is no longer present, which a large dentine exposure that occupies most of its occlusal facet and extends below the cervix onto the root, precluding to ascertain any details of lingual morphology. Nevertheless, when all these specimens are considered together, the i1 morphology recorded at CCN20 is characterized by a tall crown that displays a labiolingually compressed incisal edge (roughly horizontal with moderately developed mamelons when unworn, more inclined when worn out) but progressively becomes broader lingually until labiolingual breadth surpasses mesiodistal length before reaching the cervix. In contrast, the labial contour in mesial/distal views is convex (more markedly so toward the apex and close to the cervix). On the lingual side, the mesial and distal ridges (prestylid and poststylid) are moderately developed and subparallel until converging on the endosynclinid. There is also a broader and more bulging pillar (endocristid) that originates centrally close to the incisal edge and is slightly tilted distally. It delimits two narrow and shallow lingual depressions (prefossid and endofossid) that are similar in size and it is partially worn even at a moderate degree of wear. The crown base is not waisted at the cervix and displays marked pre- and postanticlinids. The root is quite straight and vertically aligned with the crown, being mesiodistally compressed throughout its length and progressively tapering from cervix to apex.

The sample of i2s from CCN20 is even more extensive than that of i1s, with most specimens being assigned to *P. palaeochoerus* and a few attributed to the other two suid species identified at the site (see below). Those assigned to *P. palaeochoerus* include two lightly worn specimens preserving part of the root (IPS106358 and IPS107877; Fig. 7i–j), three crowns displaying moderate wear (IPS113817, IPS28725, and IPS124322, the latter being somewhat damaged; Fig. 7g–h, l), and a specimen with more advanced wear further preserving part of the

root (IPS124327; Fig. 7k). The i2 crown is lower than the i1 and, unlike the latter, markedly asymmetric, with a mesiodistally shorter incisal edge that is tilted mesially. In mesial/distal views, the labial contour is convex, while the lingual one is only very slightly concave (almost straight in some specimens). As a result, the crown progressively becomes wider from the incisal edge to the cervix, being broader than long at its base. The lingual pillar (endocristid) is well developed as in the i1, but more obliquely oriented, originating below the distal end of the incisal margin and progressively becoming more diffuse but more bulging lingually toward the crown base. The mesial ridge (prestylid) is mesially inclined from the crown base to the incisal edge, but rather straight. In contrast, the distal ridge (poststylid) shows a marked angulation, with its lower third being distally inclined and the two upper thirds being more mesially inclined than the prestylid. Together with the endocristid, the pre- and poststylids define a shallow and variably developed prefossid mesially as well as a similarly narrow but much deeper and better defined endofossid distally, the latter being more basally located (almost reaching the cervix) than the former. The crown base is very little waisted at the cervix, with the crown appearing continuous with the root in mesial/distal views but being inclined mesialward relative to the latter in labial/lingual views. The preanticlinid is as pronounced as in the i1, whereas in contrast the postanticlinid is much shallower. The root resembles that of the i1, being mesiodistally compressed and progressively tapering toward its apex. Although none of the specimens preserves the complete root, the two basal thirds are straight and do not follow the same curvature as the crown in labial/lingual views.

Five i3s from CCN20 are also assigned to *P. palaeochoerus*. Two of them (IPS114221 and IPS114299; Fig. 7r–s) preserve the complete root and are unworn, likely corresponding to the R and L antimeres of a single individual. This might also apply to the more worn i3s IPS113840 and IPS124323 (Fig. 7p–q), which preserve most of the root (except for its apex) and in which the occlusal relief has been somewhat obscured by wear, displaying a steep wear facet on the distalmost end of the crown. However, these specimens are more dissimilar in size to one another and IPS124323 is more worn distally than IPS113840. A very worn incisor preserving the basal portion of the root (IPS113983; Fig. 7t) is also tentatively interpreted as an i3, as it fits better with the aforementioned specimens than with the I3 morphology of this taxon. Based on the remaining four specimens, the i3 crown is markedly elongate (labiolingually compressed), being higher mesially than distally. The labial aspect of the crown is convex on its mesial half but slightly depressed distally, whereas the lingual crown wall is flatter or even somewhat concave, due to the somewhat mesiolingually curved mesial portion of the crown (more markedly so in IPS113840 and IPS124323 than in IPS114221 and IPS114299). On the mesial half of the crown, unworn specimens display three distinct mamelons on the incisal edge. Except for the distalmost one, these mamelons are no longer distinguishable in IPS113840 and IPS124323 due to wear. On the distal aspect of the crown there is a subhorizontal endofossid, labially enclosed by the marked poststylid (which in the unworn specimens originates from a cuspulid-like protrusion similar to the aforementioned mamelons) and lingually delimited by a similarly long but lower and less marked endocristid that converges with the former on the distalmost end of the crown, somewhat above the cervix. The latter can only be ascertained on the unworn specimens, as the distal portion of the endofossid has been eroded away by wear in IPS113840 and IPS124323. Although the crown protrudes mesially from the root, distally the base of the crown is only very slightly waisted relative to the cervix. The latter further displays a straighter (subhorizontal) shape labially than lingually, with the marked preanticlinid extending from mesial toward lingual and the endosynclinid being located on the

distolingual end of the crown. The root is labiolingually compressed and displays a triangular shape with straight mesial and distal margins in labial/lingual views, being strongly tapering toward the pointed apex.

Besides the aforementioned partial c1m IPS95623 (Fig. 6b) and c1f germs IPS114003 (Fig. 6a) and IPS124336a (Fig. 6c), which could not be reliably measured because they are embedded in mandibular bone, the dental sample from CCN20 includes multiple isolated lower canines, most of them (three male and three female) assigned to *P. palaeochoerus*. The male specimens include a complete c1 (IPS113857) that is slightly distorted due to multiple cracks and fissures filled with sediment (Fig. 8g), a partial c1 (IPS113964) that is better preserved than but lacks the tip (Fig. 8h), and a more partial one (IPS113663) that is preserved in two fragments and lacks both the tip and the base (Fig. 8f). The three c1ms display a similar morphology, characterized by an open root, a distal face devoid of enamel, a moderate degree of apicobasal curvature in labial/lingual views, a slighter labial curvature from base to tip (particularly close to the apical portion), and a verrucosic cross section resembling an isosceles triangle with slightly convex labial, lingual, and distal margins that are subequal in size. In particular, the three specimens are similar in size and their distal aspect (13.1–13.8 mm) equals (IPS113857) or is slightly narrower than (IPS113663 and IPS113964) the labial one (13.5–14.0 mm), which in turn is slightly narrower than the lingual (14.3–16.1 mm).

The isolated c1fs from CCN20 correspond to IPS124330, IPS114311, and IPS114338. The former (Fig. 8a) is the most completely preserved one, including the complete (even if worn) crown and a large portion of the root (except for its apical portion), similar to IPS114338, although the latter shows more advanced wear and is more damaged (Fig. 8c). In turn, IPS114311 is less worn but is missing most of the root and it is damaged on its apicalmost portion (Fig. 8b). The three specimens show similar size and shape, with the crown and the root being labiolingually compressed (BLI = 66–75%) and markedly curved (the mesial convexity being more pronounced than the distal concavity) and displaying a symmetric triangular cross-section that is narrowest distally (more markedly so than in the male canines). The cervix is not well distinct and enamel extends much more rootward labially and lingually than mesially. The distal face displays a shallow groove along the root and a labially-oriented oblique wear facet against the upper canine. In the more worn specimen, there is also a mesial wear facet that shapes an acute angle with the distal facet, such that in distal/mesial views the canine apex appears truncated. Although in these three (worn) specimens the distal side of the crown is devoid of enamel, the two unworn c1f germs of IPS114003 and IPS124336a (Fig. 6a, c) indicate that originally enamel was also present on the distal face. The latter displays a shallow depression delimited by two cristids (ectocristid and postcristid) that originate from the crown apex, which is pointed and recurved backward. The root is longer than the crown but, even though it is not completely preserved in any specimen, it was probably closed originally (as it progressively tapers toward the apex).

The p1 is represented at CCN20 by five isolated specimens, of which four are assigned to *P. palaeochoerus*. The most complete is IPS107146, which preserves the lightly worn crown and almost the complete root (Fig. 9a). IPS107648 is missing most of the root (Fig. 9b) and is only slightly worn at the apex of its main cuspid. In turn, IPS95728 is an unworn germ (Fig. 9c), while IPS114342 lacks the mesial portion of the crown and preserves the root, even if damaged (Fig. 9d). The crown is low and buccolingually compressed, displaying a subelliptical contour that is much longer than broad (BLI = 42–43% in the three available complete crowns). All the specimens display a similar occlusal contour, which is markedly convex mesially and distally, moderately convex buccally, and more sinuous lingually, due to the presence of a more or less marked lingual convexity at

about crown midlength. One of the specimens (IPS107146) has a more pointed mesial end and a slightly marked protrusion at the distolingual corner of the crown, which constitutes a faint cingulid that is absent from the remaining ones. Otherwise, they all display a very similar occlusal morphology, characterized by the presence of a main cuspid (protoconid) that is located clearly at the mesial half of the crown, resulting in a very asymmetrical crown profile in buccal/lingual views. A narrow and short protoprecristid steeply descends from the protoconid apex to the mesial end of the crown, joining a variably developed prestylid. A similarly developed but less steep protopostcristid runs in distal direction from the protoconid toward a rather indistinct cuspid (metaconid). From the distal aspect of the metaconid, two distinct cristids bifurcate, delimiting (together with the fain distal marginal ridge) a triangular and narrow distal fossid. In IPS95728, the distolingual cristid constitutes a cuspulid-like structure that would correspond to the hypoconulid. The crown walls are only slightly bulging at the level of protoconid and straighter to mildly concave distally from it. There are no cingulids except for the aforementioned diffuse distolingual cingular expansion in IPS107146. IPS107146 and IPS114342 show that this premolar is uniradiculate, with a single fused root that is very compressed buccolingually and tilted distally from cervix to apex. In IPS107146 the root is slightly constricted buccally and lingually, whereas in IPS114342 the root is apicobasally broken at the junction between its mesial and distal portions, which apparently display separate apices, hinting at the presence of two fused roots. Indeed, IPS107648 shows more marked grooves at the root base than IPS107146, suggesting that the fusion of the two roots might not be complete in the former, so that the degree of p1 root fusion would be variable.

At CCN20, the p2 is represented by three isolated specimens (IPS114339, IPS28732, and IPS114256; Figs. 9f–g, i), which are all assigned to *P. palaeochoerus*, plus another specimen corresponding to the IPS107069 mandible (Fig. 9h). The isolated specimens display some variation in occlusal outline and/or relief, but generally fit with the morphology of the socketed specimen (whose tooth locus identification is secure). They are characterized by a buccolingually compressed crown (slightly less so than in the smaller p1; BLI = 41–51%), with the protoconid slightly located on the mesial moiety of the crown, a lingually tilted prestylid, and a variously developed distal cuspulid (hypoconid) located and the end of the protopostcristid close to the distal end of the crown. The most outstanding specimen is the unworn crown IPS114256 (Fig. 9i), which is longer in absolute terms than the remaining specimens and shows a more marked relief and better developed lingual and buccal anticlinids, a distinct distolingual cingulid, and a slightly compressed buccal and lingual contours. However, an alternative identification of this tooth as a P2 is considered less likely, as it lacks the more marked lingual and distal expansions characteristic of this upper premolar, which result in a relatively broader and more clearly figure-eight-shaped occlusal contour. The same applies to the more worn specimen IPS28732, which shows a broader occlusal contour than the remaining p2s, but less so than in the P2s and further lacking the characteristic buccal and lingual constrictions of the latter. The protoprecristid is sharp and straight to moderately curved lingually, ending in the mesiolingually located prestylid, which is better developed in IPS114256 and apparently worn away in IPS28732. The protopostcristid is approximately as sharp and long as the protoprecristid, but slightly more obliquely oriented, ending on the hypoconid, slightly located on the buccal half of the crown. The hypoconid is fainter in IPS107069 than in the remaining specimens, and more distally located in IPS107069 and IPS114339 than in IPS28732 and IPS114256, where a distinct but short cristid originates from the hypoconid in distobuccal direction. A smaller cuspulid-like structure (which would correspond to the metaconid) can be clearly discerned in IPS114256 and IPS114339 at the end of the

protopostcristid, just mesially from the hypoconid, resulting in a somewhat serrated edge in buccal/lingual views that can still be hinted at in IPS107069 but not in IPS28732 probably due to wear. No buccal cingulid can be discerned except for some hints at the mesiobuccal and distobuccal corners of the crown, respectively at the level of the mesial stylid and the hypoconid. The lingual cingulid is also poorly developed (only consisting of a slight basal bulging of the crown) except in IPS114256, where a narrow but distinct cingulid extends continuously from the prestylid across the protoconid level, becoming thicker and slightly ledge-like around the distolingual aspect of the crown, where it displays multiple radial enamel folds. The p2 has two well distinct roots, the mesial one being mesially tilted, whereas the distal one is slightly stouter and more verticalized.

The sample of p3s from CCN20 includes five specimens from three individuals: the R and L antimeres from IPS107069 (Figs. 5a and 9j) and IPS114386 (Figs. 5b and 9k–l), and the isolated specimen IPS113968 (Fig. 9m). The socketed specimens are larger than the p2s but display some variation in occlusal contour: elliptical (i.e., buccally and lingually bulging at crown midlength) in IPS107069 (BLI = 53%) and more buccolingually compressed with straighter buccal and lingual contours in IPS114386 (BLI = 44–46%). Otherwise, all these specimens display the same occlusal structure, with a high protoconid located toward the mesial half of the crown, a protoprecristid steeper and shorter than the protopostcristid, a distinct albeit low mesial stylid that is tilted lingually, a higher hypoconid located at the distal end of the crown, variably deep clefts on the lingual and buccal crown walls at the level of the protopostcristid, and a mild development of a cingulid on the distolingual corner of the crown. The p3s of IPS114386 display lower occlusal relief and a less distinct prestylid than those of IPS107069, to a large extent due to the more advanced wear in the former, although they all display some dentine exposure on the distal aspect of the protoconid apex and along the protopostcristid. Nevertheless, remnants of a cuspulid (which would correspond to the metaconid), originally present between the protoconid and the hypoconid, can be discerned. The isolated specimen IPS113968 preserves the complete crown and both the mesial and distal roots, although the latter is clearly constituted by two (distolingual and distobuccal) roots that are only partially fused apically from their basalmost portion. This cannot be ascertained in the socketed specimens from CCN20, from which IPS113968 differs in several details of occlusal morphology: a relatively broader suboval outline that is particularly expanded distolingually (BLI = 61%), a more subhorizontal protopostcristid due to the more elevated hypoconid, and better developed distobuccal and distolingual cingula. It is however unclear if the more subhorizontal distal outline of the crown is due to an unusual wear pattern against the upper dentition, whereas other particular features of this specimen (such as size and occlusal contour, the moderate development of the metaconid, and the presence of two roots) rule out an alternative identification as a p4 (see the description of the p4s below for further details). Interestingly, this specimen evinces more clearly than the socketed ones the presence of a metaconid just distally from the protoconid, although it is of similar size to the hypoconid and hence much smaller than the protoconid (or the p4 metaconid).

The p4s of *P. palaeochoerus* from CCN20 are represented by four teeth from two mandibular specimens, corresponding to the R and L antimeres of IPS107069 (Figs. 5a and 9n) and IPS114386 (Figs. 5b and 9o–p). Those of IPS107069 are only lightly worn and permit to ascertain all occlusal details, whereas those of IPS114386 show a somewhat more advanced degree of wear (with confluent dentine exposures on the apices of the three main cuspids) but otherwise agree in morphology with the former, merely differing slightly in occlusal contour. Thus, although occlusal proportions are similar in IPS107069 (BLI = 62–68%) and IPS114386 (BLI = 66–71%), the former displays an elliptical contour that is buccally and lingually bulging at about crown

midlength, and more markedly tapering distally than mesially, whereas IPS114386 is rather suboval and slightly broader distally than mesially. The crown is larger than that of the preceding molars, and more complex in structural terms, being dominated by a high protoconid and an arched protoprecristid that descends from the apex of the former until reaching a well-developed prestylid on the mesialmost end of the crown. On the buccal side of the protoconid and protoprecristid, the crown wall is bulging and convex, whereas the lingual one constitutes a spacious and lingually open protofossid. The latter is delimited mesially by the well-developed and somewhat beaded mesiolingual cingulid originated from the mesial stylid, distally by the metaconid, and buccally by the high lingual wall of the protoprecristid, which displays multiple radial enamel grooves. The apex of the metaconid is smaller than that of the protoconid and located on the distolingual aspect of the latter, separately by a shallow groove that extends mesiolingually toward the bottom of the protofossid. The protopostcristid is very verticalized and interrupted by the well-developed buccal and lingual clefts that separate the trigonid from the much lower and smaller talonid, which are further delimited from one another by a transverse deep groove that extend slightly onto the buccal and lingual crown walls. At the middle of the talonid there is a distinct hypoconid mesiodistally aligned with the protoconid but much lower than the trigonid cuspids. At least in IPS107169, there is a very short but thick hypopostcristid that buccally originates a distinct distobuccal cingulid, which defines a narrow distobuccal fossid; this distobuccal cingulid is narrow and smooth in IPS107169 and somewhat wider and beaded in IPS114386. On the distolingual aspect of the hypoconid, in contrast, there are no distinct fossid or cingulid, but in IPS107169 the distolingual crown margin constitutes a cuspulid-like structure on the distolingual aspect of the hypoconid, with is partly separated from the hypopostcristid by a vertical groove located slightly lingually from the distalmost end of the crown. Although all the available p4s are socketed, it can be ascertained that three roots are present, the mesial one being apparently more mesially oriented than the distal ones.

The whole lower molar series is preserved in the adult mandibles IPS107069 (Figs. 5a and 9x, c') and IPS114386 (Figs. 5b and 9s, y, d'), although the m1 is distorted in the former and too worn to ascertain occlusal morphology in the latter. However, the m1 morphology can be adequately observed in the lightly worn specimen and the unworn germs of the juvenile mandibular fragments IPS114003 (Figs. 6a and 9t) and IPS124336a–b (Figs. 6c and 9w), respectively, as well as in two complete (IPS95707 and IPS107263) and one partial (IPS28737) germs (Figs. 9r, u–v). The m2 and m3, in turn, are preserved in the two aforementioned adult mandibles (Figs. 5a–b and 9x–y, c'–d') and in the mandibular fragment IPS95623 (Figs. 6b and 9z, e'), coupled with an isolated m2 (IPS113969; Fig. 9a'), a mesial fragment of m2 (IPS113845; Fig. 9b'), and three m3 distal fragments (IPS113843, IPS107717, and IPS114049; Fig. 9f'–h'). The whole sample of lower molars from CCN20 is assigned to *P. palaeochoerus*, with the exception of an isolated m1 (IPS113818; Fig. 9q), which is very worn and was left unassigned to subfamily. The m1 and m2 display similar rectangular occlusal contour with a moderate lingual constriction and a more marked buccal one, as well as similar proportions at a different size, with the m2 being larger but tending to be only slightly broader with considerable overlap (m2 BLI = 66–78%; m1 BLI = BLI m1 = 63–70%, excluding the IPS114386 antimeres, which are somewhat broader due to interproximal wear). The crowns of both m1 and m2 display two distinct lobes: the mesial one bears the two trigonid cuspids (protoconid and metaconid), whereas the distal one is mesiodistally longer (and in the m2 also broader than the mesial more often than for the m1) and displays three main cuspids together with a well-developed hypopreconulid. The buccal cuspids are higher and slightly more mesially located than the corresponding lingual ones, but similarly extensive and non-peripheral. The hypopreconulid is centrally located

and smaller than the main cuspids, although sometimes it is transversely extended by lingual and/or buccal secondary cristids. The pentaconid is centrally located on the distalmost end of the crown and intermediate in size between the remaining main cuspids and the hypopreconulid. The m1 germs show well marked Fürchen and abundant enamel wrinkling on the cristids and cingulids. These features become progressively more indistinct at more advanced wear stages, as most clearly shown by the m2s. On the mesial end of the crown there is a marked cingulid that in unworn specimens displays a beaded morphology (with marked radial enamel grooves), and which is interrupted by a distinct mesiolingual stylid (less distinct in m2s, apparently due to wear). In most of the unworn to slightly worn m1s, just distal to the mesial cingulid, there is a long and arched protoprecristid and a shorter but similarly curved metaectocristid that join at about crown midline and form a continuous semicircular and thick crest that mesially encloses the protofossid, which is mostly occupied by the thick and short metaprecristid and the even shorter protoendocristid. However, there is some variation in these structures, as in IPS114003 the two former cristids do not merge but are separated by a distinct mesiodistal groove, whereas in IPS107263 the protoprecristid merges instead with the end of a longer and more mesially oriented metaprecristid, with the metaectocristid terminating abruptly close to the mesial cingulid (between the mesiolingual stylid and the metaprecristid). The endo- and postcristids of the protocone and metacone are similarly developed and distally oriented, ending at the transverse groove that separates the mesial and distal lobes. The metaendocristid appears somewhat thicker and displays a bifid end, although only in IPS124336 it constitutes a distinct endoconulid, which is separated from the end of the protoendocristid by a marked groove. Due to their more advanced degree of wear, the occlusal details of the mesial cristids and cingulids cannot be adequately ascertained in the m2s, although as far as it can be evaluated their morphology is consistent with that of the m1s, and in IPS107069 a distinct endoconulid linked to the metaendocristid can be discerned (as in the m1 germ IPS124336). Besides the aforementioned hypopreconulid, the transverse groove separating the two lobes is buccally enclosed by a more or less distinct (and, in the latter case, single or double) hypoectoconulid. The hypoconid and ectoconid display four cristids each. Both the endo- and hypoprecristid are directed toward the hypopreconulid, but only the end of the hypoprecristid is connected to the latter, their dentine lacunae coalescing at more advance wear stages (as shown by one of the m2s). In turn, the endo- and hypoendocristid are directed to the pentaconid, but the hypoendocristid is generally longer and thicker, sometimes more clearly reaching the pentaconid. The hypoectocristid and hypopostcristid are poorly developed, whereas in contrast the endoectocristid and the endopostcristid are more distinct and mesiodistally aligned along the distolingual crown wall. The endopostcristid is continuous with a semicircular, thick, and distally protruding distal cingulid that encircles the pentaconid and merges with the hypoendocristid on the buccal side.

The m3s display a much more elongate and distally tapering occlusal contour than the preceding molars (BLI = 50–55%), displaying three distinct lobes (with the mesial one being the broadest). Available specimens display a degree of dental wear from slight (almost no dentine exposure) to moderate (slight dentine exposure on the apices of the main cuspids). The former still permit to ascertain the presence of Fürchen, but most enamel wrinkling presumably present originally has already been obscured. As far as it can be ascertained, the configuration of the four more mesial cuspids is essentially comparable to that of the preceding molars, except that the protoprecristid appears in all instances separated from the paraectocristid by a groove and is terminally swollen, almost forming a distinct protopreconulid. As in the preceding molars, there is a small hypoectoconulid and the hypopreconulid is well developed and variably extended buccolingually along the transverse groove that

separates the mesial from the central lobe. Distally from the hypoconid and entoconid, the talonid is more elongate than in the preceding molars and displays a well-developed pentapreconulid (subequal in size to the hypopreconulid) next to the end of the hypo- and entoendocristid, as well as larger pentaconid at the distalmost end of the crown. While the pentapreconulid is centrally located and completely aligned with the hypopreconulid, the pentaconid is tilted distobuccally. On the buccal side, between the hypoconid and the pentaconid, there is no distinct pentapreconulid at the end of the pentaectocristid. On the lingual side, between the entoconid and the pentaconid, there are some cuspulids that might be interpreted as the hexaconid (distally from the entoconid and pentapreconulid) and the heptoconid (between the hexaconid and pentaconid), although they are not well individualized and their development is variable and very rudimentary at most.

Deciduous teeth Four DI1s from CCN20 are assigned to *P. palaeochoerus*, of which IPS107830 (Fig. 10a) and IPS124844 (Fig. 10d) preserve the crown and most of the root, whereas IPS95713 (Fig. 10b) and IPS113900 (Fig. 10c) preserve the crown and the basalmost portion of the root. All the specimens display a similar morphology, characterized by a moderately high crown that is slightly taller than long and longer than broad, with a moderately convex mesiolabial wall and a markedly concave distolingual aspect. The latter is flanked by the thick distal marginal crest and the shorter and fainter mesial marginal crest. There is a sharp and narrow lingual cingulum that runs in parallel to the cervix. An obliquely oriented and short endocrista originates from the mesiolingual end of the lingual cingulum and becomes progressively fainter until disappearing close to the incisal edge, separating the relatively restricted prefossa from the more extensive and somewhat deeper endofossa. The cervix more steeply descends from distal to mesial on the lingual than on the labial side, shaping a marked preanticline on the mesiolingual aspect of the crown, as well as a distinct endosyncline in distolabial position, which slightly bulges from the cervix. The root is slender and labiolingually compressed toward its base but more strongly tapers in apical direction in labial/lingual views, curving in distal direction from cervix to apex. Another DI1 (IPS107110; Fig. 10e) is completely preserved but displays an advanced degree of wear that precludes assessing any details of the lingual morphology, so we prefer to leave it unassigned. Two additional upper incisors (IPS95667 and IPS95662; Fig. 10f–g) displaying a relatively advanced degree of wear and preserving part of the root show a similar morphology than the I2 assigned to *P. palaeochoerus* (IPS107919; Fig. 3a), markedly protruding from the cervix (particularly in mesial direction). However, these specimens are mesiodistally shorter and have a slenderer root than the I2, being tentatively interpreted as DI2 of the same taxon. Yet another upper incisor (IPS124326; Fig. 10h) more closely resembles the DI1s described above at a much smaller size, with a less marked lingual cingulum and shallower fossae, being interpreted as a DI3.

With regard to the deciduous premolars, the DP2 is represented by a moderately worn R crown (IPS113741; Fig. 10i), as well as four additional partial specimens (the mesial fragment IPS124325 and the distal fragments IPS114191, IPS114228, and IPS113669; Fig. 10j–m) that display a congruent size and shape with the aforementioned complete crown. One of these specimens (IPS114191) is associated with a DP3 distal fragment and the R and L DP4 of the same individual (Fig. 10o, v–w), whereas the more completely preserved IPS113741 is associated with a partial DP3 and a complete DP4 of the same individual (Fig. 10n, u). The deciduous upper premolars of this taxon are further represented by two additional partial DP3s (IPS95632 and IPS113800; Fig. 10p–q) and a partial DP4 (IPS113914; Fig. 10x). The DP2 is a biradiculate premolar similar in size to the P1 but intermediate in occlusal shape between the P1 and P2, being characterized by an elongate (BLI = 47%) and

asymmetrical crown that is broader distally than mesially and longer lingually than buccally. The occlusal contour is markedly convex mesially and almost straight lingually, with a marked constriction on the buccal side at about crown midlength, and a very protruding distolingual expansion. In the two latter features, IPS113741 more closely resembles a P2 than a P1, suggesting that it corresponds to a DP2 instead of a P1. Otherwise, the occlusal morphology is very similar except for a comparatively somewhat higher occlusal relief. The main cusp (paracone) is located toward the mesial half of the crown and the straight and steep precrista ends at a marked prestyle. The paracone postcrista leads to an apparently well-developed (but largely worn out) metacone that is much lower than the paracone and connected to the distal marginal ridge by a very short metacone postcrista. Unlike the buccal cingulum, which is interrupted at the base of the paracone, the lingual cingulum is continuous, albeit more developed at the level of the prestyle and the metacone. In turn, the morphology of the DP3 can be best ascertained in IPS113741, which is nevertheless missing the distobuccal crown corner, further being complemented by the aforementioned remaining specimens. This DP3 crown displays a subtriangular occlusal contour that is longer than broad (BLI = 66–67%) and broader distally than mesially, with a markedly convex anterior lobe and only a slight constriction separating it from the distal lobe. There are three main cusps: the paracone, which is centrally located on the mesial lobe and despite wear it evinces the presence of three crests (the mesial precrista and the distal endocrista and postcrista); and the distal protocone and metacone. There is a mesial cingulum that extends from the mesial margin throughout most of the lingual side, but not along the buccal one, and at least IPS95632 displays a cingular development on the distobuccal crown corner. The DP4s (Fig. 10u–x) display a similar morphology to the M1s but are smaller and lower-crowned, and display a more oblique (mesiobuccally protruding) mesial contour but a similarly convex distal margin and a subrectangular (longer than broad; BLI = 77–84%) occlusal outline with two distinct (mesial and distal) lobes.

The deciduous lower incisors of *P. palaeochoerus* are represented by multiple di1s, some of them preserving most of the root and showing only minimal to moderate wear (IPS124335, IPS114535, and IPS28730; Fig. 11a–c), whereas the remaining ones (IPS106511 and IPS124845; Fig. 11d–e) are more incompletely preserved and show more advanced wear, but are consistent in preserved morphology with the former ones. The deciduous incisor sample further includes three di3s preserving the crown with the basalmost portion of the root (IPS107839, IPS95719, and IPS107685; Fig. 11i–k), whereas the di2 is only represented by a distal crown fragment (IPS124333; Fig. 11h) that is not particularly informative. The di1 displays a similar morphology to the i1, characterized by a labiolingually compressed incisal edge and a crown that slightly expands mesiodistally from cervix to apex, with moderately marked mesial and distal ridges, a more protruding and slightly inclined endocristid that basally originates from the endosynclinid but apically fades away before reaching the incisal edge, and a straight root aligned with the crown. The morphology of the di3, which can be best ascertained in the slightly worn specimen IPS107839, resembles that of the i3 in several features, especially the low and mesiodistally elongate crown that is higher mesially than distally, at a smaller size. However, unlike in the i3, in the di3 no distinct mamelons can be discerned, the mesial ridge is more distinct, the crown is proportionally lower, and the endocristid is more diffuse and less distally directed, so that the endofossid is neither enclosed nor distally directed.

With regard to the deciduous lower premolars, three isolated specimens (IPS124332, IPS107121, and IPS107099; Fig. 11l–n) and a partial crown IPS124336a (Fig. 11o) are identified as dp2s of *P. palaeochoerus*. The latter specimen is associated with the dp3–m1, which show the morphology of *P. palaeochoerus*, thereby

being unambiguously attributable to this species. IPS107121 only preserves the mesial moiety of the crown, but is consistent in size and shape with IPS124332 and IPS107099, which similarly display an extensive distal wear facet. IPS124332 displays slenderer roots than IPS107099 and IPS107121 (where they are fused at the basalmost portion but more clearly diverge toward their tips) and appears more trenchant in crown morphology, but this is likely attributable to a lesser degree of wear. All the specimens display a mesiolingually curved protoprecristid that ends on the mesialmost end of the crown without any distinct prestylid; however, IPS124332 and IPS124336a further display a second, more buccal cristid descending from the protoconid apex, which together with the protoprecristid define a shallow and steep mesiolingual fossa. Due to the degree of wear and incomplete preservation, the shape of the distal end of the crown can only be ascertained in IPS124336a, which displays a low but conspicuous cuspid (hypoconid) at the end of the protopostcristid on the distalmost end of the crown. In turn, the dp3 is represented by the R and L antimeres of IPS124336 and the R specimen of IPS114003 (Fig. 11q, t–u), both corresponding to juvenile mandibular specimens preserving the m1, as well as the R dp3 IPS124841 (associated with a mandibular fragment with partial dp4; Fig. 11r) and an isolated L dp3 IPS125679 (Fig. 11s). All the specimens display a mesially tapering elliptical occlusal contour that is about twice longer than broad (BLI = 45–50%). The dp3 crown is larger and relatively longer than that of the dp2, but the two roots are proportionally even more developed (both stouter and longer) relative to crown size, further being clearly separated from one another at the cervix level, with the mesial one being clearly tilted mesialward. The occlusal morphology of the dp3 can be better ascertained in the less worn isolated specimen (IPS125679), although most of the details can still be ascertained in the remaining dp3s despite a somewhat more advanced degree of wear. The main cuspid (protoconid) is centrally located but slightly titled toward mesial. The protoprecristid is longer and more steeply inclined than the protopostcristid, ending on a low but distinct prestylid on the mesial end of the crown. The protopostcristid, when unworn, displays a more convex profile than the protoprecristid in buccal/lingual views, and ends on a well-developed hypoconid, which is lower than the protoconid apex but much higher than the prestylid, and located close to distal end of the crown. The hypoconid base is separated from the end of the protopostcristid by a short and shallow transverse groove. No distinct cingulids can be discerned.

Finally, the dp4 is represented by the various specimens belonging to mandibular fragments (IPS124336, IPS114003, and IPS124841; Fig. 11v–x, z), coupled with the R isolated specimen IPS124842 (Fig. 11y) and two partial specimens (IPS124329 and IPS114001; Fig. 11a'–b'). These teeth are much longer than broad (BLI = 44–49%) and display three distinct lobes that increase in breadth from mesial to distal. The various lobes display convex sides and are separated from one another by more or less developed constrictions, generally more marked on the buccal side. Most of the specimens display a more or less advanced degree of wear, except for IPS124336, which only display minimal dentine exposure at the apices of the main cuspids (except for the mesial lobe of the L antimere, which displays an extensive dentine lacuna occupying most of the occlusal surface). The size, proportions, and occlusal morphology (as far as it can be ascertained) of the remaining specimens are consistent with those of IPS124336, on which the following description is based. The tooth displays six main cuspids, more or less transversely aligned by pairs and displaying each several cristids separated by distinct Fürchen. On the mesial lobe, the lingual cuspid (primonid) is somewhat more mesially located than the similarly sized buccal cuspid (paraconid), and the primonid precristid connects with a distinct parapreconulid located on the mesiolingual end of the crown; in turn, the paraendocristid gives rise to a poorly

developed endoconulid located at about the center of the crown. The cuspids of the central lobe are mesiodistally aligned with those of the mesial lobe; the protoconid is somewhat more extensive than the metaconid, and the endocristids of both cuspids end on a small endoconulid that is more distinct than that of the mesial lobe. Distobuccally from the latter, on the distal lobe, there is a slightly larger preconulid attached to the end of the hypoconid precristid; the hypoconid and, to a lesser extent, the endocristid are the most extensive cuspids. A conspicuous but small pentaconid, similar in size to the preconulid, is located on the distalmost end of the crown, being somewhat titled toward the buccal side.

Subfamily Tetraconodontinae Lydekker, 1876
Genus *Parachleuastochoerus* Golpe-Posse, 1972b
Parachleuastochoerus valentini (Filhol, 1882)
Figs. 2b–c, 3d, 4e, h, m, u, x, b', i'–j', 7m, 8d–e, 9e, 10e, r–t, y–c', 11f–g, p

Referred Material

See Table 1 for a list of referred material and Appendix Table 1 for measurements.

Description

Upper Permanent Dentition None of the upper incisors available from CCN20 fit well with the morphology of the upper permanent incisors of *Pa. valentini* described by Pickford (2014) from Sant Quirze, although it should be taken into account that the morphology of the I2 is unknown. No C1f has either been reported for this species, but one of the specimens from CCN20 (IPS106329; Fig. 3d) differs in several regards (larger crown basal dimensions as well as a stouter but shorter and straighter root) from the two other C1fs from the site (Fig. 3b–c), which display the typical morphology of *P. palaeochoerus* (see above), and is thus assigned to *Pa. valentini*. The crown is very worn, displaying an obliquely oriented wear facet against the lower canine that, in the mesial half of the crown, goes up beyond the cervix onto the root (such that enamel is only preserved in the distal moiety). A flake of enamel is also missing from the labial crown wall, whereas dentine exposure on the preserved distal crown aspect is very limited (except for two small chips of enamel missing at the cervix probably due to wear). Based on what is preserved, the crown would have originally been somewhat labiolingually compressed (about 50% longer than broad). The labial and lingual crown walls display a convex contour, whereas the distal aspect is slightly concave, being delimited on the distolabial aspect of the crown by an irregular postcrista that is much thicker than the distolingual endocrista. The root is stout, labiolingually compressed, and rather straight (displaying only a mildly convex mesial curvature and a rather vertical distal contour in labial/lingual views, such that it only tapers moderately from cervix to apex). The mesiolingual and distal aspects of the root display a more convex contour than the labial aspect, defining a faint mesial keel that extends from the wear facet to the root apex.

The tetraconodontine upper premolars available from CCN20 consist of an isolated R P2 (IPS124328; Fig. 4e) and a maxillary fragment including the R P3–P4 (IPS113819; Figs. 2b and 4h, m). Like in the other maxillary fragment from CCN20 (IPS114251), which includes the R M1–M3 (Figs. 2c and 4u, b', j'), not much

bone is preserved, being only informative from the viewpoint of dental morphology. Both maxillary fragments and the aforementioned P2 might belong to the same individual, as they are from the same side and display a consistent degree of wear—more advanced in the M1, moderate in the M2, slight in the premolars, and very slight in the M3. However, this cannot be conclusively demonstrated because, even though the three specimens come from the same area of the excavation (squares O51, M52, and O50, respectively), they were not found in close spatial association. The P2 (Fig. 4e) is biradiculate and elongate, being almost twice longer than broad (BLI = 53%), and broader distally than mesially. The crown, which is almost unworn, is high and displays a trenchant appearance. In occlusal view, it displays a rather uniformly convex buccal contour and a marked constriction midway along the lingual side, followed by a well-developed protrusion on the distal crown moiety. Such a protrusion is flanked by a shelf-like lingual cingulum that contrasts with the faint and narrow cingular remnant on the distobuccal aspect of the crown but which does not constitute any cuspule-like structure. There is a centrally located and distally tilted main cusp (paracone), from which the sharp precrista and postcrista originate. The precrista is straight but slightly obliquely oriented in mesiolingual direction, steeply descending until reaching a well-developed prestyle that is located at the mesial end of the crown, flanked by cingular notches (the lingual being more marked than the buccal). The postcrista, which terminates at the distal end of the crown, is longer, more curved, and less steeply inclined than the precrista, and unlike the latter it displays a mildly concave (instead of convex) contour in buccal/lingual views. The postcrista is slightly swollen toward its final portion but it does not constitute a distinct distal cuspule. Only the mesial root is preserved, displaying a round cross-section and being mesially tilted.

Like the P2, the P3 (Fig. 4h) is only slightly worn (with moderate dentine exposure at the tip of the paracone and along the postcrista) and displays a similar occlusal structure, mostly differing in crown size and proportions and the number of roots. In particular, the P3 is triradiculate and displays a more inflated (slightly longer but much broader) crown. The P3 crown occlusal contour (BLI = 85%) is subtriangular to suboval (albeit asymmetric), and broader distally than mesially. The buccal profile is more markedly convex than that of the P2, whereas on the lingual side a faint constriction precedes a more extensive protruding distolingual shelf. The latter is separated from the paracone base and the postcrista by a poorly defined and curved groove, and peripherally flanked by a marked thickening of the cingular margin, which (unlike in the P2) constitutes a low and diffuse cuspule-like structure that would correspond to the protocone. Similarly to the P2, the P3 crown displays a trenchant appearance, although it is comparatively much taller relative to mesiodistal length than that of the P2. Although the paracone is in a similarly centered position, unlike in the P2, the precrista and postcrista of the P3 are of similar length and both display a convex contour in buccal/lingual views. Similarly, the prestyle of the P3 is comparatively less developed (e.g., compared to the height of the paracone) than that of the P2, being of about the same size but flanked by less marked notches in the P3. In contrast, at the distal end of the P3 crown there is cuspule-like thickening of the enamel where the postcrista merges with the distal margin. There is no continuous lingual cingulum, being limited to the lingual aspect of the prestyle as well as to the distolingual shelf-like extension of the crown. The buccal crown base is slightly bulging but no buccal cingulum can be discerned except at the mesialmost and distalmost ends of the crown. The mesial root is slightly tilted mesially (as in the P2), whereas the distobuccal and distolingual roots seem to be more vertically oriented (so that only the mesial and distobuccal roots are exposed, whereas the distolingual one is socketed in the maxillary bone except for its apicalmost preserved portion; Fig. 2b).

The P4 (Figs. 2b and 4m) is a triradiculate tooth much lower-crowned than the P3. The crown displays a subtriangular occlusal contour that markedly tapers lingually and is broader than long (BLI = 123%). The lingual contour is markedly convex, whereas the buccal one displays a slight constriction at the junction between the buccal cusps; the mesial margin is more obliquely oriented than the distal relative to the crown's mesiodistal axis. There are three main cusps, given that the similarly-size paracone and metacone, even if closely packed, display well distinct apices and are separated along more than two-thirds of the buccal crown wall by a deep but narrow vertical groove. The protocone is larger than the buccal cusps and no accessory cuspules can be discerned on the protofossa (or sagittal valley). Although the protocone is located toward the mesial moiety of the crown, it is not transversely aligned with the paracone but rather intermediate in position between the latter and the metacone. The mesial and distal cingula are similarly well developed; the lingual end of the distal cingulum is particularly thickened, but separated from the short postcrista of the protocone by a deep transverse groove. On the mesiobuccal corner of the crown, at the end of the paracone ectocrista, there is a distinct and cuspule-like prestyle, which is nevertheless smaller than the preconule located on the mesiolingual aspect of the paracone.

With regard to the upper molars, the maxillary fragment with M1–M3 (IPS114251; Figs. 2c and 4u, b', j') enables to ascertain the differences in shape and proportions among molar loci within a single individual. Both the M1 and M2 display a similar subrectangular occlusal contour that is slightly longer than broad (with the M2 being essentially a larger copy of the M1 in terms of occlusal morphology), whereas the M3 displays a more elongated and subtriangular contour (being slightly broader but much longer than the M2) that tapers distally. A distal fragment of M1 (IPS113642; Fig. 4x) and a distobuccal fragment of M3 (IPS95697; Fig. 4i') are the only additional upper molars assigned to this taxon. The latter preserves the metacone and partially the hypocone, the hypopreconule, and the pentapreconule, but except for the apparently greater development of the latter it perfectly fits in occlusal morphology and overall size with the complete M3 of IPS114251. The distal M1 fragment, in contrast, allows to better ascertain the morphology of this tooth, because it is much less worn than the M1 of IPS114251, which displays a large dentine lacuna corresponding to the mesial cusps, another to the hypocone and hypopreconule, and another one to the metacone, with further dentine exposure and damage at the distal cingulum. The complete M1 displays a subrectangular contour slightly longer than broad (BLI = 91%) and slightly broader mesially than distally. The buccal and lingual contours are similarly convex and display a marked constriction between the mesial and distal lobes. The narrow transverse valley between the two lobes is interrupted midway by the mesialmost end of the hypopreconule dentine lacuna. This valley is lingually open, whereas buccally it is partially blocked by a diffuse ectoconule constituted by two enamel thickenings. A small dentine exposure located at the end of the hypocone ectocrista, distally from the buccal end of the transverse valley, corresponds to a lingual ectoconule that has been worn away. The M1 distal fragment displays some lingual flare and preserves the hypocone, the slightly smaller metacone, and the much smaller hypopreconule, which is linked to the hypocone by a short and thick precrista. The main cusps are pyramidal in shape and display marked Fürchen, as it is typical of tetraconodontines, while lacking the corrugated enamel that is characteristic of suines such as *Propotamochoerus*. There is a very thick but buccolingually short and centrally located distal cingulum that constitutes a cuspule-like enamel thickening just distal to the hypocone postcrista and endocrista.

The M2 of the maxillary fragment IPS114251 is moderately worn, with conspicuous dentine exposure only at the paracone and protopreconule, although most of the details concerning Fürchen have been eroded by wear. The M2 resembles the M1 but is larger, broader in relative terms (BLI = 94%), and broader distally than mesially (unlike the preceding molar). Furthermore, the M2 crown apparently displays greater lingual flare and more marked constrictions between the mesial and distal lobes than in the M1 (particularly the lingual one). The mesial cusps are somewhat larger and more conical in shape than the distal ones, with the protocone being slightly more distally located than the paracone, and the distal cusps being transversely aligned. The hypopreconule is flattened due to wear and quite extensive (larger than in the M1 fragment described above), but it does not block the transverse valley between the two lobes of the crown. This valley is buccally enclosed by a twinned ectoconule similar but slightly more developed than that of the M1. As in the latter, a similarly developed lingual ectoconule is present at the terminus of the hypocone ectocrista, distally from the transverse valley. A short but thick precrista of mesiolingual orientation connects the hypocone with the hypopreconule, thereby lingually enclosing the hypofossa. The mesial and distal cingula appear well developed, although the former is much more worn; the distal is less marked but buccolingually less restricted than in the aforementioned M1 distal fragment.

The lightly worn M3 is slightly broader but much longer than the M2, and displays a subtriangular contour that tapers distally, being longer on the lingual than on the buccal side due to the distally protruding pentacone. The crown is markedly constricted buccally and lingually between the mesial and central lobes. The four main cusps are conical to pyramidal in shape and quite bulbous, and display moderately developed Fürchen. The mesial cusps are somewhat larger than the distal ones, and the lingual cusps are clearly more distally located than the corresponding buccal cusps. The protocone is somewhat more extensive than the paracone and hypocone, whereas the metacone is elongate (buccolingually compressed). The mesial cingulum is very thick and tuberculate. It is interrupted by the jutting protopreconule, where it further displays a marked concavity. The protopreconule is well developed but somewhat smaller than the centrally located hypopreconule. The transverse valley is sinuous and briefly interrupted by the internal endocrista of the protocone, which connects with the mesial aspect of the hypopreconule. This valley is open lingually but buccally enclosed by an ectoconule that is simple and slightly less developed than that of the M2. A thick but very short precrista connects the hypocone with the hypopreconule, lingually enclosing the hypofossa. The pentacone, located at the distolingual corner of the crown, is broader than long and smaller than the four main cusps, but larger than the preconules. On the mesiobuccal aspect of the pentacone there is a moderately developed pentapreconule. A small secondary cuspule is present buccally from the pentapreconule, which distally encloses the narrow hypofossa. The pentacone and pentapreconule are directly located on the distal margin of the crown, not being encircled by a distal cingulum.

Lower Permanent Dentition All the i1s and i3s from CCN20 are assigned to *P. palaeochoerus*, but the most complete i2 (IPS114337; Fig. 7m) is ascribed to *P. valentini*. Although the crown is too worn to adequately ascertain its lingual morphology and overlaps in size with the i2s assigned to *P. palaeochoerus* (see above), this specimen displays tetraconodontine affinities because it has a stouter (less mesiodistally compressed) and a more curved root that displays the same curvature as the crown with less waisting at the cervix.

Regarding the lower canines, all the male specimens from CCN20 are assigned to *P. palaeochoerus*, but two isolated c1fs (IPS107072 and IPS114387; Fig. 8d–e) are instead attributed to *Pa. valentini* because they display

several relevant differences relative to those of *P. palaeochoerus*. These two specimens preserve the complete root (except for minor damage in IPS107072), which is closed, but the crown is barely preserved due to their advanced degree of wear (comparable to the most worn specimen of *P. palaeochoerus* from CCN20), displaying two (distal and mesial) wear facets. The former is subparallel to the distal face, whereas the mesial facet is more steeply oriented, so that small remnants of the crown enamel are only preserved on the lingual and labial sides. While this precludes reliably assessing crown morphology, the root appears less curved (especially distally) and more robust than in the specimens assigned to *P. palaeochoerus*, clearly becoming labiolingually more inflated relative to the crown basal dimensions throughout most of its length until apically tapering more or less abruptly along their apicalmost third. Given that two c1f morphotypes can be discerned among the CCN20 sample, it seems logical to attribute the robust one to *Pa. valentini* (in further agreement with the differences inferred for the C1fs), even though such an identification must remain tentative as far as the specimens are not associated with more diagnostic material and that the morphology of this tooth locus had never been previously reported for this taxon.

A single lower premolar from CCN20 is assigned to *Pa. valentini*, consisting of a partial p1 germ with unfinished crown (IPS95813), so that the distalmost end of the crown cannot be observed (Fig. 9e). This tooth displays a higher occlusal relief and more trenchant morphology than those assigned to *P. palaeochoerus*, with the protoconid being only slightly mesially located (resulting in a less asymmetrical profile in buccal/lingual views). The protoprecristid is similarly steep but somewhat curved mesiobuccally, ending on a better developed mesial prestylid. The protopostcristid is straighter and longer, and despite displaying a somewhat denticulated margin it lacks a distinct cuspulid. The distal end of the crown and the buccal course of the cervix cannot be adequately ascertained due to incomplete preservation. However, on the lingual side the cervix displays a distinct anticlinid.

Deciduous Dentition The sample of deciduous teeth attributable to *Pa. valentini* is quite restricted. The R DP3 IPS114230 (Fig. 10r) and two distal fragments of DP3 (IPS113955 and IPS107104; Fig. 10s–t) display a similar size and shape to those assigned to *P. palaeochoerus* (see above), except that the mesial lobe is comparatively narrower and the occlusal contour is relatively broader (BLI = 74%) with a more marked constriction between the mesial and distal lobes, being thus assigned to *Pa. valentini*. Several more or less complete (IPS114048, IPS107687, and IPS124331) and partial (IPS125678 and IPS107883) DP4 crowns (Fig. 10y–c') are also assigned to *Pa. valentini* based on the less corrugated enamel with more marked Fürchen and squarer occlusal contour (only slightly longer than broad; BLI = 86–99%), at least as far as it can be ascertained in spite of wear and incomplete preservation (the tetraconodont affinities being most clear-cut in IPS114048; Fig. 10y).

Two deciduous incisors from CCN20, the di1 germ IPS107725 (Fig. 11f) and the moderately worn crown with basal root portion IPS107976 (Fig. 11g), are tentatively assigned to *Pa. valentini* instead of *P. palaeochoerus* based on the more obliquely oriented incisal edge and seemingly better developed (broader and more lingually protruding) endocristid, although such attribution must remain tentative because this tooth position has not been thus far described for the former taxon. Finally, a deciduous lower premolar IPS114102 (Fig. 11p) from CCN20 has a more trenchant appearance than those attributed to *P. palaeochoerus* and is interpreted as a R dp2 of *Pa. valentini*. The crown is markedly longer than broad (BLI = 34%) and slightly broader distally than mesially, with a lingual constriction at about crown midlength and a somewhat protruding

distolingual crown aspect. The buccal crown wall is generally convex, whereas the lingual wall is rather concave, and the crown displays a rather trenchant appearance. The single main cuspid (protoconid) is located toward the mesial half of the crown, with the protoprecristid being shorter but steeper than the protopostcristid. The former ends on a mildly distinct prestylid on the mesialmost end of the crown, whereas the protopostcristid (which displays some dentine exposure) bears no conspicuous cuspulid but ends on a poorly developed hypoconid on the distal end of the crown. There are no cingulids except by a short cingular development lingually from the prestylid. The crown displays marked lingual and buccal anticlinids. The two roots are distinct from one another from the cervix level and well developed (the distal one being stouter and the mesial one being more mesially directed).

Subfamily Cainochoerinae Pickford, 1993
Genus *Albanohyus* Ginsburg, 1974
cf. *Albanohyus* sp.
Fig. 7n–o

Referred Material

See Table 1 for a list of referred material and Appendix Table 1 for measurements.

Description

Only two lower incisors (Fig. 7n–o) are assigned to this small suid. Both specimens preserve a quite worn crown and a large portion of the root, which display a marked mesialward curvature from root to crown apex. The crown is slightly broader than long and, despite the degree of wear, an endocristid can be discerned along the lingual side of the crown, which terminates above a moderately large and bulging endosynclinid close to the cervix.

Comparisons

Qualitative comparisons

Propotamochoerus palaeochoerus In the male cranium of *P. palaeochoerus* from Johnsdorf, the canine flange distally extends from about the P2–P3 level, with its root further extending posteriorly until mid-P3 (Mottl 1966: pl. III). Given that no remains of the flange can be ascertained in IPS28739 from CCN20, despite preserving the R P1 and both P2, this specimen most likely belongs to a female individual. The anterior root of the zygomatic also originates slightly more anteriorly (distal M1 level) than in the Johnsdorf male cranium (distal level of the M2; Mottl 1966 pls. II and III), which might also be due to sexual dimorphism.

The I2 from CCN20 agrees well in size with the published measurements for the I2 of *P. palaeochoerus* from Rudabánya (Fortelius et al. 2005) and Gau-Weinheim (Pickford 2013). Comparisons of crown shape (see Hünermann 1968: pl. 1, fig. 10) are restricted by the advanced wear of the CCN20 specimen, but as far as it can

be ascertained it resembles the I2 of *P. palaeochoerus* from Hostalets figured by Van der Made and Moyà-Solà (1989: pl. I, fig. 11), except that the latter displays a more marked distolingual cingulum. The latter structure is variable in the I3 of *P. palaeochoerus*, but an alternative identification of the CCN20 specimen as an I3 is less likely because this tooth in *P. palaeochoerus* is shorter, more triangular, and relatively less elongate (Hünermann 1968: pl. 1, fig. 11; Van der Made and Moyà-Solà 1989: pl. I, fig. 10; see measurements in Fortelius et al. 2005; Pickford 2013), and unlike the I2 it is not worn out flat but preserves its characteristic triangular profile in labial/lingual views. An alternative attribution to the tetraconodontine from CCN20 can be ruled out because the tetraconodontine upper incisors are not mesiodistally elongate (e.g., Pickford 2013b: fig. 7).

The two C1s of *Propotamochoerus* from CCN20 clearly belong to female individuals, as those of males are larger and open-rooted (Fortelius et al. 2005; see Hünermann 1968: pl. 1, figs. 25–26, 32). The CCN20 specimens are slightly larger and relatively broader than those reported from Rudabánya (Fortelius et al. 2005) and the specimen from Grytsiv (Van der Made et al. 1999). However, the somewhat larger size is in accordance with that of the postcanine dentition and the general morphology of the tooth is consistent with that from Grytsiv (Van der Made et al. 1999: pl. 2, fig. 4), except that the latter displays a slenderer and more constricted root, as well as a more convex lingual crown wall with a more marked precrista and a distally more protruding postcrista. Nevertheless, the two specimens from CCN20 assigned to *P. palaeochoerus* more closely resemble the Grytsiv specimen than the other specimen from CCN20 (assigned to the tetraconodontine) in the possession of a longer, slenderer and more curved root.

The P1s from CCN20 (BLI = 38–42%) are larger than the specimens previously measured in the literature but display similar proportions (BLI = 36–46%, N = 7; Hellmund 1995; Fortelius et al. 2005), with the exception of a specimen from Gau-Weinheim (BLI = 52%) reported by Pickford (2013), which despite its broader proportions closely resembles in occlusal shape (see Hünermann 1968: pl. 1, fig. 2; Schmidt-Kittler 1971: fig. 4) the two specimens from CCN20. The latter also match very well the occlusal contour of the P1 from the female cranium figured by Stromer (1928: pl. II, fig. 20)—originally reported from the Münchener Flinz but subsequently considered to come from the younger Schweiß-Sande (Stromer 1940)—which displays only a moderate distolingual swelling, whereas the P1s from the Johnsdorf male cranium (Mottl 1966: pl. IV) display a more bulging distolingual contour. Comparisons with the Rudabánya material are limited because the P1s were described but not figured by Fortelius et al. (2005), but the only obvious difference evidenced by their descriptions is perhaps the greater development of the cingula in the Rudabánya specimens. It is noteworthy that in the Johnsdorf cranium (Mottl 1966: pl. IV), the P1 is separated from the P2 by a longer diastema than in the CCN20 maxilla, whereas in the Münchener Flinz's female cranium (Stromer 1928: pl. II, fig. 20) such a diastema is much smaller. Besides the length of the diastema, these specimens also show variation in the orientation of the P1 mesiodistal axis, which in the cranium figured by Stromer (1928) is aligned with the posterior premolars, whereas in the Johnsdor cranium it is rotated outward, and in the CCN20 maxilla it is rotated inward. These differences might be partly related to the development of the supracanine flanges in the Johnsdorf male cranium.

The P2s from CCN20 (BLI = 53–55%) are slightly larger than those previously reported in the literature but display similar proportions (BLI = 50–59%, N = 5; Hellmund 1995; Fortelius et al. 1996), except for the specimen from Pyhra (Austria), which is narrower (BLI = 39%; Hellmund 1995). The single P2 from Rudabánya, based on the descriptions by Fortelius et al. (2005), is slightly broader (BLI = 59%) but displays a

very similar morphology to the CCN20 specimens, merely differing in the development of a distolingual cuspule from the cingular margin. The P2s from the Johnsdorf cranium, despite displaying very similar proportions to the CCN20 ones (BLI = 56%; Hellmund 1995), show a distolingual expansion of the crown much more marked than in the CCN20 maxilla (Mottl 1966: pl. IV), although due to wear it is difficult to ascertain if a cuspule (which would correspond to the protocone) was present as in the Rudabánya specimen. In any case, the morphology of the CCN20 P2s perfectly matches that of the lightly worn specimens from the cranium figured by Stromer (1928: pl. II, fig. 20). Note that all these specimens differ in occlusal morphology from the P2 figured by Hünermann (1968: pl. 1, fig. 4) as *P. palaeochoerus*, where the crown is relatively narrower and only distolingually expanded, and which was reassigned to a tetraconodont by Pickford (2013a).

The CCN20 P3s (BLI = 92–94%) are somewhat larger and more inflated than average as compared with those previously reported in the literature (BLI = 73–94, N = 24; Mottl 1966; Hellmund 1995; Fortelius et al. 2005; Pickford 2013a; Iannucci and Begun 2022); see for instance the more triangular (mesially tapering) profile of the P3s figured in Mottl (1966: pl. IV) and Fortelius et al. (2005: fig. 5) and the less protruding distolingual cusp in Stromer (1928: pl. II, fig. 20). However, some specimens from Rudabánya, Gau-Weinheim and Alsótelekes (Hünermann 1968: pl. 1, fig. 2; Iannucci and Begun 2022: fig. 2A) reach values of BLI equal or higher than 90%, similar to those displayed by the CCN20 specimens. Overall, the occlusal contour of this tooth locus appears quite variable in the comparative sample of *P. palaeochoerus*, although its occlusal configuration is essentially the same as seen in the CCN20 specimens, including the presence of a distinct protocone on the distolingually protruding portion of the crown. As in the female cranium from the Münchener Flinz (Stromer 1928: pl. II, fig. 20), in the CCN20 maxilla the P3s are only slightly obliquely implanted relative to the mesiodistal axis of the P4–M3, whereas in the male cranium from Johnsdorf (Mottl 1966: pl. IV) they are more obliquely implanted, in accordance with the more oblique mesial contour of the P4.

The comparative sample for the P4 of *P. palaeochoerus* is much larger than for the preceding premolars (BLI = 103–130%, N = 44; Hellmund 1995; Van der Made et al. 1999; Fortelius et al. 2005; Pickford 2013a; Iannucci and Begun 2022), but similarly shows that, despite some overlap in length and proportions, the CCN20 P4s are quite large and particularly broad (BLI = 123–136%) compared with previously known specimens. Nevertheless, in terms of occlusal morphology the CCN20 specimens do not show any relevant difference relative to previously figured P4s, which display the same variation in occlusal contour, from subsquare (Hünermann 1968: pl. 1, figs. 2–3; Van der Made et al. 1999: pl. 1, fig. 2 and pl. 2, fig. 1; Fortelius et al. 2005: fig. 5) to more lingually tapering (Stromer 1928: pl. II, fig. 20; Mottl 1966: pl. IV; Iannucci and Begun 2022: fig. 2A). Note, however, that the more lingually tapering specimen from Gau-Weinheim assigned by Hünermann (1968: pl. 1, fig. 5) to *P. palaeochoerus* was considered tetraconodont by Pickford (2013).

The upper molars from CCN20 are larger than average in *P. palaeochoerus*, but while the larger sample of M1s largely overlap with the upper range of the species, both the M2s and the M3s surpass to some extent the previously recorded size range for the species, as in the case of the posterior premolars. Nevertheless, in terms of BLI proportions, the upper molars from CCN20 fit quite well with previously published measurements (Mottl 1966; Hellmund 1995; Van der Made et al. 1999; Fortelius et al. 2005; Pickford 2013a, 2015; Iannucci and Begun 2022): 80–95% in CCN20 vs. 82–104% elsewhere (N = 47) for the M1; 84–90% vs. 79–102% (N = 69) for the M2; and 63–67% vs. 58–87% (N = 69) for the M3. In terms of occlusal structure, the CCN20 upper molars also fit well with those previously described or figured in the literature (Stromer 1928: pl. II, fig. 20;

Mottl 1966: pl. IV; Hünermann 1968: pl. 1, figs. 2–3; Van der Made et al. 1999: pl. 2, figs. 1–2; Fortelius et al. 2005: fig. 5; Iannucci and Begun 2022: fig. 2A), with some exceptions discussed below. In the Johnsdorf cranium (Mottl 1966: pl. IV) the M3s appear much shorter than in the CCN20 sample and other figured specimens (Hünermann 1968: pl. 1, fig. 2; Van der Made et al. 1999: pl. 2, fig. 2) due to the lesser development of the central and distal lobes, although their proportions (BLI = 78–80%; Hellmund 1995) fit with the variation documented elsewhere. The M3s are even stouter (BLI = 86–87%) in the cranium figured by Stromer (1928: pl. II, fig. 20), in which the third lobe appears particularly underdeveloped compared with those from CCN20 and other figured specimens, from which it differs by apparently lacking a pentapreconule. In contrast, the CCN20 M3s resemble this specimen and that from Grytsyv in the distolingual position of the pentacone, which is more centrally located in the Gau-Weinheim M3 figured by Hünermann (1968: pl., 1 fig. 2). In this regard, all these specimens differ from the Johnsdorf M3s, where the smaller and more centrally located pentacone is even slightly tilted buccally instead of lingually. The pentacone orientation in the Johnsdorf M3s seems thus a bit unusual, as the CCN20 M3s fit in this and other regards with the morphology described for the Rudabánya M3 sample by Fortelius et al. (2005). Indeed, these authors noted other relevant variation in M3 morphology among the Rudabánya specimens, including the minority presence of an additional distal cusp (hexacone) and the infrequent extension of the mesial cingulum along the buccal crown margin, but not in pentacone position or orientation. Furthermore, for the two variable features reported by these authors, the CCN20 specimens agree with the most common M3 morphology at Rudabánya. Overall, it can be concluded that the M3 of *P. palaeochoerus* displays some variation among the available hypodigm, but that the CCN20 M3s fit well with the M3 morphology most commonly displayed by the species.

The morphology of the i1 agrees well with that previously figured and described (Hünermann 1968: pl. 1, fig. 13; Van der Made et al. 1999, pl. 2, fig. 7; Fortelius et al. 2005; Iannuci and Begun 2022: fig. 2D), characterized by a symmetrical and labiolingually broader crown that displays a conspicuous lingual pillar and is well distinct from the root. Occlusal proportions cannot adequately be compared with those reported in the literature because labiolingual breadth is not adequately preserved in any of the CCN20 specimens (due to wear and/or incomplete preservation). However, mesiodistal length (7.5–7.9 mm) is slightly longer than in the specimens from Grytsyv, Gau-Weinheim, and Alsótelekes (Van der Made et al. 1999; Pickford 2013a; Iannuci and Begun 2022) but shorter than in those from Rudabánya (Fortelius et al. 2005).

The i2s appear somewhat larger than those of Grytsyv, Rudabánya, Eppelsheim, Gau-Weinheim, and Alsótelekes (Van der Made et al. 1999; Fortelius et al. 2005; Pickford 2013; Iannuci and Begun 2022), particularly in mesiodistal length, but show the same morphology previously described and figured for the species (Hünermann 1968: pl. 1, fig. 14; Van der Made et al. 1999: pl. 2, fig. 8; Fortelius et al. 2005; Iannucci and Begun 2022: fig. 2D), characterized by an asymmetrical crown with an angulated distal margin, a well-developed endocristid, and a deep endofossid and a mesiodistally compressed and straight root that displays a different orientation from the crown. Available information from the literature for the i3 of *P. palaeochoerus* is quite meager, being mostly restricted to the four specimens from Grytsyv measured by Van der Made et al. (1999), which purportedly would be broader than long. However, it is obvious from the figure (Van der Made et al. 1999: pl. 2, fig. 6) that these authors oriented the i3s differently as it is customary (e.g., see the i3 of *P. wui* in Van der Made and Han 1994: pl. 12, fig. 7), with the crown being mesiodistally elongate and quite compressed labiolingually in *Propotamochoerus*. This cannot be checked in the samples from Rudabánya, as Fortelius et al.

(2005) explicitly reported that no i3s had been identified (despite listing measurements for two, which might be a mistake), or the mandible from Alsótelekes, where the i3 is not preserved (Iannuci and Begun 2022). When the correct orientation is taken into account, the CCN20 i3s are larger, and especially more elongate (BLI = 48–49% in the two unworn specimens from CCN20) than those from Grytsyv (BLI = 60–69%, N = 4). Otherwise, the i3s from CCN20 match the morphology of the specimen figured by Van der Made et al. (1999: pl. 2, fig. 6), being characterized by a mesiodistally elongate and asymmetrical crown that is higher and lingually curved mesially than distally and displays a narrow distal fossid, as well as by a triangular and labiolingually compressed crown that strongly tapers from cervix to apex.

The morphology of the CCN20 c1ms (with subequal and slightly convex sides and an enamel-free distal portion) agrees well with that described by Van der Made et al. (1999) and Fortelius et al. (2005) for *P. palaeochoerus*. The latter authors described the c1m cross section of this species as "moderately scrofic to verrucosic" (Fortelius et al. 2005: p. 271), but the provided measurements are unclear and this cannot be checked. According to Van der Made et al. (1999), *P. palaeochoerus* possesses a verrucosic c1m, with the distal face approaching or even slightly surpassing the labial face, and in the single specimen from Grytsyv reported by this author the lingual side is slightly wider (11.0 mm) than the labial (10.5 mm) and distal (10.1 mm). The CCN20 specimens are larger but display similar proportions, being slightly broadest lingually and slightly narrowest distally (although in one of the specimens the labial and distal sides measure the same). The verrucosic condition of lower male canines is usually defined as having labial and lingual sides of similar length and longer than the distal one (as in *Sus verrucosus*), whereas the scrofic condition is defined as having a longest lingual side and a distal side longer than the labial (as in *Sus scrofa;* e.g., Cherin et al. 2020). This definition can be simplified by referring to the narrowest side, which would be the distal in verrucosic canines and the labial in scrofic canines (e.g., Van der Made et al. 1999). In the three c1ms from CCN20, the lingual side is the longest, but they qualify as verrucosic instead of scrofic because the distal side is the narrowest and the labial side is only slightly narrower than the lingual. In this regard, together with their slightly convex cross-section and distal enamel-free surface without a cementum band, the CCN20 specimens resemble those of *P. palaeochoerus* (Van der Made et al. 1999: pl. 2, fig. 5; see also cross-sectional drawings in Hünermann 1968: figs. 48–49, 51). In contrast, the morphology of the CCN20 c1ms excludes an attribution to *Conohyus doati* (Lartet, 1851), which like *C. simorrensis* displays a scrofic morphology with a cementum band on the distal side (Pickford 2013b: fig. 6E, 2014, 2016a; Pickford and Laurent 2014; see also Stehlin 1900: pl. VII, fig. 12 regarding *C. doati*), and also to *Versoporcus* spp., which lacks the cementum band but displays a very scrofic cross-section (Pickford 2014, 2016a: fig. 19). Probably for this reason, a specimen figured by Hünermann (1968: fig. 36) as *P. palaeochoerus,* but markedly scrofic, was reassigned by Pickford (2013a) to a tetraconodontine (either *Conohyus* or *Versoporcus*). Given that the c1m of *Pa. valentini* is unknown (see Discussion and Conclusions below) and that the genus *Parachleuastochoerus* otherwise displays a verrucosic morphology (Pickford 2014), an alternative attribution of the CCN20 specimens the former species cannot be conclusively excluded. Indeed, finding a lower male canine of *Pa. valentini* would be key for confirming or excluding its inclusion in *Parachleuastochoerus* instead of *Conohyus*.

The morphology of the c1fs from CCN20 generally agrees with that described for the sample from Rudabánya (Fortelius et al. 2005: p. 271) and the mandible from Alsótelekes (Iannucci and Begun 2022: fig. 2D)—i.e., curved and labiolingually compressed, with a rounded mesial edge, and a closed root. Although the

isolated specimens from CCN20 lack enamel on the distal face due to wear, the unworn germ from the same locality (Fig. 6a) clearly shows the presence of distal enamel, as in Alsótelekes (Iannucci and Begun 2022: fig. 2D). In contrast, the CCN20 specimens do not display a distinct groove on the distal face but a poorly defined and shallow groove along the root and a more diffuse concavity delimited by two cristids on the distal aspect of the crown apex. The CCN20 c1fs (BLI = 64–79%) overlap in size and proportions with those previously reported from Wien III, Eppelsheim, Gau-Weinheim, and Alsótelekes (BLI = 62–94%; N = 5; Hellmund 1995; Pickford 2013a; Iannucci and Begun 2022). The same applies to the two c1fs from CCN20 assigned to *Pa. valentini*, except that one displays slightly higher mesiolingual dimensions; however, they differ from those assigned to *P. palaeochoerus* in displaying a less curved and much stouter root, as well as a different wear pattern characterized by the presence of both distal and mesial wear facets. If our identification is correct, it would be the first time that the c1f morphology of *Pa. valentini* is reported in the literature.

The p1s of *P. palaeochoerus* from CCN20 are only slightly more elongate (BLI = 42–43%) than those previously reported from Grytsyv, Rudabánya, and Alsótelekes (44–52%, N = 6; Van der Made et al. 1999; Fortelius et al. 2005; Iannucci and Begun 2022) and generally agree, with only a few minor differences, with the morphology described by these authors. The specimen tentatively assigned to the species by Van der Made et al. (1999: pl. 1, fig. 3) similarly displays a mesially located protoconid, with the protoprecristid being steeper than the protopostcristid, but no secondary cuspulid can be recognized in the latter, there is neither a distinct prestylid, and besides the specimen displays two well distinct roots (the distal one being stouter than the mesial). Van der Made et al. (1999) noted that the specimen might alternatively belong to a tetraconodontine, and indeed the more convex outline of the protoprecristid in buccal view is more reminiscent to the p1 of *V. steinheimensis* figured by Chen (1984: pl. 2, fig. 2). The CCN20 specimens more closely resemble that from the Alsótelekes mandible (Iannucci and Begun 2022: fig. 2D), which undoubtedly belongs to *P. palaeochoerus*, except that the latter displays two distinct (even if closely packed roots) rather than a single fused root (as in the CCN20 specimens in which the root is preserved). The p1s of *P. palaeochorus* described (but not figured) by Fortelius et al. (2005) from Rudabánya also appear more similar to those from CCN20 in possessing a prestylid and a distinct secondary cuspulid along the protopostcristid, but similarly display two distinct roots. The specimens from CCN20 thus suggest that the degree of fusion of p1 roots might be variable in the species. The Rudabánya p1s also resemble those from CCN20 in that the protopostcristid divides into two distinct ridges distally, although Fortelius et al. (2005) described the presence of two distinct shallow fossids, one distal (as in the CCN20 specimens) and another distolingual (only recognizable in one of the CCN20 specimens in the form of a faint cingular expansion), and also distinct cingular bulges on the buccal and lingual margins that are not well recognizable in the CCN20 sample (or in the Alsótelekes mandible).

The p2s from CCN20 are slightly larger than average but show similar proportions (BLI = 41–51%) to the specimens previously reported from Grytsyv, Rudabánya, Gau-Weinheim, and Alsótelekes (BLI = 42–50%, N = 16; Van der Made et al. 1999; Fortelius et al. 2005; Pickford 2013a; Iannucci and Begun 2022). Furthermore, as far as it can be judged from published descriptions and figures (Hünermann 1968: pl. 1, fig. 6; Van der Made et al. 1999: pl. 1, figs. 1, 4–5 and pl. 2, fig. 3; Fortelius et al. 2005; Iannucci and Begun 2022: fig. 2D) they no not display important differences in occlusal morphology. The specimens described by Van der Made et al. (1999) and Fortelius et al. (2005) resemble all the CCN20 specimens in the mesially located protoconid and the distinct lingually tilted prestyle, and some (but not) all p2s from CCN20 in the elongate occlusal profile that is mildly

constricted buccally and lingually and slightly expanded distolingually. Although the Grytsiv specimens do not enable to clearly evaluate the presence of a distinct distal cuspulid (probably due to wear), this feature can be ascertained in the Rudabánya sample, where two cuspulids could be discerned distally from the protoconid in slightly worn specimens (Fortelius et al. 2005), as well as in the Alsótelekes mandible (Iannucci and Begun 2022: fig. 2D).

The p3s of *P. palaeochoerus* from CCN20 are larger than—but display similar proportions (BLI = 44–61%) to—the specimens previously reported from Grytsyv, Rudabánya, Gau-Weinheim, and a few other sites (BLI = 46–59%, N = 26; Hellmund 1995; Van der Made et al. 1999; Fortelius et al. 2005; Pickford 2013a; Iannucci and Begun 2022). In terms of occlusal morphology, they fit well with previously figured and described specimens (Hünermann 1968: pl. 1, figs. 1 and 7; Van der Made et al. 1999: pl. 1, figs. 1 and 4 and pl. 2, fig. 3; Fortelius et al. 2005; Iannucci and Begun 2022: fig. 2D), although some of the specimens from CCN20 have a more inflated or distolingually expanded contour than those from Grytsyv, which in contrast appear to have a more distinct distobuccal cingulid. However, based on the Rudabánya sample, Fortelius et al. (2005) already noted that the development of the cingulids and the degree of crown swelling around the protoconid are variable in the p3 of *P. palaeochoerus*. These authors further highlighted the presence of hypoconulid and often also metaconid at early stages of wear, as shown by the CCN20 specimens and as further observable in some of the figured p3s from Grytsyv (Van der Made et al. 1999) and Alsótelekes (Iannucci and Begun 2022).

The p4s from CCN20, like the preceding premolars, are larger than average for *P. palaeochoerus* (despite some overlap) and display slightly narrower proportions (BLI = 62–71%) than previously published specimens (BLI = 67–85%, N = 40; Helmmund 1995; Van der Made et al. 1999; Fortelius et al. 2005; Pickford 2013a; Iannucci and Begun 2022). In terms of occlusal morphology, the CCN20 p4s generally match the morphology displayed by previously figured specimens (Hünermann 1968, pl. 1, fig. 1; Van der Made et al. 1999: pl. 1, figs. 1 and 4 and pl. 2, fig. 3; Iannucci and Begun 2022: fig. 2D) as well as descriptions provided by Fortelius et al. (2005), including the variable development and beading of the distolingual and distobuccal cingulids. However, the Grytyv (Van der Made et al. 1999) and Alsótelekes (Iannucci and Begun 2022) specimens display a more distally expanded p4 crown. For the Rudabánya sample Fortelius et al. (2005: p. 271) asserted that in the p4 "The Innenhügel [i.e., the metaconid] is as large as the main cuspid [i.e., the protoconid] or larger and placed and place just distally and strongly lingually to it", whereas in the CCN20 material the metaconid occupies the same position but is somewhat smaller than the protoconid (at least in the unworn p4s of IPS107069), as in the Alsótelekes mandible (Iannucci and Begun 2022). Given the variation in morphology displayed by this and the preceding premolars, we do not consider these differences to be taxonomically relevant, particularly given that the metaconid in the CCN20 sample is nevertheless very well developed, as it is typical of the species (Van der Made et al. 1999; Iannucci and Begun 2022).

The lower molars of *Propotamochoerus* from CCN20 overlap to a large extent with those of *P. palaeochoerus* from elsewhere but are larger on average and some specimens surpass the upper range of lower molar mesiodistal length recorded elsewhere, consistent with evidence from the upper molars. However, the BLI proportions of the lower molars from CCN20 fit well with previously published measurements (Hellmund 1995; Van der Made et al. 1999; Fortelius et al. 2005; Pickford 2013a; Iannucci and Begun 2022): 63–82% in CCN20 vs. 60–79% elsewhere (N = 50) for the m1; 66–78% vs. 65–82% (N = 76) for the m2; and 50–55% vs. 47–62% (N = 85) for the m3. The occlusal morphology of the *P. palaeochoerus* lower molars from CCN20 also matches

that previously described or figured for this species in the literature (Hünermann 1968, pl. 1, fig. 1; Van der Made et al. 1999: pl. 1, figs. 1 and 4 and pl. 2, fig. 9; Fortelius et al. 2005; Iannucci and Begun 2022: fig. 2D), including the only moderately elongated and distally tapering m3 (although, according to Fortelius et al. 2005, the m3s from Rudabánya would be less distally tapering) with a continuous mesial cingulid. In the CCN20 sample, the m3 pentaconulid appears more buccally tilted than in the lectotype (Hünermann 1968: pl. 1, fig. 1) and the Grytsyv specimens (Van der Made et al. 1999: pl. 1, figs. 1 and 4 and pl. 2, fig. 9), more closely resembling in this regard the morphology of the Alsótelekes mandible m3s (Iannucci and Begun 2022: fig. 2D).

With regard to the deciduous dentition, Hünermann (1968: pl. I, figs. 12, 15, 17, 19) figured a DI2, a di2, a DP4, and a dp4 fragment of *P. palaeochoerus*. However, to our knowledge this is the first time that the DI1, DI3, DP2, DP3, di1, di3, dp2, dp3, and dp4 of this taxon are figured or described in detail (Hünermann 1968: pl. I, fig. 18 also figured a purported dp3 but this tooth was interpreted as a tetraconodont p2 by Pickford 2013a). This is because Van der Made et al. (1999) and Fortelius et al. (2005) merely reported measurements for these tooth positions (with the exception of third deciduous incisors, which were not reported) but did not figure or described them (except for a brief description of the dp4 in Fortelius et al. 2005). The assignment of the described DP3, DP4, and lower deciduous premolars to *P. palaeochoerus* is conclusively supported by their association with permanent first molars that display the morphology of this taxon, while that of the DP2, di1, and di3 are based on their similarities with permanent teeth of *P. palaeochoerus* (the P1–P2, i2, and i3, respectively). The assignment of the upper deciduous incisors to *P. palaeochoerus* is thus somewhat more tentative, albeit the DI1 does not show a tetraconodont morphology but rather more closely resembles the figured specimen of *P. wui* (Van der Made and Han 1994: pl. 12, fig. 8), supporting its attribution to *P. palaeochoerus*. In agreement with the permanent cheek teeth, the upper and lower deciduous premolars from CCN20 are generally larger (longer and/or broader) than those previously reported (Van der Made et al. 1999; Fortelius et al. 2005; Pickford 2013a).

Parachleuastochoerus valentini The presence of a large-bodied tetraconodont of similar dental size to *P. palaeochoerus* at CCN20 is supported by the existence of two different morphotypes for multiple tooth loci. Thus, *Pa. valentini* is apparently characterized by a stouter and less curved root of the female C1 and c1; more trenchant P2 with a non-constricted buccal contour and a well-developed prestyle; more trenchant, taller, and relatively more elongate P3; the subtriangular (more lingually tapering) P4; the more constricted occlusal contour of the DP3; the less elongate DP4 and upper molars, which further display less corrugated enamel (better ascertainable in the M3); and particularly an M3 that does not markedly taper distally displays a lesser developed pentacone; and the more trenchant and relatively narrower dp2 and p1 (the latter further displaying a better developed prestylid).

Determining the taxonomic identity of the tetraconodont recorded at CCN20 is hindered by the different taxonomic opinions about Middle to Late Miocene tetraconodontines from Europe (compare Pickford 2016a with Van der Made 2020). For the reasons exposed in greater detail in the Discussion and Conclusions section, here we provisionally follow Pickford's (2016a) taxonomy (see also Pickford 2014; Pickford and Laurent 2014; McKenzie et al. 2022). This implies that, based on size, the large tetraconodont from CCN20 could be attributable to either *Pa. valentini* or *C. doati* (which are both considered junior subjective synonyms of *C. simorrensis* by Van der Made 2020), given that the two species of *Versoporcus—V. steinheimensis* and

Versoporcus grivensis (Gaillard, 1899), both synonymized with *Parachleuastochoerus steinheimensis* by Van der Made (2020)—are smaller than the CCN20 material (Pickford 2013a, 2014, 2016a; Van der Made et al. 2014; McKenzie et al. 2022). Other differences that rule out an attribution of the CCN20 tetraconodont material to *Versoporcus* spp. (Hünermann 1968: pl. I, fig. 46; Chen 1984: pls. I–II, IV; Van der Made et al. 2014: figs. 3–4, 8; Pickford 2014: figs. 19F, 30–33, 2016: figs. 6, 15, 18–20, 24)—see also the diagnosis of the genus in Pickford (2014: p. 203)—include: a distolingually expanded P2 without a mesial cingular swelling or a distinct distal cuspule; P3 with a greater buccal convexity and a more protruding distolingual shelf; a more lingually tapering P4 that displays a fainter buccal cingulum, a more developed protocone that is not transversely aligned with the paracone, and more distinct paracone and metacone apices (at least compared with *V. steinheimensis*); and a more buccolingually compressed and higher-crowned p1, with a more trenchant protoconid.

With regard to comparisons with *Pa. valentini* and *C. doati*, neither species is particularly well known, as multiple tooth loci have not been described yet, and the inclusion of the former species in *Parachleuastochoerus* instead of *Conohyus* would require, as remarked by McKenzie et al. (2022), to confirm that the former does not display the diagnostic c1m morphology of *Conohyus* (Pickford and Laurent 2014; Pickford 2016a; see Discussion and Conclusions for further details). Based on the CCN20 material, here we first report the morphology of several tooth positions for *Pa. valentini* (C1f, P2, c1f, di1, and dp2). No remains from these tooth positions are either known for *C. doati*, such that they are not useful to confirm or reject an attribution to *Pa. valentini* instead of *C. doati*. The morphology of the upper and lower female canines is consistent (displaying a straighter and stouter root than in *P. palaeochoerus*) and in our opinion they can be confidently assigned to the tetraconodont recorded at CCN20, whereas in contrast the attribution of two di1s from CCN20 to *Pa. valentini* (based on minor differences compared with those of *P. palaeochoerus*) must be deemed more tentative. The morphology of the *Pa. valentini* P2 is also first described here because only two distal P2 fragments had previously been reported from Sant Quirze (Pickford 2014). The CCN20 P2 fits well in morphology with the figured partial specimen from Sant Quirze (Pickford 2014: fig. 14B) except for a more marked distolingual crown extension, resulting in a somewhat greater BL measurement. No definitive conclusions can be drawn from this tooth because the morphology of the CCN20 specimen fits with the diagnoses of both *Parachleuastochoerus* (P2 “elongated with slightly swollen distal end”; Pickford 2014: p. 171) and *Conohyus* (“crowns of anterior premolars slightly sectorial without marked mesial and distal buccal expansion and with quite tall, pointed main cusp”; Pickford and Laurent 2014: p. 5). However, the P2 from CCN20 (BLI = 53%) is relatively broader than those of *C. simorrensis* (the type species of *Conohyus*; BLI = 35–41%, N = 3; Pickford 2016a; Van der Made 2020), thus rather supporting an assignment to *Parachleuastochoerus*. The greater distolingual expansion of the CCN20 P2 as compared with the partial specimens from Sant Quirze might simply represent intraspecific variation (as documented for the P3), although it should be taken into account that, in terms of preserved crown size and shape, the Sant Quirze specimen figured by Pickford (2014) might alternatively be interpreted as a P1 (see Pickford 2014: fig. 14A, G–I). In turn, the dp2 from CCN20 assigned to *Pa. valentini* clearly differs in shape and proportions from those assigned to *P. palaeochoerus*, and is smaller and relatively narrower than the single dp3 previously reported for *Pa. valentini* by Pickford (2016a), being thus confidently attributable to the large tetraconodont recorded at CCN20.

Several other tooth loci available for *Pa. valentini* from CCN20 were previously known for the species but not for *C. doati*. These include the i2 (purportedly, see below), the p1, the DP3, and the DP4, the two latter tooth

positions probably being the least informative. However, it is noteworthy that, despite the somewhat larger size, the more complete DP3 from CCN20 (BLI = 74%) shows similar proportions to the single previously reported specimen of *Pa. valentini* from Sant Quirze (BLI = 72%; Pickford 2014). The same applies to the three more complete DP4s from CCN20 (BLI = 89–98%) as compared with those from Sant Quirze (BLI = 81–94%; Pickford 2014: fig. 16A). Therefore, both the DP3 and DP4 tetraconodont specimens from CCN20 are consistent with an attribution to *Pa. valentini*.

In turn, the single i2 from CCN20 assigned to *Pa. valentini* is unfortunately very worn, which precludes assessing the lingual morphology details, although it clearly differs from those of *P. palaeochoerus* by displaying a uniform curvature throughout the crown and root across the cervix (instead of showing a vertically oriented crown with a marked angulation at about one-third of the distal marginal ridge height, as in *P. palaeochoerus*). This specimen can be compared with the i1 and i2 from Mira (attributed by Pickford 2014: fig. 16A–B to *Pa. valentini*, but see below), although they only preserve the basal portion of the root and do not allow us to conclusively ascertain the above-mentioned feature. The same applies to the i2 of *Pa. valentini* from Wartenberg bei Erding (Pickford 2016a: fig. 21A), which only preserves the crown. As such, the only reliable comparison is restricted to a lower incisor of *Pa. valentini* from Sant Quirze (Pickford 2014: fig. 13B) that the latter author identified as an i2, probably because the distal margin is very inclined (so that the crown tapers apically from the cervix to the incisal edge). However, in our opinion, the Sant Quirze lower incisor could alternatively be interpreted as an i1, given that the crown is vertically aligned with the root and that the endocristid is also very verticalized. If our interpretation is correct, the i2 of *Pa. valentini* would be expected to display a more obliquely oriented crown, both mesially and distally, than in other tetraconodonts such as *V. grivensis* (Pickford 2014: fig. 32; Van der Made et al. 2014: fig. 4b). This interpretation fits well with the morphology of the lower incisor from CCN20, which is thus interpreted as an i2. That said, more complete material would be required to confirm our tooth loci identifications for this incisor and that from Sant Quirze.

With regard to the p1 assigned to *Pa. valentini*, unfortunately it corresponds to a partial (unfinished) germ, which hinders the comparisons to some extent. However, the specimen clearly differs from p1s assigned to *P. palaeochoerus* (see above) in the following features: the more buccolingually compressed crown with a more trenchant morphology; a less mesially positioned protoconid; a curved protoprecristid that ends in a better developed prestylid; a longer protopostcristid with no secondary cuspulid; and a marked indentation of the cervix midway along the lingual side. In these features, the CCN20 specimen is consistent in size and shape with the single p1 of *Pa. valentini* reported so far from Sant Quirze (Pickford 2014: fig. 14D), which is very buccolingually compressed (BLI = 31%), at least if it is assumed that the distal fourth of the crown was still pending to be formed (i.e., including the distal cuspulid as well as the more marked extension of the cervix onto the root). Although comparisons with *C. doati* are not possible because this tooth locus is unknown for the species, the p1 of *C. simorrensis* (see Pickford 2013b: fig. 2) is indeed larger and distally broader than the CCN20 specimen, which displays a much better developed prestylid as well as steeper protoprecristid and protopostcristid. All the remaining permanent lower premolars from CCN20 are assigned to *P. palaeochoerus* because they show a typically dicoryphocoerin morphology (Van der Made and Moyà-Solà 1989; Van der Made et al. 1999). This is most clear-cut in the case of the p4s, which display a well-developed metaconid distolingually from the protoconid, as it is typical of *P. palaeochoerus* (see above). However, none of the p2 and p3 from CCN20 displays the trenchant morphology that would be expected for a tetraconodont, and while the p2

of *Pa. valentini* thus far remains unknown, the p3s reported from various sites by Pickford (2014: fig. 17C, 2016a: fig. 9A–B, fig. 13A) differ from the CCN20 ones in displaying larger and more inflated crowns, with a less distinct prestylid but a more trenchant, centrally located, and distally tilted protoconid.

Given all of the above, a conclusive attribution of the CCN20 tetraconodont to *Pa. valentini* instead of *C. doati* can only be conclusively substantiated based on the posterior upper premolars (P3 and P4) and molars (M2 and M3), which have previously been reported for both species, even though the sample available for *C. doati* is very limited. The morphology of the P3 from CCN20 fits with the diagnosis of the genus *Parachleuastochoerus* (Pickford 2014: p. 171) in the possession of a weak lingual cingulum and a small and low distolingual cuspule (corresponding to the protocone). The available sample of *Pa. valentini* P3s displays some variation in occlusal contour, with the CCN20 specimen closely matching the specimen from Kleineisenbach (Pickford 2016a: fig. 13B) and especially one of the P3 from Saint-Gaudens (Pickford 2014: fig. 11A) in the marked distolingual protrusion of the crown, which is less accentuated in the Saint-Gaudens holotype (Pickford 2014: fig. 9A) and in the P3s from Hollabrunn (Pickford 2016a: fig. 7A–B). Nevertheless, all these specimens resemble that from CCN20 in the possession of a marked distolingual cingulum with a low protocone, contrasting with the P3 from Mira (Pickford 2014: fig. 18C). Although the latter specimen was assigned to *Pa. valentini* by Pickford (2014), it displays a morphology more similar to that of *C. simorrensis*, which is characterized by a poorly-developed distolingual cingulum and a buccally (rather than distolingually) protruding occlusal contour. It is thus possible that the Mira sample belongs to *Conohyus*, as argued by Van der Made (2020), instead of *Pa. valentini*. Unfortunately, comparisons of the CCN20 P3 with that attributed to *C. doati* (from Hammerschmiede) are hindered by the fact that Pickford (2016a) did not figure it and merely described it as “inflated”. Indeed, this specimen displays similar size and proportions (BLI = 76%) to the specimens of *Pa. valentini* (BLI = 66–81%, N = 6, or 66–78% if the Mira specimen is excluded; Pickford 2014, 2016a), which are slightly less inflated than the CCN20 P3 (BLI = 85%). Occlusal proportions thus do not justify discounting an assignment of the CCN20 P3 to *C. doati*, particularly given that the P3s of *C. simorrensis* seem to be more inflated (BLI = 78–93%, N = 4; Ginsburg 1977; Pickford 2016a) than those of *Pa. valentini*, in further agreement with the CCN20 specimen. Nevertheless, it should be taken into account that the sample reported from Hammerschmiede is very restricted (a P3 and an M3; Pickford 2016), such that its assignment to *C. doati* instead of *Pa. valentini* would need to be substantiated further. Moreover, the CCN20 P3 differs from the P3 of *C. simorrensis* (Ginsburg 1977: fig. 1.3; Pickford 2016a: fig. 31) and Mira (see above) by displaying a much more developed distolingual expansion with a more distinct, even if low, cuspule (protocone), thereby supporting an assignment to *Parachleuastochoerus* instead of *Conohyus*.

In terms of P4 morphology, this tooth locus is also somewhat variable among the available sample of *Pa. valentini* (Pickford 2014: figs. 9A, 14C, 2016a: fig. 7A–B), with the CCN20 specimen (BLI = 123%) overlapping with the lower range of BLI of previously known specimens of *Pa. valentini* (BLI = 123–140, N = 8; Pickford 2014, 2016a). Nevertheless, the CCN20 P4 fits well with this sample in terms of occlusal shape, including the subtriangular contour that markedly tapers lingually, the distinct apices of the similarly developed paracone and metacone, the non-peripheral and more extensive protocone (somewhat intermediate in position between the paracone and metacone), and the faintly developed buccal cingulum. In contrast, the P4 from CCN20 displays some differences relative to the homologous tooth from Nuri Yamut (Van der Made and Tuna 1999: fig. 3), assigned to *C. doati* by Pickford (2016a). The two specimens display a similar occlusal contour and

relative position between the protocone and the buccal cusps, but the Nuri Yamut specimen differs from the CCN20 one (and the remaining P4s assigned to *Pa. valentini*) by displaying a paracone larger than both the protocone and metacone, and less distinct buccal cusps (with the paracone and protocone being merely separated by a short and shallow groove toward their apices). Therefore, if this material actually belongs to *C. doati* (as argued by Pickford 2016a), it would support the distinction of this species from *Pa. valentini* and exclude an attribution of the CCN20 material to the former. Unfortunately, the lack of further material from Nuri Yamut as well as additional P4s of *C. doati* from elsewhere makes the taxonomic attribution of this material somewhat uncertain.

As compared to molars, it is noteworthy that, while the P3 from CCN20 is narrower than the available upper molars from the same site, the P4 is only somewhat broader than the M1 (but not the M2 or the M3). Assuming that the two maxillary fragments (with P3–P4 and M1–M3) belong to the same individual, this agrees relatively well with the diagnosis of *Parachleuastochoerus* by Pickford (2014: p. 171), according to which the posterior upper premolars of this genus are larger than the anterior ones but not broader than the molars. Indeed, having a P4 broader than the M1 is characteristic of many tetraconodonts (Pickford 2016a), and while not all individuals of *Pa. valentini* display such proportions, it is noteworthy that both in the holotype of *Pa. valentini* and the L maxillary fragments from Sant Quirze the P4s are also broader than the M1s but not the remaining molars (Pickford 2014). The proportions of the M1 from CCN20 (BLI = 91%) are similar to the M1 proportions of *Pa. valentini* from elsewhere (BLI = 89–106, N = 9; Pickford 2014, 2016a), but the lack of M1 assigned to *C. doati* renders this comparison of little utility. In contrast, the proportions of the M2 and M3 from CCN20 can be compared with both *Pa. valentini* and *C. doati*. The M2 from CCN20 (BLI = 94%) overlaps with the variability range of *Pa. valentini* from elsewhere (BLI = 88–105%, N = 11; Pickford 2014, 2016a), whereas the single M2 assigned to *C. doati*—a specimen from Geiselberg (Pickford 2016a: fig. 4E) formerly assigned to *P. palaeochoerus* by Zapfe (1949)—appears somewhat narrower. This tends to support an attribution of the CCN20 tetraconodont to *Pa. valentini* instead of *C. doati*, although it should be taken into account that differences are not very pronounced and that the variability range of the latter species is unknown.

Regarding the M3, the sample available for *C. doati* is larger than for other upper cheek teeth but comparisons are hampered by the greater intraspecific variability typically displayed by this tooth position. In terms of size and proportions, the CCN20 M3 (MD = 32.3 mm, BL = 24.1 mm, BLI = 75%) is somewhat larger than, but fits well in proportions with, the M3s assigned to both *C. doati* (MD = 25.2–28.5 mm, BL = 20.0–22.4 mm, BLI = 74–86%, N = 5; Pickford 2013a, 2016a; Van der Made 2020) and *Pa. valentini* (MD = 22.8–31.7 mm, BL = 16.8–21.6 mm, BLI = 62–81%, N = 12; Pickford 2014, 2016a). In terms of occlusal shape, the CCN20 specimen differs in several regards from both the lectotype of *C. doati* from Bonnefond (Stehlin 1900: pl. I, fig. 7; Pickford 2014: fig. 19A; Pickford and Laurent 2014: fig. 6) and the holotype of *Pa. valentini* from Valentine in Saint-Gaudens (Pickford 2013: fig. 6A, 2014: figs. 9, 19D). In particular, the CCN20 M3 differs from the *C. doati* lectotype (MD = 25.2 mm, BL = 21.6 mm, BLI = 86%; Van der Made 2020) in the larger size but relatively narrower proportions, the lesser development of Fürchen and secondary cuspules (including a much less developed ectoconule), the more distinct and larger pentacone (which is more distolingually protruding and mesiodistally aligned with the remaining lingual cusps), and the lack of distal cingulum. Other M3s assigned to *C. doati* include a specimen from Hammerschmiede (BLI = 83%; Pickford 2016a, not figured) and three specimens from Gau-Weinheim (BLI = 74–77%; Pickford 2013a: figs. 6D, 7A–B, D), which had

previously been assigned to *P. palaeochoerus* by Hünermann (1968). These specimens are somewhat smaller than the CCN20 M3 but larger than the lectotype of *C. doati*, and display overall proportions (BLI = 74–77%, N = 3; Pickford 2013a) much closer to the former, further falling within the BLI range of *Pa. valentini* (see above). The CCN20 M3 also closely resembles the Gau-Weinheim specimens in the general arrangement and development of the main cusps and other cuspules, although the orientation of the pentacone is variable (from mesiodistally aligned with the lingual cusps to more centrally located or even tilted buccally). In turn, the CCN20 M3 differs from those of the holotype of *Pa. valentini* (MD = 26.2–26.5 mm, BL = 20.0–21.2 mm, BLI = 76–81%; Pickford 2014) in the larger size and less distally tapering occlusal contour (despite displaying overall proportions only minimally broader in relative terms), with a less distally protruding pentacone that is not tilted toward buccal. Other M3s assigned to *Pa. valentini* include another one from Saint-Gaudens (Pickford 2014, not figured), two from Sant Quirze (Pickford 2014: figs. 14H, 15C), one from Mira (Pickford 2014: figs. 18E), three from Hollabrunn (Pickford 2016a: fig. 7A–C), two from Wartenberg bei Erding (Pickford 2016a: fig. 22F), and one from Kleineisenbach (Pickford 2016a: fig. 13C). Overall, these specimens denote considerable variation in size and shape, particularly regarding the development and degree of individualization of the pentacone, which is not surprising for this tooth locus. When this variation is taken into account, the CCN20 M3 and those from Gau-Weinheim assigned to *C. doati* more closely resemble the M3 sample of *Pa. valentini* than the lectotype of *C. doati*, except for the somewhat broader proportions of the former. Therefore, the question arises as to why the Gau-Weinheim specimens were assigned to *C. doati* instead of *Pa. valentini*, as this was not explicitly discussed by Pickford (2013a, 2016a). When discussing the attribution of the Wartenberg bei Erding M3s, Pickford (2016a) justified the attribution to *Pa. valentini* based on the relatively elongated talon. However, it is noteworthy that the unfigured specimen from this site had previously been assigned by Pickford and Laurent (2014) to *C. doati*, and that the figured specimen, unlike most (but not all) of the M3s assigned to *Pa. valentini* (except those from Kleineisenbach an Mira), does not display a particularly elongated talon or a well individualized pentacone. The Mira M3 differs from the lectotype of *C. doati* in the possession of a distolingually protruding pentacone, but otherwise it does not markedly differ in occlusal morphology from it, which is relevant given the more *Conohyus*-like morphology of the P3 in the Mira sample (see above). Given the extensive degree of variation of the M3s assigned to *Pa. valentini* and *C. doati*, and the possibility of misclassification based on this tooth position alone, we consider that the relatively broader proportions of the M3s from both CCN20 and Gau-Weinheim can be accommodated within the variability range of *Pa. valentini*.

cf. *Albanohyus* The curvature of the crown and root of two lower incisors from CCN20 (Fig. 7n–o) indicate that they are not central incisors, while their size is too small to be di2 of the two other suids recorded at the site (Appendix Table 1). Instead, their size and shape fit well with the material of *Albanohyus castellensis* from Castell de Barberà (Golpe Posse 1977). Given the paucity of the material and doubts about the species distinction between *A. castellensis* (Golpe Posse 1977) and *Albanohyus pygmaeus* (Depéret, 1892), the type species of the genus (see Tomàs et al. 2011), we refrain from making a species attribution and assign the specimens only tentatively to *Albanohyus* sp. until more material becomes available.

Quantitative comparisons

Dental size and proportions Given that the dental size of the *Propotamochoerus* specimens from CCN20 exceeds that previously recorded elsewhere for *P. palaeochoerus* for most tooth positions, we decided to compare them with those of similarly sized species of the same genus (*P. aegaeus*, *P. hysudricus*, *P. hyotherioides*, and *P. provincialis*), as well as the larger *H. major*; *P. wui* was not considered because it is clearly smaller. Our comparisons (Figs. 12–15) indicate that *P. palaeochoerus* metrically differs from *P. hysudricus* in multiple tooth loci, with the former displaying on average longer P2 and dp4, as well as larger DP4, P3, P4, M1, p3, p4, and m1. *Propotamochoerus palaeochoerus* also differs by possessing smaller P2, M2, and M3 than the remaining species of the genus analyzed (albeit with a substantial overlap with *P. aegaeus*), P3 intermediate in size between those of *P. aegaeus/P. provincialis* and those of *P. hyotherioides*, smaller P4 on average (with substantial overlap) and narrower dp4 than *P. hyotherioides*, larger m1 than *P. aegaeus* and smaller m2 than *P. provincialis* on average (with some overlap), and smaller m3 than both *P. provincialis* and *P. hyotherioides*. Differences are more marked regarding *H. major*, which shows larger tooth dimensions than *Propotamochoerus* spp. for all the tooth positions investigated, with only moderate to minimal overlap for most tooth loci, and most clear-cut differences in M2, M3, and m3.

The deciduous premolars of *Propotamochoerus* from CCN20 are generally larger (longer and/or broader) than those of *P. palaeochoerus* from elsewhere, but fit even worse with the variability of *H. major*, with the DP3 and dp4 more closely resembling in size and proportions those of *P. hyotherioides*, and the DP4 fitting reasonably well with both *P. palaeochoerus* and *H. major*. The upper and lower permanent premolars from CCN20 fit better with the size variation of *H. major* (and, in the case of the P2, that of later *Propotamochoerus* species), even though the p2 and p4 (like the M1, m1, and m2) overlap with both species. However, the M2 and M3 from CCN20 are intermediate in size between those of *P. palaeochoerus* and *H. major* (which do not overlap for these tooth positions), more closely resembling those of *P. hyotherioides*, whereas the m3 fits much better with *P. palaeochoerus* (albeit overlapping with its uppermost size range and only approaching the condition of *P. hyotherioides*). Indeed, the upper and lower third molars from CCN20 are smaller than those of *P. provincialis*, which are somewhat intermediate between those of other *Propotamochoerus* species (except *P. hyotherioides*) and those of *H. major*. These comparisons show that the CCN20 sample lacks the elongation of third molars characteristic of *Hippopotamodon* (and, to a lesser extent, *P. provincialis* and *P. hyotherioides*), whereas in terms of premolar and, especially, first molar size and proportions, the CCN20 sample most closely resembles *P. palaeochoerus* despite displaying on average larger dimensions.

With regard to *Pa. valentini*, the specimens from the comparative sample differ in several regards from those of *P. palaeochoerus*, including a longer DP3, P1, and P3, a broader P4 and dp4, a larger p3, and somewhat smaller m2 and m3. These differences are not surprising given that, as a tetraconodont, *Pa. valentini* must be characterized by comparatively larger premolars than a suine like *Propotamochoerus*. The remains from CCN20 attributed to *Pa. valentini* are also generally larger than those previously reported for the species, including the DP3, DP4, P4, M2, and M3, whereas only the P3 and M1 of *Pa. valentini* from CCN20 falls reasonably close the variability of previously known specimens (comparisons are not possible for the P2, as that from CCN20 is the first complete specimen reported for the species). These differences must not necessarily be taxonomically relevant, as sample sizes available for *Pa. valentini* are quite small and all the permanent upper premolars and molars from CCN20 might belong to a single specimen. As such, the CCN20 tetraconodont specimens might simply expand the known range of variability of *Pa. valentini*. Although the dental remains of this species from

CCN20 generally resemble in size and proportions those of *P. palaeochoerus* from the same site, it is noteworthy that the DP4 and M2 of the former are somewhat shorter, while the P3 and P4 are somewhat longer, than those of *P. palaeochoerus* from CCN20, thereby paralleling the differences evinced by the previously known samples of these species from elsewhere.

Principal Components Analysis The two PCAs based on upper and lower cheek teeth yielded three and two PCs explaining more than 5% variance, respectively (Online Resource 2), with PC1 explaining more than two-thirds of the variance in both cases. The scores for each individual and the loadings for each Mosimann shape variable regarding these PCs are reported in Online Resources 2 and 3, respectively. In the PCA based on upper cheek teeth (Fig. 16a–b), the PC1 (66% of variance) discriminates well between *Hippopotamodon* (positive scores) from *Propotamochoerus* spp. (mildly positive to negative scores). This axis is mostly driven by M3 MD (and, to a lesser extent, M3 BL and M2 MD) toward positive scores, as well as, to a lesser extent, by premolar size toward negative scores. This accords well with the relative larger M3s of *Hippopotamodon* and the relatively larger premolars of tetraconodonts. The CCN20 *Propotamochoerus* individual falls between the two *P. palaeochoerus* specimens and those of *P. aegaeus* along this axis, supporting its attribution to the genus but not necessarily *P. palaeochoerus*. *Parachleuastochoerus valentini* from CCN20 shows more negative values along PC1 than the *P. palaeochoerus* specimen from the same locality but overlaps with other individuals from this species and shows less extremely negative values than the other tetraconodonts included in the analysis (*V. steinheimensis* and *C. simorrense*). However, the results for *Pa. valentini* from CCN20 should be taken with cautious because they are based on three specimens that must not necessarily belong to a single individual and no other specimen from this species is included in the analysis. In turn, PC2 (11% of variance), which is mostly driven by posterior premolar and, especially, molar breadth toward positive scores, and tooth length (especially M2 MD) and P2 BL toward negative scores, shows substantial overlap among the included genera and is not useful to discriminate any of the analyzed taxa. In contrast, along PC3 (7% of variance), which is mostly driven by P2 BL toward negative scores, *Pa. valentini* from CCN20 shows more extremely negative scores than the rest of the sample, thereby supporting its attribution to a different taxon.

The PCA based on lower cheek teeth (Fig. 16c) yields very similar results to that based on the upper cheek teeth, with PC1 explaining a large amount of variance (74%) and separating *Hippopotamodon* (with positive scores) from *Propotamochoerus* (mildly positive to moderately negative scores) and the tetraconodontines *Versoporcus* and *Parachleuastochoerus* (extremely negative scores). This axis is mostly driven by m2 and m3 size (especially m3 MD) toward positive scores (in agreement with the enlarged third molars of *Hippopotamodon*), as well as and by p2 and p3 MD and p3 BL toward negative scores (in agreement with the larger premolars of tetraconodonts). In turn, PC2 (13% of variance) is mostly driven by p4, m1 and m2 MD toward positive scores and p2 MD toward negative scores. Although different taxa substantially overlap along this axis, *P. aegaeus* from the Turolian of eastern Europe differs from the rest of the sample by displaying more strongly negative scores (in agreement with its comparatively larger p2). In turn, the *Propotamochoerus* individual from CCN20 is clearly closer to the three specimens of *P. palaeochoerus* when PC1 and PC2 are considered together (even displaying higher PC2 scores than the rest of the analyzed sample except for one of the *P. palaeochoerus* individuals), thereby supporting an attribution to the latter species.

Discussion and conclusions

Taxonomic attribution

Propotamochoerus More than three-quarters of the suid remains from CCN20 belong to a dicoryphochoerin suine that we attribute to *Propotamochoerus* on the basis of occlusal shape and size. Dicoryphochoerins are characterized by the morphology of the p4 (which, among other features, displays a buccally located protoconid and a well-developed but more distolingually located metaconid) and the incisors (including an elongated I2 with a distolingual cingulum), as well as by elongate molars (Van der Made and Moyà-Solà 1989). Two genera are known from the Late Miocene of Europe, the smaller and more conservative *Propotamochoerus* and the larger and more derived *Hippopotamodon*, the latter formerly often included in *Microstonyx* (see review in Pickford 2015). *Propotamochoerus* and *Hippopotamodon* apparently evolved from a *Hyotherium* ancestor in southern Asia during the late Middle Miocene, and subsequently dispersed into Europe during the Late Miocene (Pickford 2015). They appear to be closely related to one another, given the possession of several synapomorphies, such as enlarged canine flanges, sagittal cuspules in the P4, and the p4 metaconid morphology, among other features (Pickford 2015). The two genera basically differ in size, cranial morphology, and some details of the dentition—with *Hippopotamodon* being characterized by larger tooth size, longer I3, and more hypsodont i3, among other features (Van der Made et al. 1992). The type species of genus *Propotamochoerus* is *P. hysudricus* (see discussion in Pickford 1988; de Bonis and Bouvrain 1996). For many years, *P. palaeochoerus* was included in *Hyotherium* (e.g., Golpe-Posse 1972b) until Schmidt-Kittler (1971) erected the genus *Korynochoerus* to accommodate it. This proposal was initially accepted by most subsequent authors (e.g., Ginsburg 1980; Pickford 1988; Van der Made and Moyà-Solà 1989), although Pickford (1988, 1993) already noted the similarities between the type species of *Korynochoerus* with *P. hysudricus*, justifying their congeneric status. The former species was thus formally transferred to *Propotamochoerus* by Fortelius et al. (1996) and most subsequent authors (e.g., Van der Made et al. 1999; Fortelius et al. 2005). Both species overlap in chronostratigraphic range (Pickford 1988) and in overall dimensions, unlike the later Miocene species from China and Myanmar, *P. wui*, which is clearly distinct by its much smaller dental size as compared with both *P. hysudricus* and *P. palaeochoerus* (Van der Made and Han 1994; Sein et al. 2009). Nevertheless, Van der Made et al. (1999) noted that *P. hysudricus* differs from *P. palaeochoerus* in the generally simpler (even if large) third lobe of the m3 and the size of particular tooth loci. Other species of *Propotamochoerus* recognized in Europe are *P. provincialis* and *P. aegaeus* from eastern Europe and Turkey (Geraads et al. 2008; Pickford 2013; Lazaridis 2015; Iannucci et al. 2021; Kostopoulos and Sylvestrou 2022; Lazaridis et al. 2022), both recorded during the Turolian and whose distinction has been disputed (Iannucci et al. 2021), whereas *P. hyotherioides* is recorded in the latest Miocene of China (Van der Made and Han 1994; Hou et al. 2019).

Our bivariate plots indicate that the material of *Propotamochoerus* from CCN20 is generally larger than previously reported for *P. palaeochoerus*, sometimes even overlapping with the lower size range of *H. major*. However, the CCN20 material lacks the characteristic enlargement of third molars of *Hippopotamodon*, and in this regard more closely resembles the material of *P. palaeochoerus* than that of both *P. provincialis* and *P. hyotherioides*, which is somewhat intermediate in this regard. Our bivariate plots further confirm that *P. palaeochoerus* and *P. hysudricus* differ in dental proportions, with the former displaying on average larger

premolars and first molars but similarly sized second and third molars. In this regard, the CCN20 material most closely resembles *P. palaeochoerus* despite the somewhat larger dental size. This is confirmed by the results of our multivariate analyses of cheek tooth proportions, which show closer morphometric affinities with European *Propotamochoerus* species rather than *Hippopotamodon*, and in the case of the lower dentition very close affinities with *P. palaeochoerus*. Therefore, we conclude that CCN20 records a paleodeme (sensu Howell 1999; see also Antón et al. 2016) of *P. palaeochoerus* that was characterized by somewhat larger dental size that the populations recorded in central and eastern Europe. It is not entirely unconceivable that a different species of *Propotamochoerus* is recorded in the MN9 of the Vallès-Penedès Basin, as other Vallesian immigrants that dispersed from the east show some degree of endemism related to vicariance (e.g., *Hippotherium*, with different species being recorded in the early Vallesian of the Iberian Peninsula as compared to Central Europe; Bernor 2021). However, except for the somewhat larger dental size, the occlusal morphology of the *Propotamochoerus* sample from CCN20 fits well with that previously described for this species based on remains from multiple localities throughout Europe, from Spain to Ukraine (Mottl 1966; Hünermann 1968; Schmidt-Kittler 1971; Golpe-Posse 1972b; Van der Made et al. 1999; Fortelius et al. 2005; Iannucci and Begun 2022). We therefore conclude that not even open nomenclature (i.e., either 'cf.' or 'aff.') is required and that an attribution of the CCN20 sample to *P. palaeochoerus* is warranted. It remains to be seen if the larger average size of the CCN20 individuals is characteristic of the species in westernmost Europe (as other remains from the Vallès-Penedès Basin, currently under study, were not included in the comparative sample) or of the earliest Vallesian representatives of the species (as most of the comparative sample comes from central European sites, such as Rudabánya, which are much younger than CCN20). If the size differences displayed by the CCN20 material were found to be consistent in chronologic and/or geographic terms by means of the study of samples from other sites, a subspecies distinction might be warranted. The morphological and morphometric study of additional material of *Propotamochoerus* from other sites of the Vallès-Penedès Basin, including the roughly coeval site of Castell de Barberà as well as younger MN9 sites such as Can Poncic and Can Llobateres, will hopefully clarify this question. Incidentally, although our bivariate comparisons and PCA substantitate the differences in cheek tooth size and proportions between *P. aegaeus* and *P. provincialis* (see Lazaridis et al. 2022), they further stress that their joint variability could be accommodated within a single species—at least, when the size variation of *P. palaeochoerus* is considered.

Parachleuastochoerus Besides *Propotamochoerus*, another large-bodied suid that corresponds to a tetraconodontine is recorded at CCN20. The recent revision of European Tetraconodontinae performed by Pickford (2014, 2016a; see also Pickford and Laurent 2014) has led to a substantial systematic rearrangement of several taxa, but is not exempt of criticism (Van der Made et al. 2020; Iannucci and Begun 2022). For the purposes of this paper, the following changes in the systematics of this subfamily must be highlighted: (1) the erection of a distinct genus (*Versoporcus*) for *V. steinheimensis* (previously included in *Parachleuastochoerus*) and the resurrection of another species included in this genus (*Versoporcus grivensis*), formerly considered a subjective junior synonym of the former; and (2) the resurrection and inclusion in *Parachleuastochoerus* of another large species of tetraconodont (*Parachleuastochoerus valentini*). Such taxonomic decisions stem in part from the rediscovery of long forgotten material and their respective designation as lectotypes of *C. simorrensis* by Pickford and Laurent (2014) and of *Pa. valentini* by Pickford (2014). These nomenclatural decisions and their

taxonomic implications have been questioned by Van der Made (2020), according to whom *Pa. valentini* and *C. doati* would be subjective junior synonyms of *C. simorrensis*, *Versoporcus* would be a junior subjective synonym of *Parachleuastochoerus*, and *Pa. steinheimensis* would include the two species included by Pickford (2016a) in *Versoporcus*. Resolving these taxonomic disagreements is outside the scope of this paper, but they are discussed below in some detail and some conclusions are drawn regarding *Pa. valentini* and *C. doati*. With regard to *Versoporcus*, we follow McKenzie et al. (2022) in tentatively distinguishing *V. steinheimensis* and *V. grivensis*, although we acknowledge that the distinction between the two species of this genus, and even the distinctiveness of the genus *Versoporcus*, should be subject to further scrutiny. It is however noteworthy that the inclusion of *V. steinheimensis* in *Parachleuastochoerus* has also been subject to considerable debate. Decades ago, this species was considered either a subspecies (e.g., Thenius 1956) or a junior subjective synonym (e.g., Hünnerman 1968) of *C. simorrensis*, until Chen (1984) convincingly argued it was a distinct species (i.e., *C. steinheimensis*). This view was followed by Van der Made (1990a) and Pickford (1993), but the former already remarked similarities with *Parachleuastochoerus*, and Fortelius et al. (1996) formally transferred *C. steinheimensis* to *Parachleuastochoerus*. Such a proposal was followed by several authors (Van der Made 1997a, 1999, 2020; Pickford 2012, 2013a; Van der Made et al. 2014) but not by others, who kept the species in *Conohyus* (Bernor et al. 2004; Fortelius et al. 2005; Harris and Liu 2007; Pickford 2013b). In our opinion, including this species in *Conohyus* is no longer warranted, at least after the emended diagnosis and lectotype designation by Pickford and Laurent (2014), as the c1m morphology of *Versoporcus* differs from that of *C. simorrensis*. In turn, deciding whether a distinct genus *Versoporcus* is warranted largely depends on whether *Pa. valentini* is included in *Parachleuastochoerus* or in *Conohyus*.

We concur with Pickford (2014, 2016a, 2016b) that the presence, in multiple MN7+8 and MN9 sites from Europe, of a large tetraconodontine other than *V. steinheimensis* had previously remained unnoticed, owing to confusion with both *Versoporcus* and *P. palaeochoerus*. We further agree that this large tetratocondontine must be included in a different genus than *V. steinheimensis*. However, without cranial material of *Parachleuastochoerus crusafonti* Golpe-Posse, 1972 (the type species of the genus *Parachleuastochoerus*), it seems difficult to conclusively ascertain whether the previously overlooked large tetraconodont must be included in *Parachleuastochoerus* (as advocated by Pickford 2014, 2016a) or *Conohyus* (as contended by Van der Made 2020). This issue is further complicated by the distinction, advocated by Pickford (2013, 2014, 2016a) and Pickford and Laurent (2014), of a roughly coeval second large tetraconodontine, *C. doati*. We concur with Pickford (2014, 2016a) that *Pa. valentini* is different from *C. simorrensis* (at least at the species rank), as remarked in the comparisons provided about, but we consider that the distinction of *C. doati* from both *Pa. valentini* and *C. simorrensis* is much more questionable. Van der Made (2020) formally synonymized both *C. doati* and *Pa. valentini* with *C. simorrensis* s.l., while noting that the c1m and the lectotype M3 from the type locality of the former were compatible with a large form of either *Conohyus* or *Parachleuastochoerus.* Indeed, the c1m of *C. doati* displays a band of cementum on the distal enamel-free surface of the crown that has been considered diagnostic of the genus *Conohyus* based on its type species (Pickford 2013b, 2016a; Pickford and Laurent 2014). However, the size of the M3 lectotype does not justify a distinct species status for *C. doati* relative to *C. simorrensis*, thereby supporting Van der Made's (2020) contention that the former might be a junior subjective synonym of the type species of *Conohyus*. We concur with Pickford (2014, 2016a) that *Pa. valentini* shows a priori greater similarities to the much smaller *Pa. crusafonti* (the type species of the genus)

than *Versoporcus* spp. do, but such similarities could also be consistent with the inclusion of *Pa. valentini* in *Conohyus*. Furthermore, as discussed in the Comparisons section above, there is the possibility that some remains (particularly M3s) assigned to *C. doati* by Pickford (2013a, 2016a) do belong innstead to *Pa. valentini*. For example, Pickford and Laurent (2014) attributed to *C. doati* an M3 from Wartenberg bei Erding that was subsequently assigned by Pickford (2016a) to *Pa. valentini*, illustrating that confusion between the two species is not unlikely, especially regarding the upper molars. Unfortunately, the c1m of *Pa. valentini* is currently unknown because the only specimen attributed to it so far (measured but not figured by Pickford 2014 as IPS31067 [VP1113] from Sant Quirze) in all probability corresponds to the specimen listed as IPS1113 in Golpe Posse (1971) as coming from the MN5 site of Puente Vallecas, Spain, which must thus belong to a different taxon. As such, the purported synonymy between *Pa. valentini* and *C. simorrensis*, or at least their potential congeneric status, cannot be currently discounted on the basis of this tooth locus. All these taxonomic uncertainties illustrate that the systematics of European tetraconodontines is far from being settled and suggest that the definition of the genera *Conohyus* and *Parachleuastochoerus* should be clarified further based on cladistic analyses—although the study of additional remains of *Pa. valentini* (e.g., from Abocador de Can Mata and Castell de Barberà) would be of much help to thrown light on the genus ascription of this species.

The tetracondont material from CCN20 is scarce and the most informative specimens are the two maxillary fragments with upper cheek teeth that might belong to a single individual. The morphology of the P3 and P4 from CCN20 fits better with *Pa. valentini* than with species of the genus *Conohyus*, with the exception of the P3 from Mira, which was attributed to *Pa. valentini* by Pickford (2014) but might belong to *Conohyus* instead (Van der Made 2020; see below for further discussion). In turn, the M3 from CCN20 differs from that of the lectotype of *C. doati* but more closely resembles the M3s from Gau-Weinheim, assigned to *C. doati* by Pickford (2016a), apparently given their less distally tapering occlusal contour as compared with specimens assigned to *Pa. valentini*. However, in other regards the Gau-Weinheim specimens more closely resemble those of *Pa. valentini* than the lectotype of *C. doati*, leading to the conclusion that they might have been misattributed. Similarly, given the differences relative to the lectotype of *C. doati*, we consider that an attribution of the CCN20 specimen to *Pa. valentini* is also warranted. The taxonomic validity of *C. doati* is indeed questionable because, as noted by Van der Made (2020), its M3 lectotype is only slightly larger than the lectotype of *C. simorrensis* designated by Pickford and Laurent (2014). Therefore, we concur with Van der Made (2020) that *C. doati* is likely a junior subjective synonym of *C. simorrensis*, with the *C. doati* hypodigm as conceived by Pickford (2016a) apparently mixing remains attributable to both *C. simorrensis* and *Pa. valentini*. This would also apply to the hypodigm of *Pa. valentini* as conceived by Pickford (2014, 2016a), particularly regarding the material from Mira: besides the *Conohyus*-like morphology of the P3 mentioned above, the Mira M3 is also reminiscent of the lectotype of *C. doati*, and the buccally protruding contour of the p4 from Mira also more closely resembles the morphology of *C. simorrensis* than that of other specimens attributed to *Pa. valentini*. In this regard, it is noteworthy that Pickford (2016a) correlated the type locality of *C. doati* (Bonnefond) to MN8–MN9 and Mira to MN9. However, we have been unable to find a justification for the age determination of Bonnefond, whereas an MN9 age for Mira is not supported by the accompanying fauna. Mira was indeed tentatively considered Vallesian by Golpe-Posse (1972b, 1974), but Van der Made (1990a, 1990b) correlated it with MN6, and the micromammal assemblage (in particular, the presence of *Megacricetodon collongensis*) supports a correlation to MN5 (local zone Dd; Agustí et al. 1988; Oliver Pérez 2015). Such an ancient chronology is completely at odds with an

assignment to *Pa. valentini* but is perfectly compatible with the range of *C. simorrensis* (e.g., Pickford 2016a). The material from Mira was originally used to describe the species *Conohyus melendezi* Golpe-Posse, 1972b, which was considered a junior synonym of *Pa. valentini* by Pickford (2014) and Pickford and Laurent (2014). Nevertheless, based on its premolar morphology (and in further agreement with its early Middle Miocene age), we concur with Van der Made (1990a, 1990b, 2020) that *C. melendezi* is best interpreted as a synonym of *C. simorrensis*. The remaining material assigned by Pickford (2013a, 2016a) to *C. doati* might belong to either *C. simorrensis* or *Pa. valentini*. The mandible from Fonte de Pinheiro, Portugal (Roman 1907: pl. V, fig. 1), attributed by Van der Made (1989) to *Conohyus ebroensis* Azanza, 1986, resembles in premolar morphology the material from Mira and can be attributed to *C. simorrensis*, as argued by Van der Made (2020), whereas this is less clear in the case of the type material of *C. ebroensis* from El Buste and La Ciesma, Spain (Azanza 1986, pl. I; Van der Made 1989). This species was also synonymized with *C. simorrensis* by Van der Made (2020), but we prefer to leave the material unassigned because the morphology of the p4 cannot be adequately ascertained and *C. ebroensis* could alternatively be a junior synonym of *Pa. valentini*. Except for the material from Gau-Weinheim (which we reassign to *Pa. valentini*), the same applies to the remaining material assigned by Pickford (2013a, 2016a) to *C. doati*, including that from Gaiselberg and Bayraktepe (which does not preserve the premolars), Hammerschmiede (not figured by Pickford 2016a), and Nuri Yamut (although an assignment to *Pa. valentini* can be discounted based on P4 morphology).

In summary, *C. simorrensis* and *Pa. valentini* might have overlapped in time during the latest Middle Miocene, but there is no conclusive evidence that a different species of *Conohyus* was present during the early Vallesian (contra Pickford 2016a). The large tetraconodont present in Europe during MN9 appears different from both *C. simorrensis* and *Versoporcus* spp. and, as argued by Pickford (2014, 2016a), can be recognized as *Pa. valentini* (contra Van der Made 2020). As in the case of *P. palaeochoerus*, the remains of *P. valentini* from CCN20 are generally somewhat larger than those previously reported, but it should be taken into account that the comparative sample available for *Pa. valentini* from the literature is quite small and thus likely to underrepresent the variation of the species in terms of dental size. If our identification of the CCN20 tetraconodont is correct, then this is the first time that the female canines, the P2, and the dp2 of *Pa. valentini* are described. However, the study of additional tetraconodont remains from other sites (such as Abocador de Can Mata and Castell de Barberà), currently underway, would be required to further characterize all tooth loci and determine the variability of this species, in order to substantiate further its taxonomic validity as well as its inclusion in *Parachleuastochoerus* instead of *Conohyus*.

Albanohyus After much confusion with peccary-like small suoids, *Albanohyus* was recognized as a suid by Van der Made (1996a), being subsequently included in the superfamily Chainochoerinae (Van der Made 1997, 2010; Harris and Liu, 2007; Orliac et al. 2010). The type species (*A. pygmaeus*) is known from MN6 and MN7+8 of Slovakia and France (Depéret 1892; Ginsburg 1974; Van der Made 1996a; Maridet et al. 2000; Mein and Ginsburg 2002; Sabol et al. 2004), and it has been also tentatively reported (*A.* cf. *pygmaeus*) from the early Vallesian (MN9) of Austria (Daxner-Höck and Bernor 2009). In the Vallès-Penedès, the most abundant material of *Albanohyus* comes from the MN7+8 of Abocador de Can Mata (being largely unpublished; Tomàs et al. 2011) and the earliest Vallesian of Castell de Barberà (Golpe-Posse 1975, 1977). The latter material was used by Golpe-Posse (1977) to describe *Barberahyus castellensis*, but subsequently included in *Albanohyus* (Fortelius et

al. 1996; Van der Made 1996a, 1997a; Tomàs et al. 2011). The differences between *A. pygmaeus* and *A. castellensis* are slight and basically consist in the somewhat larger dental size of the former, so that they might be synonymous (Fortelius et al. 1996). Nevertheless, following Van der Made (1996a) most authors have accepted the distinction between the two species (Van der Made 1997a, 1997b, 2010; Orliac et al. 2006; Harris and Liu 2007; Daxner-Höck and Bernor 2009), with *A. castellensis* having been further reported from other MN7+8 and MN9 sites from Spain, France, and tentatively Poland (Chen 1984; Van der Made 1990a, 1990a, 1996a; Álvarez Sierra et al. 2003). The largely unpublished material from Abocador de Can Mata, provisionally attributed to *Albanohyus* sp. by Tomàs et al. (2011), is closer in age to the type locality of *A. pygmaeus* (La Grive Saint-Alban, MN7+8), and hence will be useful in the future to evaluate the purported distinct species status of *A. castellensis*. The material from CCN20 is roughly coeval with that from Castell de Barberà, but the available material (two lower incisors) does not allow a confident attribution. The two lower incisors from CCN20 fit well in both size and shape with those from Castell de Barberà, thereby supporting a tentative assignment to cf. *Albanohyus*. This is reinforced by the fact that peccary-like small suoids of genera *Pecarichoerus* and *Choeromorus* (Van der Made 2010; Pickford 2012, 2017) are unknown from the MN7+8 and MN9 of the Vallès-Penedès Basin (Tomàs et al. 2011), although more diagnostic material should be required to confirm such an attribution.

Biochronological and paleoenvironmental implications

Besides the aforementioned problem with the age of Mira, the dating of some other sites in which *Pa. valentini* is recorded (Charmoille, Hollabrunn, Klein Hadersdorf, Kleineisenbach, Wartenberg bei Erding) is uncertain, whereas others are securely correlated to either MN7+8 (Saint-Gaudens, Sant Quirze) or MN9 (Hinterauerbach bei Wartenberg, Tutzing; Pickford 2014, 2016a). The same applies to the genus *Albanohyus*, which is already recorded from MN7+8 localities of the Vallès-Penedès Basin and elsewhere (Van der Made 1996a; Alba et al. 2006; Tomàs et al. 2011). Similarly, since the late 1980s, several authors have considered that the first appearance datum of *P. palaeochoerus* dates to the late MN7+8 (Van der Made and Moyà-Solà 1989; Van der Made 1990a, 1990b; Van der Made et al. 1999; Agustí et al. 2001; Fortelius et al. 2005; Alba et al. 2006). This contention has been most recently echoed by Iannucci and Begun (2021) and Kostopoulos and Sylvestrou (2022), in the case of the former based on the incorrect assumption that the species is present at Sant Quirze (e.g., Van der Made 1990a, 1997a) and Saint-Gaudens (Ginsburg 1974, 1980). As shown by Pickford (2014, 2016a), the previous citations of *P. palaeochoerus* in these MN7+8 localities stems from a confusion with the large tetraconodontine *Pa. valentini*, and the same applies to the citation from the MN7+8 of Abocador de Can Mata (Pickford 2016a; D.M.A., pers. obs.), whereas the previous citation from Castell de Barberà (Van der Made 1990a, 1997a) is correct (authors' unpublished data; contra Pickford 2016a) but the site is now conclusively dated to the earliest Vallesian (Alba et al. 2019). Given that *P. palaeochoerus* is not securely recorded until MN9 (Pickford 2016a), including the earliest Vallesian site of Castell de Barberà, this species might have dispersed from the east synchronously with *Hippotherium* and thus has the potential to be a biochronological marker of the Vallesian (Alba et al. 2022). This possibility is further reinforced by the results of this paper, which show that *P. palaeochoerus* is recorded at CCN20, which records the first appearance datum of *Hippotherium* in the Vallès-Penedès Basin (Agustí et al. 1997; Garcés et al. 1997).

The suid assemblage from CCN20, dominated by *P. palaeochoerus*, is much less diverse than that from the roughly coeval site of Castell de Barberà, despite the fact that both localities have about the same age (~11.2 Ma) and are located within the Vallès Sector of the Vallès-Penedès Basin (only ~10 km away). Golpe-Posse (1971, 1972b) initially identified three species from the latter site—*Hyotherium palaeochoerus* (currently in *Propotamochoerus*), *Hyotherium soemmeringi*, and *Listriodon splendens* Von Meyer, 1846—but subsequently the small suid *A. castellensis* was further reported (Golpe-Posse 1977; Van der Made 1996a, 1997a; Fortelius et al. 1996; Tomàs et al. 2011). The revision of Iberian suids performed by Van der Made (1990a, 1990b, 1996a, 1996b, 1997a, 1999) further refined the taxonomic assignment of the remaining suids from Castell de Barberà, leading to the recognition of as much as five species: *A. castellensis*, the listriodontine *L. splendens* (part of the material being figured by van der Made 1996b), the tetraconodontines *Pa. steinheimensis* (formerly in *Conohyus* and currently in *Versoporcus*, including most of Golpe-Posse's 1972b, 1974 citations of *H. soemmeringi*) and *Pa. huenermanni*, and the suine *P. palaeochoerus*. Ongoing work focused on the Castell de Barberà suids by some of the authors of this paper, by taking into account Pickford's (2014, 2016a) recent revision of European tetraconodonts, indicates that there are only two tetraconodonts at Castell de Barberà (a species of *Versoporcus* and a larger tetraconodontine that might correspond to *Pa. valentini*). In contrast, the previous citation of *Pa. huenermanni* does not stand close scrutiny, being apparently based on mislabeled specimens of *Pa. crusafonti* from Can Llobateres. Given that several thousand macrommamal remains have been recovered from both CCN20 and Castell de Barberà, the absence of *Listriodon* and *Versoporcus* from the former site, and the apparent rarity of *Albanohyus* (contrasting with the abundance of both *Listriodon* and *Albanohyus* at Castell de Barberà) is unlikely to be attributable to a sampling bias.

It is noteworthy that Castell de Barberà displays notable differences in the composition of the vertebrate assemblage as compared with CCN20, suggesting important paleoenvironmental differences between the two sites. In particular, the fauna from Castell de Barberà is indicative of a closed and humid forested environment with permanent water masses, whereas that of CCN20 (with less abundant castorids and arboreal rodents, more abundant hipparionin horses, and no primates thus far) is suggestive of a more open and arid environment (see Alba et al. 2019 for further details). This would explain the scarcity of *Albanohyus* from CCN20 (as very small suoids are generally interpreted as forest-adapted forms; Fortelius et al. 1996) but is apparently at odds with the absence of *L. splendens* from this site. This is because the latter taxon has been interpreted as a browser that abandoned rooting as a main feeding strategy and relied mostly on low vegetation with occasional input of grass and fruit in relatively open environments (Hunter and Fortelius 1994; Fortelius et al. 1996; Van der Made 1996b; Aiglstorfer et al. 2014; Van der Made et al. 2014). In fact, *L. splendens* is also frequently recorded in humid and densely forested paleoenvironments such as those recorded at the hominoid-bearing sites of Castell de Barberà and ACM/BCV1 (Casanovas-Vilar et al. 2008)—suggesting that, despite a specialization for browsing folivory, this species was quite generalist in the sense that it could successfully exploit a variety of habitats. The well-developed (and, in some cases, heavily worn) lower incisors of both *P. palaeochoerus* and *Pa. valentini* indicate that these species frequently engaged in rooting behaviors (Van der Made 2010), a typical behavior of suoids, of variable intensity throughout the year, which enables them to survive when other types of food are scarce (Van der Made et al. 2014). The hypothesized lack of rooting behaviors in *L. splendens* might thus explain its absence from CCN20, where it might have been outcompeted by the other suid species during the unfavorable season due to a lower vegetation productivity as compared with Castell de Barberà. On dental grounds, *P. palaeochoerus*

has been considered to be somewhat better adapted for rooting than tetraconodonts such as *Parachleuastochoerus*/*Versoporcus* (Van der Made et al. 2014), even though isotopic data indicate that the latter also frequently relied on underground resources (Aiglstorfer et al. 2014; Eastham et al. 2016, 2017; Iannucci and Begun 2021). Indeed, isotopic data from Rudabánya indicate that *Parachleuastochoerus* was more dependent on underground resources than *Propotamochoerus* (Eastham et al. 2016, 2017), suggesting that the latter might have displayed a more varied diet further including fruits and leaves, while being able to more efficiently look for underground food items by means of rooting behaviors when other resources were scarce (Iannucci and Begun 2021). This would further agree with the greater development of secondary molar cusps characteristic of suines, generally interpreted as indicative of an omnivorous diet (Fortelius et al. 1996). It is thus likely that the less diverse suid assemblage of CCN20, dominated by *P. palaeochoerus* instead of tetraconodonts, *Albanohyus*, and *L. splendens* reflects a more open, arid, and seasonal environment without permanent water masses, in which rooting behaviors were more essential for survival than at Castell de Barberà. This hypothesis could be tested by means of isotopic and tooth wear analysis of *P. palaeochoerus* and *Pa. valentini* from both localities, as it would predict a higher incidence of rooting behaviors, at least in the former taxon, at CCN20 as compared with Castell de Barberà.

Acknowledgments We are particularly indebted to the following people: the landowner of the CCN20 parcel, for giving us permission to carry out the fieldwork; Salvador Moyà-Solà, for codirecting some fieldwork campaigns; Manel Llenas, Manel Méndez, and Víctor Vinuesa, for various assistance and their implication during the excavations; Josep M. Robles, for geological field assistance and collection management; Guillem Pons-Monjo, for further collection assistance; Xènia Aymerich and the rest of the staff of the ICP Preparation & Conservation Area, for the preparation of the specimens; Martin Pickford, for providing relevant literature; and the two reviewers (Alessio Iannucci and an anonymous one) and the Editor-in-Chief (Darin A. Croft) for constructive comments that helped improve a previous draft of this paper. We also thank all the other researchers, students, and volunteers that have participated in the CCN20 fieldwork campaigns over the years, and we further acknowledge the collaboration of the Servei d'Arqueologia i Paleontologia of the Generalitat de Catalunya. This work is part of the PhD dissertation of the first author, in the framework of the PhD Programme in Geology of the Universitat Autònoma de Barcelona.

Funding This work is part of R+D+I projects PID2020-117289GBI00, PID2020-116220GBI00, and PID2020-116908GB-I00 funded by the Agencia Estatal de Investigación of the Spanish Ministry of Science and Innovation (MCIN/AEI/10.13039/501100011033/). Research has also been supported by the Generalitat de Catalunya/CERCA Programme, a predoctoral fellowship from the Confederated Tribes of Grand Ronde (CTGR) to S.M.; a predoctoral FI AGAUR fellowship funded by the Secretaria d'Universitats i Recerca of the Generalitat de Catalunya and the European Social Fund (2020 FI_B1 00131) to L.S.; and the Programa Postdoctoral Beatriu de Pinós of the Secretaria d'Universitats i Recerca of the Generalitat de Catalunya (2019 BP 00154) to À.H.L. Fieldwork was funded by the Departament de Cultura of the Generalitat de Catalunya (2014/100609, CLT009/18/00071, and ARQ001SOL-136-2022). Some of the authors are members of the consolidated research groups 2017 SGR 116 GR and 2017 SGR 960 GR of the Agència de Gestió d'Ajuts Universitaris i de Recerca of the Generalitat de Catalunya.

Data Availability The fossil material studied in this paper is housed and adequately curated in the Institut Català de Paleontologia Miquel Crusafont, and it is accessible to other researchers. All the data generated in the course of this study are provided in the paper or the supplementary information.

Author Contributions S.M., D.DM., and D.M.A. designed the study. S.A., M.P., J.A., À.H.L., and D.DM. directed the fieldwork. S.M. took the photographs and measurements and drafted the descriptions. D.M.A. prepared the figures. L.S. performed the statistical analyses. S.M., M.C., and D.M.A. identified the material. S.M. and D.M.A. wrote the manuscript with input from all authors after reviewing the manuscript.

Declarations

Conflicts of Interest The authors have no competing interests to declare that are relevant to the content of this article.

References

Agustí J, Anadón P, Ginsburg L, Mein P, Moissenet E (1988) Araya et Mira: nouveaux gisements de Mammifères dans le Miocène inférieur-moyen des Chaînes Ibériques orientales et méditerranéennes. Conséquences stratigraphiques et structurales. Paleontol Evol 22:83–101

Agustí J, Galobart À (1998) Noves localitats amb mamífers fòssils en el miocè de la Conca del Vallès-Penedès. Trib Arqueol 1996–1997:9–23

Agustí J, Cabrera L, Garcés M, Parés JM (1997) The Vallesian mammal succession in the Vallès-Penedès basin (northeast Spain): Paleomagnetic calibration and correlation with global events. Palaeogeogr Palaeoclimatol Palaeoecol 133:149–180

Agustí J, Cabrera L, Garcés M, Krijgsman W, Oms O, Parés JM (2001) A calibrated mammal scale for the Neogene of Western Europe. State of the art. Earth-Sci Rev 52:247–260

Aiglstorfer M, Bocherens H, Böhme M (2014) Large mammal ecology in the late Middle Miocene Gratkorn locality (Austria). Palaeobio Palaeoenv 94:189–213

Alba DM, Moyà-Solà S, Casanovas-Vilar I, Galindo J, Robles JM, Rotgers C, Furió M, Angelone C, Köhler M, Garcés M, Cabrera L, Almécija S, Obradó P (2006). Los vertebrados fósiles del Abocador de Can Mata (els Hostalets de Pierola, l'Anoia, Cataluña), una sucesión de localidades del Aragoniense superior (MN6 y MN7+8) de la cuenca del Vallès-Penedès. Campañas 2002-2003, 2004 y 2005. Estud Geol 62:295–312

Alba DM, Carmona R, Bertó Mengual JV, Casanovas-Vilar I, Furió M, Garcés M, Galindo J, Luján ÀH (2012) Intervenció paleontològica a l'Ecoparc de Can Mata (els Hostalets de Pierola, conca del Vallès-Penedès). Trib Arqueol 2010–2011:115–130

Alba DM, Garcés M, Casanovas-Vilar I, Robles JM, Pina M, Moyà-Solà S, Almécija S (2019) Bio- and magnetostratigraphic correlation of the Miocene primate-bearing site of Castell de Barberà to the earliest Vallesian. J Hum Evol 132:32–46

Alba DM, Robles JM, Casanovas-Vilar I, Beamud E, Bernor RL, Cirilli O, DeMiguel D, Galindo J, Llopart I, Pons-Monjo G, Sánchez IM, Vinuesa V, Garcés M (2022) A revised (earliest Vallesian) age for the hominoid-bearing locality of Can Mata 1 based on new magnetostratigraphic and biostratigraphic data from Abocador de Can Mata (Vallès-Penedès Basin, NE Iberian Peninsula). J Hum Evol 170:103237

Álvarez Sierra MA, Calvo JP, Morales J, Alonso-Zarza A, Azanza B, García Paredes I, Hernández Fernández M, van der Meulen AJ, Peláez-Campomanes P, Quiralte V, Salesa MJ, Sánchez IM, Soria D (2003) El tránsito Aragoniense-Vallesiense en el área de Daroca-Nombrevilla (Zaragoza, España). Col-Pa Vol. Ext. 1:25–33

Antón SC, Taboada HG, Middleton ER, Rainwater CW, Taylor AB, Turner TR, Turnquist JE, Weinstein KJ, Williams SA (2016) Morphological variation in *Homo erectus* and the origins of developmental plasticity. Phil Trans R Soc B 371:20150236

Aslam S, Khan AM, Ahmad RM, Iqbal A, Waseem MT (2021) Systematic study of the new remains of *Propotamochoerus hysudricus* (Suidae, Mammalia) from the Late Miocene–Early Pliocene of Middle Siwaliks (Pakistan). Arab J Geosci 14:73

Azanza B (1986) Estudio geológico y paleontológico del Mioceno del sector oeste de la Comarca de Borja. Cuad Estud Borj 17–18:63–126

Batool A, Khan MA, Qureshi NA (2015) New fossils of Suidae (Mammalia, Artiodactyla) from the Hasnot Late Miocene, northern Pakistan. J An Plant Sci 25:578–590

Bernor RL, Bi S, Radovčić J (2004) A contribution to the evolutionary biology of *Conohyus olujici* n. sp. (Mammalia, Suidae, Tetraconodontinae) from the early Miocene of Lučane, Croatia. Geodiversitas 26:509–534

Bernor RL, Kaya F, Kaakinen A, Saarinen J, Fortelius M (2021). Old world hipparion evolution, biogeography, climatology and ecology. Earth Sci Rev 221:103784

Blainville HMD de (1847) Ostéographie ou Description Iconographique Comparée du Squelette et du Système Dentaire des Cinq Classes d'Animaux Vertébrés Récents et Fossiles pour Servir de Base à la Zoologie et à la Géologie. Tome Quatrième Quaternatés—Maldentés. A. Bertrand, Paris

Carmona R, Alba DM, Casanovas-Vilar I, Furió M, Garcés M, Bertó Mengual JV, Galindo J, Luján ÀH (2011) Intervención paleontológica en la serie del Mioceno Superior del Ecoparc de Can Mata (cuenca del Vallès-Penedès, NE de la península Ibérica). In Pérez-García A, Gascó F, Gasulla JM, Escaso F (eds) Viajando a Mundos Pretéritos. Ayuntamiento de Morella, Morella, pp 65–74

Casanovas-Vilar I, Alba DM, Moyà-Solà S, Galindo J, Cabrera L, Garcés M, Furió M, Robles JM, Köhler M, Angelone C (2008) Biochronological, taphonomical and paleoenvironmental background of the fossil great ape *Pierolapithecus catalaunicus* (Primates, Hominidae). J Hum Evol 55:589–603

Casanovas-Vilar I, Furió M, Agustí J (2006) Rodents, insectivores and paleoenvironment associated to the first-appearing hipparionine horses in the Vallès-Penedès Basin (Northeastern Spain). Beitr Paläontol 30:89–107

Casanovas-Vilar I, Madern A, Alba DM, Cabrera L, García-Paredes I, Van den Hoek Ostende LW, DeMiguel D, Robles JM, Furió M, Van Dam J, Garcés M, Angelone C, Moyà-Solà S (2016a) The Miocene mammal record of the Vallès-Penedès Basin (Catalonia). C R Palevol 15:791–812

Casanovas-Vilar I, Garcés M, Van Dam J, García-Paredes I, Robles JM, Alba DM (2016b) An updated biostratigraphy for the late Aragonian and the Vallesian of the Vallès-Penedès Basin (Catalonia). Geol Acta 14:195–217

Chen G (1984) Suidae and Tayassuidae (Artiodactyla, Mammalia) from the Miocene of Steinheim a. A. (Germany). Palaeontogr Abt A 184:79–93

Cherin M, Alba DM, Crotti M, Menconero S, Moullé P-E, Sorbelli L, Madurell-Malapeira J (2020) The post-Jaramillo persistence of *Sus strozzii* (Suidae, Mammalia) in Europe: New evidence from the Vallparadís Section (NE Iberian Peninsula) and other coeval sites. Quat Sci Rev 233:106234

Colbert EH (1935) Siwalik mammals in the American Museum of Natural History. Trans Am Phil Soc 26, 1–401

Crusafont M, Truyols J (1954) Catálogo Paleomastológico del Mioceno del Vallés-Penedés y de Calatayud-Teruel. Segundo Cursillo Internacional de Paleontología. Museo de la Ciudad de Sabadell, Sabadell.

Crusafont Pairó M (1950) La cuestión del llamado Meótico español. Arrahona 1950:41–48

Crusafont Pairó M (1951) El sistema miocénico en la depresión española del Vallés-Penedés. In International Geological Congress "Report of the Eighteenth Session, Great Britain, 1948", Part XI, pp 33–42

Crusafont Pairó M (1952) Los jiráfidos fósiles de España. Mem Comun Inst Geol 8:1–239

Crusafont Pairó M (1953) El sistema miocénico en la depresión española del Vallés-Penedés. Mem Comun Inst Geol Prov 10:13–23

Crusafont Pairó M, Lavocat R (1954). "Schizochoerus", un nuevo género de Súidos del Pontiense inferior (Vallesiense), del Vallés-Penedés. Not Comun Inst Geol Min Esp 36:1–12

Crusafont M, Villalta JF de, Truyols J (1955) El Burdigaliense continental de la cuenca del Vallés-Penedés. Mem Comun Inst Geol 12:1–272

Crusafont-Pairó M, Golpe JM (1972). Dos nuevos yacimientos del Vindoboniense en el Vallés. Acta Geol Hisp 7:71–72

Crusafont Pairó M, Truyols Santonja J (1960) Sobre la caracterización del Vallesiense. Not Comun Inst Geol Min Esp 60:109–125

Cuccu A, Valenciano A, Azanza B, DeMiguel D (2022) A new lynx mandible from the Early Pleistocene of Spain (La Puebla de Valverde, Teruel) and a taxonomical multivariate approach of medium-sized felids. Hist Biol. https://doi.org/10.1080/08912963.2021.2024181

Dar FY, Aftab K, Babar MA, Khan MA, Abbas SG, Shahid R, Asim M (2019) New fossils of Suidae (Mammalia) from Dhok Pathan Formation of Siwaliks, Punjab, Pakistan. J An Plant Sci 29:1198–1203

Daxner-Höck G, Bernor RL (2009) The early Vallesian vertebrates of Atzelsdorf (Late Miocene, Austria) 8. *Anchitherium*, Suidae and Castoridae (Mammalia). Ann Naturhist Mus Wien 111A:557–584

de Bonis L, Bouvrain G (1996) Suidae du Miocène supérieur de Grèce. Bull Mus Natl Hist Nat Paris 18:107–132

de Bruijn H, Doukas C, van den Hoek Ostende LW, Zachariasse JW (2012) New finds of rodents and insectivores from the Upper Miocene at Plakias (Crete, Greece). Swiss J Palaeontol 131:61–75

Depéret C (1887) Recherches sur la succession des faunes des vertébrés miocénes de la vallée du Rhône. Arch Mus Hist Nat Lyon 4:45–313

Depéret C (1892) La faune de Mammifères Miocènes de La Grive-Saint-Alban (Isère) et de quelques autres localités du bassin du Rhone. Arch Mus Hist Nat Lyon 5:1–95

Eastham LC, Feranec RS, Begun DR (2016) Stable isotopes show resource partitioning among the early Late Miocene herbivore community at Rudabánya II: Paleoenvironmental implications for the hominoid, *Rudapithecus hungaricus*. Palaeogeogr Palaeoeclimatol Palaeoecol 454:161–174

Eastham LC, Feranec RS, Begun DR (2017) Trace element analysis provides insight into the diets of early Late Miocene ungulates from the Rudabánya II locality (Hungary). Geol Acta 15:231–243

Filhol H (1882) Note relative à une nouvelle espèce de *Sus* fossile trouvée dans les argiles à *Dinotherium* de Valentine (Haute-Garonne). Bull Soc Phil Paris 6:123–124

Fortelius M, van der Made J, Bernor RL (1996) Middle and Late Miocene Suoidea of Central Europe and the Eastern Mediterranean: Evolution, Biogeography, and Paleoecology. In: Bernor RL, Fahlbusch V, Mittmann H-M (eds) The Evolution of Western Eurasian Neogene Faunas. Columbia University Press, New York, pp 348–377

Fortelius M, Armour-Chelu M, Bernor RL, Fessaha N (2005) Systematics and palaeobiology of the Rudabánya Suidae. Palaeontogr Ital 90:259–278

Fraas O (1870) Die Fauna von Steinheim. Mit Rüecksicht auf die miocänen Säugethier- und Vogelreste des Steinheimer Beckens. Jahresh Ver vaterl Naturkd Württemb. 26:145–306

Fujita M, Kawamura Y, Murase N (2000) Middle Pleistocene wild boar remains from NT Cave, Niimi, Okayama Prefecture, west Japan. J Geosci Oska City Univ 43:57–95

Gaillard C (1899) Mammifères miocènes nouveaux ou peu connus de La Grive-Saint-Alban (Isère). Archiv Mus Hist Nat Lyon 7:1–78

Gallai G (2006) Sistematica, paleoecologia, paleogeografia dei Suidae fossili italiani. Dissertation, Università degli Studi di Firenze, Florence

Gallai G, Rook L (2006) *Propotamochoerus* sp. (Suidae, Mammalia) from the Late Miocene of Gravitelli (Messina, Sicily, Italy) rediscovered. Riv Ital Paleontol Stratigr 112:317–321

Gallai G, Rook L (2011) *Propotamochoerus provincialis* (Gervais, 1859) (Suidae, Mammalia) from the latest Miocene (late Messinian; MN13) of Monticino Quarry (Brisighella, Emilia-Romagna, Italy). Boll Soc Paleontol Ital 50:29–34

Garcés M (1995) Magnetoestratigrafía de las sucesiones del Mioceno Medio y Superior del Vallès Occidental (Depresión del Vallès-Penedès, N.E. de España): Implicaciones biocronológicas y cronoestratigráficas. Dissertation, Universitat de Barcelona, Barcelona

Garcés M, Agustí J, Cabrera L, Parés JM (1996) Magnetostratigraphy of the Vallesian (late Miocene) in the Vallès-Penedès Basin (northeast Spain). Earth Plant Sci Lett 142:381–396

Garcés M, Cabrera L, Agustí J, Parés JM (1997) Old World first appearance datum of *"Hipparion"* horses: Late Miocene large-mammal dispersal and global events. Geology 25:19–22

Geraads D, Spassov N, Garevski R (2008) New specimens of *Propotamochoerus* (Suidae, Mammalia) from the late Miocene of the Balkans. N Jb Geol Paläont Abh 248:103–113

Gervais P (1850 [1848–1852]) Zoologie et Paléontologie Françaises. Nouvelles Recherches sur les Animaux Vivants et Fossiles de la France. Arthus Bertrand, Paris.

Ginsburg L (1974) Les faunes de Mammifères burdigaliens et vindoboniens des bassins de la Loire et de la Garonne. Mém Bur Rech Géol Min France 78:153–167

Ginsburg L (1980) *Xenohyus venitor*, suidé nouveau *(Mammalia, Artiodactyla)* du Miocène Inférieur de France. Geobios 13:861–877

Ginsburg L (1988) Contributions a l'étude du gisement Miocène Supérieur de Montrédon (Herault). Les grands mammifères. 4 – Les artiodactyles Suidae. Palaeovertebrata Mém. extr.:57–64

Golpe Posse JM (1971) Suiformes del Terciario Español y sus Yacimientos. Dissertation, Universidad de Barcelona, Barcelona

Golpe Posse JM (1972a) Suiformes del Terciario español y sus yacimientos (Resumen). Acta Geol Hisp 7:18–21

Golpe-Posse JM (1972b) Suiformes del Terciario español y sus yacimientos (Tesis doctoral-Resumen) (revisado y reimprimido en Diciembre de 1972). Paleontol Evol 2:1–197

Golpe-Posse JM (1974) Faunas de yacimientos con suiformes en el Terciario español. Paleontol Evol 8:1–87

Golpe-Posse JM (1975) Un nuevo tayasuido en el Vindoboniense terminal de Castell de Barberà (Cuenca del Vallès, España). Bol Inf Inst Paleontol Sabadell 7:39–43

Golpe-Posse JM (1977) *Barberahyus castellensis* n.g.n.sp., Tayasuido del Vindoboniense terminal de Castell de Barberà (Cuenca del Vallès, España). Paleontol Evol 12:31–43

Golpe Posse JM (1978) Presencia del género *Microstonyx* Pilgrim, 1926, en el Vallesiense superior de Terrassa (Barcelona, Cuenca del Vallès). Butll Inf Inst Paleontol Sabadell 10:28–33

Golpe Posse JM (1980) Notas sobre la dentición anterior de *Microstonyx antiquus* (Kaup, 1833). Acta Geol Hisp 1:109–111

Golpe Posse JM (1981) Precisiones acerca de *Palaeochoerus minus* (Suidae, Artiodactyla) del Burdigaliense de la Cuenca del Vallès (Cataluña, España). Paleontol Evol 16:25–28

Gray JE (1821) On the natural arrangement of vertebrose animals. Lond Med Repos Rec 15:296–310

Hammer Ø, Harper DAT, Ryan PD (2001) PAST: Paleontological statistics software package for education and data analysis. Palaeontol Electron 4:4

Harris JH, Liu L-P (2007) Superfamily Suoidea. In: Prothero DR, Foss EF (eds), The Evolution of Artiodactyls. Johns Hopkins University Press, Baltimore, pp 130–150

Heissig K (1989) *Conohyus huenermanni* n. sp., eine kleine Schweineart aus der Oberen Süßwassermolasse Bayerns. Mitt Bayer Staatssamml Paläontol Hist Geol 29:235–240

Hellmund M (1995) The Vertebrate Locality Maramena (Macedonia, Greece) at the Boundary Turolian-Ruscinian Boundary (Neogene). 13. Suidae (Artiodactyla, Mammalia). Munch Geowiss Abh 28:143–156

Hou S, Su DF, Kelley J, Deng T, Jablonski NG, Flynn LJ, Ji X, Cao J, Yang X (2019) New fossil suid specimens from the terminal Miocene hominoid locality of Shuitangba, Zhaotong, Yunnan Province, China. J Mamm Evol 26:557–571

Howell FC (1999) Paleo-demes, species clades, and extinctions in the Pleistocene hominin record. J Anthropol Res 55:191–243

Hünermann KA (1968) Die Suidae (Mammalia, Artiodactyla) aus den Dinotheriensanden (Unterpliozän = Pont) Rheinhessens (Sudwestdeutschland). Schweiz Paläontol Abh 86:1–96

Hunter JP, Fortelius M (1994) Comparative dental occlusal morphology, facet development, and microwear in two sympatric species of *Listriodon* (Mammalia: Suidae) from the Middle Miocene of Western Anatolia (Turkey). J Vertebr Paleontol 14:105–126

Iannucci A, Begun DR (2022) Suidae (Mammalia, Artiodactyla) from the late miocene hominoid locality of Alsótelekes (Hungary). Geobios 71:39–49

Iannucci A, Cherin M, Sorbelli L, Sardella R (2021) Suidae transition at the Miocene-Pliocene boundary: a reassessment of the taxonomy and chronology of *Propotamochoerus provincialis*. J Mamm Evol 28:323–335

Jungers WL (1984) Aspects of size and scaling in primate biology with special reference to the locomotor skeleton. Yearb Phys Anthropol 27:73–97

Kaup J-J (1833) Description d'Ossements Fossiles de Mammifères Inconnus jusqu'à Présent, qui se Trouvent au Muséum Grand-Ducal de Darmstadt. Second Cahier. J.G. Heyer, Darmstadt

Kaup J-J (1859) Beitraege zur naeheren Kenntniss der urweltlichen Saeugethiere. Viertes Heft. Eduard Zernin, Darmstadt

Khan MA, Akhtar M, Iqbal M (2010) The late Miocene artiodactyls in the Dhok Pathan type locality of the Dhok Pathan formation, the Middle Siwaliks, Pakistan. Pakistan J Zool Supplementary Series 10:1–88

Kostopoulos D (1994) *Microstonyx major* (Suidae, Artiodactyla) from the late Miocene locality of "Nikiti-1", Macedonia, Greece; some remarks about the species. Bull Geol Soc Greece 30:341–355

Kostopoulos DS, Spassov N, Kovachev D (2001) Contribution to the study of *Microstonyx*: evidence from Bulgaria and the SE European populations. Geodiversitas 23:411–437

Kostopoulos DS, Sylvestrou I (2022) The fossil record of suoids (Mammalia: Artiodactyla: Suoidea) in Greece. In: Vlachos E (ed.) Fossil vertebrates of Greece Vol. 2. Laurasiatherians, artiodactyles, perissodactyles, carnivorans, and island endemics. Springer, Cham, pp 249–269

Kubiak H (1981) Suidae and Tayassuidae (Artiodactyla, Mammalia) from the Miocene of Przewomo in Lower Silesia. Acta Geol Pol 31:59–70

Lartet E (1851) Notice sur la Colline de Sansan, suivie d'une Récapitulation des Diverses Espèces d'Animaux Vertébrés Fossiles, Trouvés soit a Sansan, soit dans d'autres Gisements du Terrain Tertiaire Miocène dans le Bassin Sous-Pyréneen. J.-A. Portes, Auch

Lazaridis G (2015) Study of the late Miocene vertebrate locality of Kryopigi and other localities of Kassandra Peninsula, Chalkidiki (Greece). Systematics, Taphonomy, Paleoecology, Biochronology. Dissertation, Aristotle University of Thessaloniki, Thessaloniki (in Greek)

Lazaridis G, Tsoukala E, Kostopoulos DS (2022) Validation of a prematurely abolished new *Propotamochoerus* Pilgrim, 1925 species (Mammalia, Suidae) from SE Mediterranean. C R Palevol 21:531–549

Lydekker R (1876) Part II. Molar teeth and other remains of Mammalia. In: Palaeontologia Indica. Ser. X. Indian Tertiary and post-Tertiary Vertebrata. Vol. I. Memoirs of the Geological Survey of India, Calcutta, pp 19–87

Maridet O, Berthet D, Mein P (2000) Un nouveau gisement karstique polyphasé miocène moyen de Four (Isère) : étude des Cricetidae (Mammalia, Rodentia) et description de *Democricetodon fourensis* nov. sp. Géol France 2:71–79

McKenzie S, Casanovas-Vilar I, Alba DM (2022) Tetraconodont dental remains (Suidae, Tetraconodontinae) from the Middle Miocene site of Ca l'Almirall (Vallès-Penedès Basin, NE Iberian Peninsula). Hist Biol, https://doi.org/10.1080/08912963.2022.2056840

Mein P, Ginsburg L (2002) Sur l'âge relatif des différents dépôts karstiques miocènes de La Grive-Saint-Alban (Isère). Cah Sci 2/2002:7–47

Morales J (1984) Venta del Moro: Su macrofauna de mamíferos, y biostratigrafía continental del Mioceno terminal mediterráneo. Dissertation, Universidad Complutense de Madrid, Madrid

Mosimann JE, James FC (1979) New statistical methods for allometry with application for Florida red-winged blackbirds. Evolution 33:444–459

Mottl M (1966) Neue Säugetierfunde aus dem Jungtertiär der Steiermark. VII. Ein vollständiger *Hyotherium palaeochoerus*-Schädel aus dem Altpliozän (Pannon) Südost-Österreichs. Mitt Mus Bergb Geol Techn Landesmus Joanneum Graz 28:73–101

Ogg JG (2012) Geomagnetic polarity time scale. In: Gradstein FM, Ogg JG, Schmitz MD, Ogg GM (eds) The Geologic Time Scale 2012, Volume 1. Elsevier, Amsterdam, pp 85–113

Oliver Pérez A (2015) Evolution of *Megacricetodon* from the Aragonian and Vallesian (Miocene) of the Iberian Peninsula. Dissertation, Universidad Complutense de Madrid, Madrid

Orliac MJ (2006) *Eurolistriodon tenarezensis*, sp. nov., from Montreal-du-Gers (France): Implications for the systematics of the European Listriodontinae (Suidae, Mammalia). J Vertebr Paleontol 26:967–980

Orliac MJ, Antoine P-O, Duranthon F (2006) The Suoidea (Mammalia, Artiodactyla), exclusive of Listriodontinae, from the early Miocene of Béon 1 (Montréal-du-Gers, SW France, MN4). Geodiversitas 28:685–718

Orliac MJ, Antoine P-O, Ducrocq S (2010) Phylogenetic relationships of the family Suidae (Mammalia, Cetartiodactyla), new insights on the relationships within Suoidea. Zool Scr 39:315–330

Owen R (1848) Description of teeth and portions of jaws of two extinct Anthracotherioid quadrupeds (*Hyopotamus vectianus* and *Hyop. bovinus*) discovered by the Marchioness of Hastings in the Eocene deposits on the N.W. coast of the Isle of Wight: with an attempt to develop Cuvier's idea of the classification of pachyderms by the number of their toes. Quart J Geol Soc Lond 4:103–141

Pickford M (1981) *Parachleuastochoerus* (Mammalia, Suidae). Estud Geol 37:313–320

Pickford M (1988) Revision of the Miocene Suidae of the Indian subcontinent. Münch Geowiss Abh A 12:1–91

Pickford M (1993) Old World suoid systematics, phylogeny, biogeography and biostratigraphy. Paleontol Evol 26–27:237–269

Pickford M (2012) Les Suoidea (Artiodactyla) de Sansan : systématique, paléoécologie, biogéographie et biochronologie. Mem Mus Natl Hist Nat 203:249–277

Pickford M (2013a) Reassessment of Dinotheriensande Suoidea: Biochronological and biogeographic implications (Miocene Eppelsheim Formation). Mainz Naturwiss Arch 50:155–193

Pickford M (2013b) *Conohyus simorrensis* (Lartet, 1851) (Suidae, Mammalia) from the Middle Miocene of Carpetana (Madrid, Spain). Spanish J Palaeontol 28:91–102

Pickford M (2013c) Re-assessment of the suids from the Sables marins de Montpellier and selection of a lectotype for *Sus provincialis* Blainville, 1847. Geodiversitas 35:655–689

Pickford M (2014) *Sus valentini* Filhol (1882) from St Gaudens (MN 8–9) France: blighted from the outset but a key to understanding late Middle Miocene Tetraconodontinae (Suidae, Mammalia) of Europe. Mainz Naturwiss Arch 51:167–220

Pickford M (2015) Late Miocene Suidae from Eurasia: *Hippopotamodon* and *Microstonyx* problem revisited. Münch Geowiss Abh A 42:1–126

Pickford M (2016a) Biochronology of European Miocene Tetraconodontinae (Suidae, Artiodactyla, Mammalia) flowing from recent revision of the subfamily. Ann Naturhist Mus Wien A 118:175–244

Pickford M (2016b) Revision of European Hyotheriinae (Suidae) and *Doliochoeridae* (Mammalia). Münch Geowiss Abh A 44:1–270

Pickford M (2016c) *Hippopotamodon erymanthius* (Suidae, Mammalia) from Mahmutgazi, Denizli-Çal Basin, Turkey. Foss Impr 72:183–201

Pickford M (2017) Revison of "peccary-like" Suoidea (Artiodactyla: Mammalia) from the Neogene of the Old World. Münch Geowiss Abh A 46:1–144

Pickford M, Laurent Y (2014) Valorisation of palaeontological collections: nomination of a lectotype for *Conohyus simorrensis* (Lartet, 1851), Villefranche d'Astarac, France, and description of a new genus of tetraconodont. Estud Geol 70:e002

Pickford M, Morales J (2003) New Listriodontinae (Mammalia, Suidae) from Europe and a review of listriodont evolution, biostratigraphy and biogeography. Geodiversitas 25:347–404

Pickford M, Moyà Solà S (1994) *Taucanamo* (Suoidea, Tayassuidae) from the Middle Miocene (MN04a) of Els Casots, Barcelona, Spain. C R Acad Sci Paris 319:1569–1575

Pickford M, Moyà Solà S (1995) *Eurolistriodon* gen. nov., (Suoidea, Mammalia) from Els Casots, early middle Miocene, Spain. Proc Kon Ned Akad v Wetensch 98:343–360

Pilgrim G (1925) Presidential address to the geological section of the 12th Indian Science Congress. In: Proceedings of the 12th Indian Science Congress, pp 200–218

Robles JM, Alba DM, Fortuny J, De Esteban-Trivigno S, Rotgers C, Balaguer J, Carmona R, Galindo J, Almécija S, Bertó JV, Moyà-Solà S (2013) New craniodental remains of the barbourofelid *Albanosmilus jourdani* (Filhol, 1883) from the Miocene of the Vallès-Penedès (NE Iberian Peninsula) and the phylogeny of the Barbourofelini. J Syst Palaeontol 11:993–1022

Sabol M, Joniak P, Holec P (2004) Succession(-s) of mammalian assemblages during the Neogene - a case study from the Slovak part of the Western Carpathians. Scripta Fac Sci Nat Univ Masaryk Brunensis 31–32:65–84

Sarwar HMA, Waseem MT, Khan AM, Ahmad RM (2016) *Propotamochoerus hysudricus* remains from late Miocene deposits of Hasnot, Pakistan. Punjab Univ J Zool 31:243–248

Schlosser M (1903) Die fossilen Säugetiere Chinas nebst einer Odonlographie der rezenten Antilopen. Abh math-phys Cl Königl Bayer Akad Wiss 22:1–221

Schmidt-Kittler N (1971) Die obermiozäne Fossillagerstätte Sandelzhausen 3. Suidae (Artiodactyla, Mammalia). Mitt Bayer Staatssamml Paläontol Hist Geol 11:129–170

Sein C, van der Made J, Rössner GE (2009) New material of *Propotamochoerus* (Suidae, Mammalia) from the Irrawaddy Formation, Myanmar. N Jb Geol Paläont Abh 251:17–31

Smith JB, Dodson P (2003) A proposal for a standard terminology of anatomical notation and orientation in fossil vertebrate dentitions. J Vertebr Paleontol 23:1–12

Stehlin HG (1899) Ueber die Geschichte des Suiden-Gebisses. Erster Teil. Abh Schweiz Paläontol Ges 26:1–336

Stromer E (1928) Wirbeltiere im obermiocänen Flinz Münchens. Abh Bayer Akad Wiss Math-naturwiss Abteil 32:1–71

Stromer E (1940) Die jungtertiäre Fauna des Flinzes und des Schweiß-Sandes von München. Nachträge und Berichtigungen. Abh Bayer Akad Wiss Math-naturwiss Abteil 48:1–102

Sylvestrou IA, Kostopoulos DS (2006) The late Miocene vertebrate locality of Perivolaki, Thessaly, Greece. 7. Suidae. Palaeontographica 276:121–133

Sylvestrou IA, Kostopoulos DS (2009) The Late Miocene mammal faunas of the Mytilinii Basin, Samos Island, Greece: New collection. 12. Suidae. Beitr Paläont 31:283–297

Thaung-Htike, Tsubamoto T, Takai M, Egi N, Zin-Maung-Maung-Thein, Chit-Sein, Maung-Maung (2006) Discovery of *Propotamochoerus* (Artiodactyla, Suidae) from the Neogene of Myanmar. Asian Paleoprimatol 4:173–185

Thenius E (1950) *Postpotamochoeros* nov. subgen. *hyotherioides* aus dem Unterpliozän von Samos (Griechenland) un die Herkunft der Potamochoeren. Sitz-Ber Akad Wiss Math-naturwiss Kl 159:26–36

Thenius E (1956) Die Suiden und Tayassuiden des steirischen Tertiärs. Beiträge zur K enntnis der Säugetierreste des steirischen Tertiärs VIII. Sitz Österr Akad Wiss Math-naturwiss Kl 165:337–382

Tomàs M, Alba DM, Robles JM, Rotgers C, Carmona R, Galindo J, Almécija S, Bertó JV, Casanovas-Vilar I, Balaguer J, Moyà-Solà S (2011) Small suoids from the Middle Miocene of Abocador de Can Mata (Vallès-Penedès Basin, NE Iberian Peninsula): A preliminary assessment. In: Pérez-García A, Gascó J, Gasulla JM, Escaso F (eds) Viajando a Mundos Pretéritos. Ayuntamiento de Morella, Morella, pp 389–398

Van der Made J (1989) A *Conohyus*-lineage (Suidae, Artiodactyla) from the Miocene of Europe. Rev Esp Paleontol 4:19–28

Van der Made J (1990a) A range-chart for European Suidae and Tayassuidae. Paleontol Evol 23:99–104

Van der Made J (1990b) Iberian Suoidea. Paleontol Evol 23:83–97

Van der Made J (1996a) *Albanohyus*, a small Miocene pig. Acta Zool Cracov 39:293–303

Van der Made J (1996b) Listriodontinae (Suidae, Mammalia), their evolution, systematics and distribution in time and space. Contrib Tert Quater Geol 33:3–254

Van der Made J (1997a) Los Suoidea de la Península Ibérica. In: Calvo JP, Morales J (eds) Avances en el Conocimiento del Terciario Ibérico. Cuenca, pp 109–112

Van der Made J (1997b) Systematics and stratigraphy of the genera *Taucanamo* and *Schizochoerus* and a classification of the Palaeochoeridae (Suoidea, Mammalia). Proc Kon Ned Akad v Wetensh 100:127–139

Van der Made J (1997c) The fossil pig from the Late Miocene of Dorn Dürkheim 1 in Germany. Cour Forsch-Inst Senck 197:205–230

Van der Made J (1998) *Aureliachoerus* from Oberdorf and other Aragonian pigs from Styria. Ann Naturhist Mus Wien 99A:225–277

Van der Made J (1999) Biometrical trends in the Tetraconodontinae, a subfamily of pigs. Trans R Soc Edinburgh Earth Sci 89:199–225

Van der Made J (2003) Suoidea (Artiodactyla). In: Fortelius M, Kappelman J, Sen S, Bernor RL (eds) Geology and Paleontology of the Miocene Sinap Formation, Turkey. Columbia University Press, New York, pp 308–327

Van der Made J (2010) The pigs and "Old World peccaries" (Suidae and Palaeochoeridae, Suoidea, Artiodactyla) from the Miocene of Sandelzhausen (southern Germany): phylogeny and an updated classification of the Hyotheriinae and Palaeochoeridae. Paläont Zeits 84:43–121

Van der Made J (2020) The Suoidea from the Middle Miocene of Gračanica (Bugojno Basin, Bosnia and Herzegovina)—evolution, taxononomy, and biostratigraphy. Palaeobiodiv Palaeoenvir 100:321–349

Van der Made J, Aiglstorfer M, Böhme M (2014) Taxonomic study of the pigs (Suidae, Mammalia) from the late Middle Miocene of Gratkorn (Austria, Syria). Palaeobio Palaeoenv 94:595–617

Van der Made J, Belinchón M (1991) *Korynochoerus palaeochoerus* from the uppermost Miocene of Alcoy. Rev Esp Paleontol Vol. Ext.:173–184

Van der Made J, Güleç E, Erkman AC (2013) *Microstonyx* (Suidae, Artiodactyla) from the Upper Miocene of Hayranlı-Haliminhanı, Turkey. Turkish J Zool 37:106–122

Van der Made J, Han D (1994) Suoidea from the Upper Miocene hominoid locality of Lufeng, Yunnan province, China. Proc Kon Ned Akad v Wetensch 97:27–82

Van der Made J, Hussain ST (1989) *"Microstonyx" major* (Suidae, Artiodactyla) from the type area of the Nagri Formation, Siwalik group, Pakistan. Estud Geol 45:409–416

Van der Made J, Krakhmalnaya T, Kubiak H (1999) The pig *Propotamochoerus palaeochoerus* from the Upper Miocene of Grytsiv, Ukraine. Estud Geol 55:283–292

Van der Made J, Montoya P, Alcalá L (1992) *Microstonyx* (Suidae, Mammalia) from the Upper Miocene of Spain. Geobios 25:395–413

Van der Made J, Morales J (1999) *Aureliachoerus* (Suidae, Mammalia) from Agreda and other Miocene localities of Spain. Geobios 32:901–914

Van der Made J, Moyà-Solà S (1989) European Suinae (Artiodactyla) from the Late Miocene onwards. Boll Soc Paleontol Ital 28:329–339

Van der Made J, Salesa MJ (2004) Early remains of the pig *Conohyus simorrensis* from the Middle Aragonian of Somosaguas near Madrid - Its dispersal into Europe and evolution. N Jb Geol Paläont Abh 233:153–168

Van der Made J, Tuna V (1999) A tetraconodontine pig from the Upper Miocene of Turkey. Trans R Soc Edinburgh Earth Sci 89:227–230

von Meyer H (1846) Mittheilungen an Professor Bronn gerichtet. N Jb Min Geol Geog Petref 1846:462–476

Zapfe H (1949) Die Säugetierfauna aus dem Unterpliozän von Gaiselberg bei Zistersdorf in Niederösterreich. Jb Geol Bundes 93:83–97

Figure captions

Fig. 1 a–b. Aerial photographs from 1994 (**a**) and 2019 (**b**) showing the location of CCN20 (asterisk) on the western margin of the former quarry of Creu de Conill, subsequently transformed into the debris deposit of Can

Guitard, and currently restored; base images © Institut Cartogràfic i Geològic de Catalunya; coordinates UTM (ETRS89) 31N 418105 E, 4598340 N. **c–e**. Different views of the CCN20 excavation in 2016 (**c**), 2019 (**d**), and 2018 (**e**); pictures by the authors, © Institut Català de Paleontologia Miquel Crusafont. **f**. Simplified geological map of the Vallès-Penedès Basin within the Iberian Peninsula, indicating the location of Creu de Conill localities (CCN, yellow star); modified from Casanovas-Vilar et al. (2016a)

Fig. 2 Suid maxillary remains from CCN20. **a**. IPS28739, maxilla with R P2–M3 and L P2–M3 of *Propotamochoerus palaeochoerus*, in L lateral (*above*), R lateral (*below*), and occlusal (*right*) views; **b**. IPS113819, R maxillary fragment with P3–P4 of *Parachleuastochoerus valentini*, in lingual (*left*), buccal (*middle*), and occlusal (*right*) views; **c**. IPS114251, R maxillary fragment with M1–M3 of *Pa. valentini*, in lingual (*above*), buccal (*below*), and occlusal (*right*) views. Scale bar equals 1 cm

Fig. 3. Suid permanent upper incisors and canines from CCN20. **a**. IPS107919, L I2 of *Propotamochoerus palaeochoerus*, in lingual (*left*), mesial (*midle left*), labial (*middle right*), and distal (*right*) views; **b**. IPS124843, R C1f of *P. palaeochoerus*, in lingual (*left*), mesial (*midle left*), labial (*middle right*), and distal (*right*) views; **c**. IPS113643, L C1f of *P. palaeochoerus*, in lingual (*left*), mesial (*midle left*), labial (*middle right*), and distal (*right*) views; **d**. IPS106329, R C1f of *Parachleuastochoerus valentini*, in lingual (*left*), mesial (*midle left*), labial (*middle right*), and distal (*right*) views. Scale bar equals 1 cm

Fig. 4. Suid permanent upper cheek teeth from CCN20. **a, c–d, f–g, i–j, n–o, y–z, f'–g'**. IPS28739, maxilla of *Propotamochoerus palaeochoerus*: R P1 (**a**), in occlusal (*left*), lingual (*middle*), and buccal (*right*) views; R P2 (**c**), in occlusal (*left*) and buccal (*right*) views; L P2 (**d**), in occlusal (*left*) and buccal (*right*) views; R P3 (**f**), in occlusal (*left*) and buccal (*right*) views; L P3 (**g**), in occlusal (*left*) and buccal (*right*) views; R P4 (**i**), L P4 (**j**), R M1 (**n**), L M1 (**o**), R M2 (**y**), L M2 (**z**), R M3 (**f'**), and L M3 (**g'**), in occlusal views; **b**. IPS114242, L P1 of *P. palaeochoerus*, in occlusal (*left*), lingual (*middle*), and buccal (*right*) views; **e**. IPS124328, R P2 of *Parachleuastochoerus valentini*, in occlusal (*left*), lingual (*middle*), and buccal (*right*) views; **h, m**. IPS113819, maxillary fragment of *Pa. valentini*: R P3 (**h**), in lingual (*left*), buccal (*middle*), and occlusal (*right*) views; R P4 (**m**), in occlusal view; **k**. IPS107194, R P4 of *P. palaeochoerus*, in occlusal view; **l**. IPS124437, L P4 (buccal fragment) of *P. palaeochoerus*, in occlusal view; **p**. IPS128040, R M1 of *P. palaeochoerus*, in occlusal view; **q**. IPS113741, R M1 germ of *P. palaeochoerus*; **r**. IPS107114, partial R M1 germ of *P. palaeochoerus*, in occlusal view; **s**. IPS114191, R M1 of *P. palaeochoerus*, in occlusal view; **t**. IPS114098, L M1 of *P. palaeochoerus*, in occlusal view; **u, b', j'**. IPS114251, maxillary fragment of *Pa. valentini*: R M1 (**u**), R M2 (**b'**), and R M3 (**j'**), in occlusal views; **v**. IPS95729, R M1 germ (mesial fragment) of *P. palaeochoerus*, in occlusal view; **w**. IPS125680, R M1 germ (mesiolingual fragment) of *P. palaeochoerus*, in occlusal view; **x**. IPS113642, R M1 (distal fragment) of *Pa. valentini*, in occlusal view; **a'**. IPS128039, R M2 of *P. palaeochoerus*, in occlusal view; **c'**. IPS114227, R M2 germ (mesial and distal fragments) of *P. palaeochoerus*, in occlusal view; **d'**. IPS114241, L M2 germ (mesial fragment) of *P. palaeochoerus*, in occlusal view; **e'**. IPS107901, L M2 germ (mesial fragment) of *P. palaeochoerus*, in occlusal view; **h'**. IPS128038, R M3 of *P. palaeochoerus*, in occlusal view; **i'**. IPS95697, L M3 (distobuccal fragment) of *Pa. valentini*, in occlusal view. Scale bar equals 1 cm

Fig. 5. Suid mandibular remains from CCN20. **a**. IPS107069, crushed mandible with R p2–m3 and L p3–m3 of *Propotamochoerus palaeochoerus*, in L lateral (*above*), R lateral (*below*), and occlusal (*right*) views: **b**. IPS114386, partial mandible with R p3–m3 and L p3–m3 of *P. palaeochoerus*, in L lateral (*above*), R lateral (*below*), and occlusal (*right*) views. Scale bar equals 1 cm

Fig. 6. Suid mandibular remains from CCN20. **a**. IPS114003, R mandibular fragment with c1f germ and dp3–m1 of *Propotamochoerus palaeochoerus*, in lingual (*above*), buccal (*below*), and occlusal (*right*) views; **b**. IPS95623, R mandibular fragment with c1m fragment and m2–m3 of *P. palaeochoerus*, in lingual (*above*), buccal (*below*), and occlusal (*right*) views; **c–d**. IPS124336a (**c**), L mandibular fragment with dp4–m1, and IPS124336b (**d**), R mandibular fragment with dp3–m1 of *P. palaeochoerus*, in lingual (*above*), buccal (*below*), and occlusal (*right*) views. **e**. IPS124841, R mandibular fragment with partial dp4 of *P. palaeochoerus*, in lingual (*above*), buccal (*below*), and occlusal (*right*) views. Scale bar equals 1 cm

Fig. 7. Suid permanent lower incisors from CCN20. **a**. IPS107181, R i1 (apical crown fragment) of *Propotamochoerus palaeochoerus*, in lingual (*left*), mesial (*middle left*), labial (**a3**), and distal (**a4**) views; **b**. IPS107801, L i1 (apical crown fragment) of *Propotamochoerus palaeochoerus*, in lingual (*left*), mesial (*middle left*), labial (*middle right*), and distal (*right*) views; **c**. IPS114264, R i1 (partial crown) of *Propotamochoerus palaeochoerus*, in lingual (*left*), mesial (*middle left*), labial (*middle right*), and distal (*right*) views; **d**. IPS107212, R i1 (root) of *P. palaeochoerus*, in lingual (*left*), mesial (*middle left*), labial (*middle right*), and distal (*right*) views; **e**. IPS124324, L i1 of *P. palaeochoerus*, in lingual (*left*), mesial (*middle left*), labial (*middle right*), and distal (*right*) views; **f**. IPS114496, R i1 (mesial fragment) of *P. palaeochoerus*, in lingual (*left*), mesial (*middle*), and labial (*right*) views; **g**. IPS113817, R i2 (crown) of *P. palaeochoerus*, in lingual (*left*), mesial (*middle left*), labial (*middle right*), and distal (*right*) views; **h**. IPS28725, R i2 (crown) of *P. palaeochoerus*, in lingual (*left*), mesial (*middle left*), labial (*middle right*), and distal (*right*) views; **i**. IPS106358, L i2 of *P. palaeochoerus*, in lingual (*left*), mesial (*middle left*), labial (*middle right*), and distal (*right*) views; **j**. IPS107877, R i2 of *P. palaeochoerus*, in lingual (*left*), mesial (*middle left*), labial (*middle right*), and distal (*right*) views; **k**. IPS124327, L i2 of *P. palaeochoerus*, in lingual (*left*), mesial (*middle left*), labial (*middle right*), and distal (*right*) views; **l**. IPS124322, L i2 of *P. palaeochoerus*, in lingual (*left*), mesial (*middle left*), labial (*middle right*), and distal (*right*) views; **m**. IPS114337, R i2 of *Parachleuastochoerus valentini*, in lingual (*left*), mesial (*middle left*), labial (*middle right*), and distal (*right*) views; **n**. IPS124334, L i2 of cf. *Albanohyus* sp., in lingual (*left*), mesial (*middle left*), labial (*middle right*), and distal (*right*) views; **o**. IPS113932, R i2 of cf. *Albanohyus* sp., in lingual (*left*), mesial (*middle left*), labial (*middle right*), and distal (*right*) views; **p**. IPS113840, R i3 of *P. palaeochoerus*, in lingual (*left*), mesial (*middle left*), labial (*middle right*), and distal (*right*) views. **q**. IPS124323, L i3 of *P. palaeochoerus*, in lingual (*left*), mesial (*middle left*), labial (*middle right*), and distal (*right*) views; **r**. IPS114221, R i3 of *P. palaeochoerus*, in lingual (*left*), mesial (*middle left*), labial (*middle right*), and distal (*right*) views; **s**. IPS114299, L i3 of *P. palaeochoerus*, in lingual (*left*), mesial (*middle left*), labial (*middle right*), and distal (*right*) views; **t**. IPS113983, L i3 of *P. palaeochoerus*, in lingual (*left*), mesial (*middle left*), labial (*middle right*), and distal (*right*) views. Scale bar equals 1 cm

Fig. 8. Suid permanent lower canines from CCN20. **a.** IPS124330, R c1f of *Propotamochoerus palaeochoerus*, in lingual (**a1**), mesial (**a2**), labial (**a3**), and distal (**a4**) views; **b**. IPS114311, partial R c1f of *P. palaeochoerus*, in lingual (**b1**), mesial (**b2**), labial (**b3**), and distal (**b4**) views; **c**. IPS114338, R c1f (damaged) of *P. palaeochoerus*, in lingual (**c1**), mesial (**c2**), labial (**c3**), and distal (**c4**) views; **d**. IPS107072, R c1f of *Parachleuastochoerus valentini*, in lingual (**d1**), mesial (**d2**), labial (**d3**), and distal (**d4**) views; **e**. IPS114387, R c1f of *Pa. valentini*, in lingual (**e1**), mesial (**e2**), labial (**e3**), and distal (**e4**) views; **f**. IPS113663, partial R c1m of *P. palaeochoerus*, in lingual (**f1**), mesial (**f2**), labial (**f3**), and distal (**f4**) views; **g**. IPS113857, L c1m (damaged) of *P. palaeochoerus*, in lingual (**g1**), mesial (**g2**), labial (**g3**), and distal (**g4**) views; **h**. IPS113964, partial R c1m of *P. palaeochoerus*, in lingual (**h1**), mesial (**h2**), labial (**h3**), and distal (**h4**) views. Scale bar equals 1 cm

Fig. 9. Suid permanent lower cheek teeth from CCN20. **a**. IPS107146, L p1 of *Propotamochoerus palaeochoerus*, in occlusal (*left*), lingual (*middle*), and buccal (*right*) views; **b**. IPS107648, R p1 crown of *P. palaeochoerus*, in occlusal (*left*), lingual (*middle*), and buccal (*right*) views; **c**. IPS95728, R p1 germ of *P. palaeochoerus*, in occlusal (*left*), lingual (*middle*), and buccal (*right*) views; **d**. IPS114342, R p1 (distal fragment) of *P. palaeochoerus*, in occlusal (*left*), lingual (*middle*), and buccal (*right*) views; **e**. IPS95813, R p1 germ (partial) of *Parachleuastochoerus valentini*, in occlusal (*left*), lingual (*middle*), and buccal (*right*) views; **f**. IPS114339, L p2 of *P. palaeochoerus*, in occlusal (*left*), lingual (*middle*), and buccal (*right*) views; **g**. IPS28732, R p2 of *P. palaeochoerus*, in occlusal (*left*), lingual (*middle*), and buccal (*right*) views; **h, j, n, x, c'**. IPS107069, mandible of *P. palaeochoerus*: R p2 (**h**), in occlusal (*left*) and buccal (*right*) views; L p3 (**j**), in occlusal (*left*), lingual (*middle*), and buccal (*right*) views; L p4 (**n**), in occlusal (*left*), lingual (*middle*), and buccal (*right*) views; L m2 (**x**) and L m3 (**c'**), in occlusal views; **i**. IPS114256, R p2 of *P. palaeochoerus*, in occlusal (*left*), lingual (*middle*), and buccal (*right*) views; **k–l, o–p, s, y, d'**. IPS114386, partial mandible of *P. palaeochoerus*: L p3 (**k**), in occlusal (*left*) and buccal (*right*) views; R p3 (**l**), in occlusal (*left*) and buccal (*right*) views; L p4 (**o**), in occlusal (*left*) and buccal (*right*) views; R p4 (**p**), in occlusal (*left*) and buccal (*right*) views; L m1 (**s**), R m2 (**y**), and L m3 (**d'**), in occlusal views; **m**. IPS113968, L p3 of *P. palaeochoerus*, in occlusal (*left*), lingual (*middle*), and buccal (*right*) views; **q**. IPS113818, R m1 of Suidae indet., in occlusal view; **r**. IPS28737, L m1 germ (mesial fragment) of *P. palaeochoerus*, in occlusal view; **t**. IPS114003, R m1 of *P. palaeochoerus*, in occlusal view; **u**. IPS95707, R m1 germ of *P. palaeochoerus*, in occlusal view; **v**. IPS107263, R m1 germ of *P. palaeochoerus*, in occlusal view; **w**. IPS124336a, L m1 of *P. palaeochoerus*, in occlusal view; **z, e'**. IPS95623, mandibular fragment of *P. palaeochoerus*: R m2 (**z**) and R m3 (**d'**), in occlusal views; **a'**. IPS113969, L m2 of *P. palaeochoerus*, in occlusal view; **b'**. IPS113845, R m2 (mesial fragment) of *P. palaeochoerus*, in occlusal view; **f'**. IPS113843, R m3 (distal fragment) of *P. palaeochoerus*, in occlusal view; **g'**. IPS107717, R m3 (talonid fragment) of *P. palaeochoerus*, in occlusal view; **h'**. IPS114049, L m3 (talonid fragment) of *P. palaeochoerus*, in occlusal view. Scale bar equals 1 cm

Fig. 10. Suid deciduous upper teeth from CCN20. **a**. IPS107830, R DI1 of *P. palaeochoerus*, in lingual (*left*), mesial (*middle left*), labial (*middle right*), and distal (*right*) views; **b**. IPS95713, L DI1 of *P. palaeochoerus*, in lingual (*left*), mesial (*middle left*), labial (*middle right*), and distal (*right*) views; **c**. IPS113900, R DI1 crown of *P. palaeochoerus*, in lingual (*left*), mesial (*middle left*), labial (*middle right*), and distal (*right*) views; **d**. IPS124844, L DI1 of *P. palaeochoerus*, in lingual (*left*), mesial (*middle left*), labial (*middle right*), and distal

(*right*) views; **e**. IPS107110, L DI1 of Suidae indet., in lingual (*left*), mesial (*middle left*), labial (*middle right*), and distal (*right*) views; **f**. IPS95667, R DI2 of *P. palaeochoerus*, in lingual (*left*), mesial (*middle left*), labial (*middle right*), and distal (*right*) views; **g**. IPS95662, L DI2 of *P. palaeochoerus*, in lingual (*left*), mesial (*middle left*), labial (*middle right*), and distal (*right*) views; **h**. IPS124326, L DI3 of *P. palaeochoerus*, in lingual (*left*), mesial (*middle left*), labial (*middle right*), and distal (*right*) views; **i, n, u**. IPS113741, isolated teeth of *P. palaeochoerus*: R DP2 (**i**), in occlusal (*left*), lingual (*middle*), and buccal (*right*) views; partial R DP3 (**n**) and R DP4 (**u**), in occlusal views; **j**. IPS124325, L DP2 (mesial fragment) of *P. palaeochoerus*, in occlusal (*left*), lingual (*middle*), and buccal (*right*) views; **k, o, v–w**. IPS114191, isolated teeth of *P. palaeochoerus*: distal fragment of R DP2 (**k**), in occlusal (*left*), lingual (*middle*), and buccal (*right*) views; distal fragment of L DP3 (**n**), R DP4 (**v**), and L DP4 (**w**), in occlusal views; **l**. IPS114228, L DP2 (distal fragment) of *P. palaeochoerus*, in occlusal (*left*), lingual (*middle*), and buccal (*right*) views; **m**. IPS113669, partial R DP2 of *P. palaeochoerus*, in occlusal (*left*), lingual (*middle*), and buccal (*right*) views; **p**. IPS95632, R DP3 (distal fragment) of *P. palaeochoerus*, in occlusal view; **q**. IPS113800, partial R DP3 of *P. palaeochoerus*, in occlusal view; **r**. IPS114230, L DP3 of *Pa. valentini*, in occlusal view; **s**. IPS113955, R DP3 germ (distal fragment) of *Pa. valentini*, in occlusal view; **t**. IPS107104, L DP3 (distal fragment) of *Pa. valentini*, in occlusal view; **x**. IPS113914, L DP4 (buccal fragment) of *P. palaeochoerus*, in occlusal view; **y**. IPS114048, R DP4 of *Pa. valentini*, in occlusal view; **z**. IPS107687, L DP4 of *Pa. valentini*, in occlusal view; **a'**. IPS124331, L DP4 of *Pa. valentini*, in occlusal view; **b'**. IPS125678, L DP4 (buccal fragment) of *Pa. valentini*, in occlusal view; **c'**. IPS107883, L DP4 (buccal fragment) of *Pa. valentini*, in occlusal view. Scale bar equals 1 cm

Fig. 11. Suid deciduous lower teeth from CCN20. **a**. IPS124335, L di1 of *Propotamochoerus palaeochoerus*, in lingual (*left*), mesial (*middle left*), labial (*middle right*), and distal (*right*) views; **b**. IPS114535, R di1 of *P. palaeochoerus*, in lingual (*left*), mesial (*middle left*), labial (*middle right*), and distal (*right*) views; **c**. IPS28730, R di1 of *P. palaeochoerus*, in lingual (*left*), mesial (*middle left*), labial (*middle right*), and distal (*right*) views; **d**. IPS106511, L di1 of *P. palaeochoerus*, in lingual (*left*), mesial (*middle left*), labial (*middle right*), and distal (*right*) views; **e**. IPS124845, L di1 crown of *P. palaeochoerus*, in lingual (*left*), mesial (*middle left*), labial (*middle right*), and distal (*right*) views; **f**. IPS107725, L di1 germ of cf. *Parachleuastochoerus valentini*, in lingual (*left*), mesial (*middle left*), labial (*middle right*), and distal (*right*) views; **g**. IPS107976, L di1 of cf. *Pa. valentini*, in lingual (*left*), mesial (*middle left*), labial (*middle right*), and distal (*right*) views; **h**. IPS124333, R di2 (distal fragment) of *P. palaeochoerus*, in lingual (*left*) and distal (*right*) views; **i**. IPS107839, R di3 of *P. palaeochoerus*, in lingual (*left*), mesial (*middle left*), labial (*middle right*), and distal (*right*) views; **j**. IPS95719, L di3 of *P. palaeochoerus*, in lingual (*left*), mesial (*middle left*), labial (*middle right*), and distal (*right*) views; **k**. IPS107685, L di3 of *P. palaeochoerus*, in lingual (*left*), mesial (*middle left*), labial (*middle right*), and distal (*right*) views; **l**. IPS124332, R dp2 (distally damaged) of *P. palaeochoerus*, in occlusal (*left*), lingual (*middle*), and buccal (*right*) views; **m**. IPS107121, L dp2 (mesial fragment) of *P. palaeochoerus*, in occlusal (*left*), lingual (*middle*), and buccal (*right*) views; **n**. IPS107099, R dp2 of *P. palaeochoerus*, in occlusal (*left*), lingual (*middle*), and buccal (*right*) views; **o, t–w**. IPS124336a–b, mandibular fragments of *P. palaeochoerus*: partial L dp2 (**o**), in occlusal (*left*), lingual (*middle*), and buccal (*right*) views; R dp3 (**t**), in occlusal (*left*), lingual (*middle*), and buccal (*right*) views; L dp3 (**u**), in occlusal (*left*), lingual (*middle*), and buccal (*right*) views; L dp4 (**v**) and R dp4 (**w**), in occlusal views; **p**. IPS114102, R dp2? of cf. *Pa. valentini*, in occlusal (*left*), lingual (*middle*), and buccal

(*right*) views; **q, x**. IPS114003, mandibular fragment of *P. palaeochoerus*: R dp3 (**q**), in occlusal (*left*), lingual (*middle*), and buccal (*right*) views; R dp4 (**x**), in occlusal view; **r, z**. IPS124841, mandibular fragment of *P. palaeochoerus*: R dp3 crown (**r**), in occlusal (*left*), lingual (*middle*), and buccal (*right*) views; R dp4 mesial fragment (**z**), in occlusal view; **s**. IPS125679, L dp3 of *P. palaeochoerus*, in occlusal (*left*), lingual (*midle*), and buccal (*right*) views; **y**. IPS124842, R dp4 of *P. palaeochoerus*, in occlusal view; **a'**. IPS124329, L dp4 (mesial fragment) of *P. palaeochoerus*, in occlusal view; **b'**. IPS114001, L dp4 (distal fragment) of *P. palaeochoerus*, in occlusal view. Scale bar equals 1 cm

Fig. 12. Bivariate plots of BL vs. MD in the deciduous and permanent upper premolars of *Propotamochoerus palaeochoerus* and *Parachleuastochoerus valentini* from CCN20 as compared with *P. palaeochoerus* and *Pa. valentini* from elsewhere, as well as *Propotamochoerus aegaeus*, *Propotamochoerus hyotherioides*, *Propotamochoerus hysudricus*, *Propotamochoerus provincialis*, and *Hippopotamodon major*. Data for the CCN20 remains are reported in Appendix Table 1, while those for the comparative sample have been taken from the literature (see Materials and Methods for details on the published sources).

Fig. 13. Bivariate plots of BL vs. MD in the upper molars of *Propotamochoerus palaeochoerus* and *Parachleuastochoerus valentini* from CCN20 as compared with *P. palaeochoerus* and *Pa. valentini* from elsewhere, as well as *Propotamochoerus aegaeus*, *Propotamochoerus hyotherioides*, *Propotamochoerus hysudricus*, *Propotamochoerus provincialis*, and *Hippopotamodon major*. Data for the CCN20 remains are reported in Appendix Table 1, while those for the comparative sample have been taken from the literature (see Materials and Methods for details on the published sources).

Fig. 12. Bivariate plots of BL vs. MD in the deciduous and permanent lower premolars of *Propotamochoerus palaeochoerus* and *Parachleuastochoerus valentini* from CCN20 as compared with *P. palaeochoerus* and *Pa. valentini* from elsewhere, as well as *Propotamochoerus aegaeus*, *Propotamochoerus hyotherioides*, *Propotamochoerus hysudricus*, *Propotamochoerus provincialis*, and *Hippopotamodon major*. Data for the CCN20 remains are reported in Appendix Table 1, while those for the comparative sample have been taken from the literature (see Materials and Methods for details on the published sources).

Fig. 15. Bivariate plots of BL vs. MD in the lower molars of *Propotamochoerus palaeochoerus* from CCN20 as compared with *P. palaeochoerus* and *Parachleuastochoerus valentini* from elsewhere, as well as *Propotamochoerus aegaeus*, *Propotamochoerus hyotherioides*, *Propotamochoerus hysudricus*, *Propotamochoerus provincialis*, and *Hippopotamodon major*. Data for the CCN20 remains are reported in Appendix Table 1, while those for the comparative sample have been taken from the literature (see Materials and Methods for details on the published sources).

Fig. 16. Results of the principal components analyses (PCAs) based on Mosimann shape variables derived from upper and lower cheek tooth measurements (see Online Resources 1–3), as depicted by bivariate plots of: **a**. PC2 vs. PC1 (upper cheek teeth); **b**. PC3 vs. PC1 (upper cheek teeth); **c**. PC2 vs. PC1 (lower cheek teeth).

Percentages of variance explained by each axis are reported within parentheses. The biplot with the variable loadings is depicted for each plot.

Table 1 List of suid dental remains from CCN20 described in this paper, including taxonomic attribution, anatomical identification, and the figure(s) where each specimen is depicted.

Catalog No.	Species	Description	Figures
IPS28739	*P. palaeochoerus*	Maxilla with R P2–M3 and L P2–M3 + isolated R P1	Figs. 2a and 4a, c–d, f–g, i–j, n–o, y–z, f'–g'
IPS113819	*Pa. valentini*	R maxillary fragment with P3–P4	Figs. 2b and 4h, m
IPS114251	*Pa. valentini*	R maxillary fragment with M1–M3	Figs. 2c and 4u, b', j'
IPS107069	*P. palaeochoerus*	Crushed mandible with R p2–m3 and L p3–m3	Figs. 5a and 9h, j, n, x, c'
IPS114386	*P. palaeochoerus*	Partial mandible with R p3–m3 and L p3–m3	Figs. 5b and 9k–l, o–p, s, y, d'
IPS114003	*P. palaeochoerus*	R mandibular fragment with c1f germ and dp3–m1	Figs. 6a, 9t, 11q, x
IPS95623	*P. palaeochoerus*	R mandibular fragment with c1m fragment and m2–m3	Figs. 6b and 9z, e'
IPS124336a–b	*P. palaeochoerus*	L (a) + R (b) mandibular fragments with dp3–m1 (+ isolated L dp2 crown)	Figs. 6c–d, 9w, 11o, t–w
IPS124841	*P. palaeochoerus*	R mandibular fragment with dp4 (partial) + isolated R dp3 crown	Figs. 6e and 11r, z
IPS107919	*P. palaeochoerus*	L I2	Fig. 3a
IPS124843	*P. palaeochoerus*	R C1f	Fig. 3b
IPS113643	*P. palaeochoerus*	L C1f	Fig. 3c
IPS106329	*Pa. valentini*	R C1f	Fig. 3d
IPS114242	*P. palaeochoerus*	L P1	Fig. 4b
IPS124328	*Pa. valentini*	R P2	Fig. 4e
IPS107194	*P. palaeochoerus*	R P4	Fig. 4k
IPS124437	*P. palaeochoerus*	L P4 (labial fragment)	Fig. 4l
IPS128040	*P. palaeochoerus*	R M1	Fig. 4p
IPS113741	*P. palaeochoerus*	R DP2 + R DP3 + R DP4 + R M1 germ	Figs. 4q and 10i, n, u
IPS107114	*P. palaeochoerus*	R M1 germ (partial)	Fig. 4r
IPS114191	*P. palaeochoerus*	R DP2 (distal fragment) + L DP3 (distal fragment) + R DP4 + L DP4 + R M1	Figs. 4s and 10k, o, v–w

IPS114098	*P. palaeochoerus*	L M1	Fig. 4t
IPS95729	*P. palaeochoerus*	R M1 germ (mesial fragment)	Fig. 4v
IPS125680	*P. palaeochoerus*	R M1 germ (mesiolingual fragment)	Fig. 4w
IPS113642	*Pa. valentini*	R M1 (distal fragment)	Fig. 4x
IPS128039	*P. palaeochoerus*	R M2 (damaged)	Fig. 4a'
IPS114227	*P. palaeochoerus*	R M2 germ (mesial and distal fragments)	Fig. 4c'
IPS114241	*P. palaeochoerus*	L M2 germ (mesial fragment)	Fig. 4d'
IPS107901	*P. palaeochoerus*	L M2 germ (mesial fragment)	Fig. 4e'
IPS128038	*P. palaeochoerus*	R M3 (distalmost end missing)	Fig. 4h'
IPS95697	*Pa. valentini*	L M3 (distobuccal fragment)	Fig. 4i'
IPS107181	*P. palaeochoerus*	R i1 (apical crown fragment)	Fig. 7a
IPS107801	*P. palaeochoerus*	L i1 (apical crown fragment)	Fig. 7b
IPS114264	*P. palaeochoerus*	R i1 (partial crown)	Fig. 7c
IPS107212	*P. palaeochoerus*	R i1 (root)	Fig. 7d
IPS124324	*P. palaeochoerus*	L i1	Fig. 7e
IPS114496	*P. palaeochoerus*	R i1 (mesial fragment)	Fig. 7f
IPS113817	*P. palaeochoerus*	R i2 (crown)	Fig. 7g
IPS28725	*P. palaeochoerus*	R i2 (crown)	Fig. 7h
IPS106358	*P. palaeochoerus*	L i2	Fig. 7i
IPS107877	*P. palaeochoerus*	R i2	Fig. 7j
IPS124327	*P. palaeochoerus*	L i2	Fig. 7k
IPS124322	*P. palaeochoerus*	L i2 (crown)	Fig. 7l
IPS114337	*Pa. valentini*	R i2	Fig. 7m
IPS124334	*Albanohyus* sp.	L i2	Fig. 7n

IPS113932	*Albanohyus* sp.	R i2	Fig. 7o
IPS113840	*P. palaeochoerus*	R i3	Fig. 7p
IPS124323	*P. palaeochoerus*	L i3	Fig. 7q
IPS114221	*P. palaeochoerus*	R i3	Fig. 7r
IPS114299	*P. palaeochoerus*	L i3	Fig. 7s
IPS113983	*P. palaeochoerus*	L i3	Fig. 7t
IPS124330	*P. palaeochoerus*	R c1f	Fig. 8a
IPS114311	*P. palaeochoerus*	R c1f (partial)	Fig. 8b
IPS114338	*P. palaeochoerus*	R c1f (damaged)	Fig. 8c
IPS107072	*Pa. valentini*	R c1f	Fig. 8d
IPS114387	*Pa. valentini*	R c1f	Fig. 8e
IPS113663	*P. palaeochoerus*	R c1m (partial, in two fragments)	Fig. 8f
IPS113857	*P. palaeochoerus*	L c1m (damaged)	Fig. 8g
IPS113964	*P. palaeochoerus*	R c1m (tip missing)	Fig. 8h
IPS107146	*P. palaeochoerus*	L p1	Fig. 9a
IPS107648	*P. palaeochoerus*	R p1 crown	Fig. 9b
IPS95728	*P. palaeochoerus*	R p1 germ	Fig. 9c
IPS114342	*P. palaeochoerus*	R p1 (distal fragment)	Fig. 9d
IPS95813	*Pa. valentini*	R p1 germ (partial)	Fig. 9e
IPS114339	*P. palaeochoerus*	L p2	Fig. 9f
IPS28732	*P. palaeochoerus*	R p2	Fig. 9g
IPS114256	*P. palaeochoerus*	R p2	Fig. 9i
IPS113968	*P. palaeochoerus*	L p3	Fig. 9m
IPS113818	Suidae indet.	R m1	Fig. 9q

IPS28737	*P. palaeochoerus*	L m1 germ (mesial fragment)	Fig. 9r
IPS95707	*P. palaeochoerus*	R m1 germ	Fig. 9u
IPS107263	*P. palaeochoerus*	R m1 germ	Fig. 9v
IPS113969	*P. palaeochoerus*	L m2	Fig. 9a'
IPS113845	*P. palaeochoerus*	R m2 (mesial fragment)	Fig. 9b'
IPS113843	*P. palaeochoerus*	R m3 (distal fragment)	Fig. 9f'
IPS107717	*P. palaeochoerus*	R m3 (talonid fragment)	Fig. 9g'
IPS114049	*P. palaeochoerus*	L m3 (talonid fragment)	Fig. 9h'
IPS107830	*P. palaeochoerus*	R DI1	Fig. 10a
IPS95713	*P. palaeochoerus*	L DI1	Fig. 10b
IPS113900	*P. palaeochoerus*	R DI1 crown	Fig. 10c
IPS124844	*P. palaeochoerus*	L DI1	Fig. 10d
IPS107110	Suidae indet.	L DI1	Fig. 10e
IPS95667	*P. palaeochoerus*	R DI2	Fig. 10f
IPS95662	*P. palaeochoerus*	L DI2	Fig. 10g
IPS124326	*P. palaeochoerus*	L DI3	Fig. 10h
IPS124325	*P. palaeochoerus*	L DP2 (mesial fragment)	Fig. 10j
IPS114228	*P. palaeochoerus*	L DP2 (distal fragment)	Fig. 10l
IPS113669	*P. palaeochoerus*	Partial R DP2 (mesial end missing)	Fig. 10m
IPS95632	*P. palaeochoerus*	R DP3 (distal fragment)	Fig. 10p
IPS113800	*P. palaeochoerus*	R DP3 (partial)	Fig. 10q
IPS114230	*Pa. valentini*	R DP3	Fig. 10r
IPS113955	*Pa. valentini*	R DP3 germ (distal fragment)	Fig. 10s
IPS107104	*Pa. valentini*	R DP3 (distal fragment)	Fig. 10t

IPS113914	*P. palaeochoerus*	L DP4 (buccal fragment)	Fig. 10x
IPS114048	*Pa. valentini*	R DP4	Fig. 10y
IPS107687	*Pa. valentini*	L DP4	Fig. 10z
IPS124331	*Pa. valentini*	L DP4	Fig. 10a'
IPS125678	*Pa. valentini*	L DP4 (buccal fragment)	Fig. 10b'
IPS107883	*Pa. valentini*	L DP4 (buccal fragment)	Fig. 10c'
IPS124335	*P. palaeochoerus*	L di1	Fig. 11a
IPS114535	*P. palaeochoerus*	R di1	Fig. 11b
IPS28730	*P. palaeochoerus*	R di1	Fig. 11c
IPS106511	*P. palaeochoerus*	L di1	Fig. 11d
IPS124845	*P. palaeochoerus*	L di1 crown	Fig. 11e
IPS107725	cf. *Pa. valentini*	L di1 germ	Fig. 11f
IPS107976	cf. *Pa. valentini*	L di1	Fig. 11g
IPS124333	*P. palaeochoerus*	R di2 (distal fragment)	Fig. 11h
IPS107839	*P. palaeochoerus*	R di3	Fig. 11i
IPS95719	*P. palaeochoerus*	L di3	Fig. 11j
IPS107685	*P. palaeochoerus*	L di3	Fig. 11k
IPS124332	*P. palaeochoerus*	R dp2 (distally damaged)	Fig. 11l
IPS107121	*P. palaeochoerus*	L dp2 (mesial fragment)	Fig. 11m
IPS107099	*P. palaeochoerus*	R dp2	Fig. 11n
IPS114102	cf. *Pa. valentini*	R dp2?	Fig. 11p
IPS125679	*P. palaeochoerus*	L dp3	Fig. 11s
IPS124842	*P. palaeochoerus*	R dp4	Fig. 11y
IPS124329	*P. palaeochoerus*	L dp4 (mesial fragment)	Fig. 11a'

IPS114001 *P. palaeochoerus* L dp4 (distal fragment) Fig. 11b'

Appendix Table 1 Measurements of the suid dental remains from CCN20 described in this paper (in mm). La, Li, and Di measurements refer to c1m only. Measurements within parentheses are estimates, whereas a 'greater than' (>) or 'less than' (<) symbols denotes that the actual measurement would have been higher or lower, respectively, than that provided due to damage, and an 'em dash' (—) indicates that no meaningful measurement can be taken owing to incomplete preservation.

Catalog No.	Species	Tooth	Side	MD	BL/La	BLm/Li	BLd/Di
IPS28725	*P. palaeochoerus*	i2	R	9.1	13.0		
IPS28730	*P. palaeochoerus*	di1	R	4.5	6.1		
IPS28732	*P. palaeochoerus*	p2	R	15.0	7.6		
IPS28737	*P. palaeochoerus*	m1	L	—	13.4		
IPS28739	*P. palaeochoerus*	P1	R	14.2	6.0		
IPS28739	*P. palaeochoerus*	P2	R	16.4	8.7		
IPS28739	*P. palaeochoerus*	P3	R	18.0	16.6		
IPS28739	*P. palaeochoerus*	P4	R	14.3	19.4		
IPS28739	*P. palaeochoerus*	M1	R	19.6	18.7	18.6	18.7
IPS28739	*P. palaeochoerus*	M2	R	25.0	22.6	22.1	22.6
IPS28739	*P. palaeochoerus*	M3	R	34.7	22.5	22.5	21.6
IPS28739	*P. palaeochoerus*	P2	L	16.5	9.1		
IPS28739	*P. palaeochoerus*	P3	L	17.5	16.4		
IPS28739	*P. palaeochoerus*	P4	L	15.6	20.0		
IPS28739	*P. palaeochoerus*	M1	L	20.2	(19.2)	19.0	19.2
IPS28739	*P. palaeochoerus*	M2	L	25.3	22.7	22.7	22.6
IPS28739	*P. palaeochoerus*	M3	L	34.6	21.8	21.8	21.0
IPS95623	*P. palaeochoerus*	m2	R	25.0	17.9	17.2	17.9
IPS95623	*P. palaeochoerus*	m3	R	34.5	18.2	18.2	16.8
IPS95632	*P. palaeochoerus*	DP3	R	—	11.2		

IPS95662	*P. palaeochoerus*	L DI2	L	12.6	6.8		
IPS95667	*P. palaeochoerus*	R DI2	R	12.5	7.0		
IPS95697	*Pa. valentini*	M3	L	>15.5	>11.2	—	—
IPS95707	*P. palaeochoerus*	m1	R	23.0	14.4	14.1	14.4
IPS95713	*P. palaeochoerus*	DI1	L	8.5	5.8		
IPS95719	*P. palaeochoerus*	di3	L	10.0	4.7		
IPS95728	*P. palaeochoerus*	p1	R	12.2	5.1		
IPS95813	*Pa. valentini*	p1	R	>11.2	4.4		
IPS106329	*Pa. valentini*	C1f	R	15.0	10.2		
IPS106358	*P. palaeochoerus*	i2	L	9.2	11.1		
IPS106511	*P. palaeochoerus*	di1	L	4.2	5.5		
IPS107069	*P. palaeochoerus*	p2	R	15.1	7.0		
IPS107069	*P. palaeochoerus*	p3	R	19.5	10.4		
IPS107069	*P. palaeochoerus*	p4	R	21.2	13.2		
IPS107069	*P. palaeochoerus*	m1	R	21.6	(15.1)	(14.7)	(15.1)
IPS107069	*P. palaeochoerus*	m2	R	27.1	(17.8)	(16.6)	(17.8)
IPS107069	*P. palaeochoerus*	m3	R	34.5	(18.9)	(18.9)	(17.6)
IPS107069	*P. palaeochoerus*	p3	L	19.0	10.1		
IPS107069	*P. palaeochoerus*	p4	L	20.4	13.9		
IPS107069	*P. palaeochoerus*	m1	L	<25.2	14.6	(14.4)	14.6
IPS107069	*P. palaeochoerus*	m2	L	25.5	17.9	17.9	17.3
IPS107069	*P. palaeochoerus*	m3	L	36.7	18.5	18.5	(16.5)
IPS107072	*Pa. valentini*	c1f	R	(14.7)	9.4		
IPS107099	*P. palaeochoerus*	dp2	R	(9.0)	4.6		

IPS107104	*Pa. valentini*	DP3	R	—	11.0		
IPS107110	Suidae indet.	DI1	L	8.7	5.4		
IPS107114	*P. palaeochoerus*	M1	R	22.0	(17.8)	>17.6	17.8
IPS107121	*P. palaeochoerus*	dp2	L	—	4.5		
IPS107146	*P. palaeochoerus*	p1	L	12.8	5.5		
IPS107181	*P. palaeochoerus*	i1	R	7.5	>8.6		
IPS107194	*P. palaeochoerus*	P4	R	15.1	17.9		
IPS107212	*P. palaeochoerus*	i1	R	>7.7	—		
IPS107263	*P. palaeochoerus*	m1	R	21.0	13.8	13.3	13.8
IPS107648	*P. palaeochoerus*	p1	R	12.5	5.2		
IPS107685	*P. palaeochoerus*	di3	L	9.4	4.6		
IPS107687	*Pa. valentini*	DP4	L	16.0	15.8	15.7	15.8
IPS107717	*P. palaeochoerus*	m3	R	—	>12.0	—	—
IPS107725	cf. *Pa. valentini*	di1	L	4.9	>5.0		
IPS107801	*P. palaeochoerus*	i1	L	7.6	>8.1		
IPS107830	*P. palaeochoerus*	DI1	R	9.2	6.4		
IPS107839	*P. palaeochoerus*	di3	R	10.0	4.5		
IPS107877	*P. palaeochoerus*	i2	R	9.7	11.8		
IPS107883	*Pa. valentini*	DP4	L	>16.1	—	—	—
IPS107901	*P. palaeochoerus*	M2	L	—	>19.1	—	>19.1
IPS107919	*P. palaeochoerus*	I2	L	15.7	6.9		
IPS107976	cf. *Pa. valentini*	di1	L	4.5	6.0		
IPS113642	*Pa. valentini*	M1	R	—	>16.3	—	>16.3
IPS113643	*P. palaeochoerus*	C1f	L	12.8	9.0		

IPS113663	*P. palaeochoerus*	c1m	R		14.0	14.3	13.1
IPS113669	*P. palaeochoerus*	DP2	R	>10.6	5.9		
IPS113800	*P. palaeochoerus*	DP3	R	17.6	11.6		
IPS113857	*P. palaeochoerus*	c1m	L		13.5	15.1	13.5
IPS113741	*P. palaeochoerus*	DP2	R	14.4	6.7		
IPS113741	*P. palaeochoerus*	DP3	R	18.6	12.5		
IPS113741	*P. palaeochoerus*	DP4	R	18.6	15.2	15.2	14.5
IPS113741	*P. palaeochoerus*	M1	R	21.2	17.4	17.4	16.8
IPS113817	*P. palaeochoerus*	i2	R	8.4	11.9		
IPS113818	Suidae indet.	m1	R	17.3	13.1	12.9	13.1
IPS113819	*Pa. valentini*	P3	R	19.2	16.3		
IPS113819	*Pa. valentini*	P4	R	16.5	20.3		
IPS113840	*P. palaeochoerus*	i3	R	12.0	6.3		
IPS113843	*P. palaeochoerus*	m3	R	—	>13,2	—	—
IPS113845	*P. palaeochoerus*	m2	R	—	—	16.1	—
IPS113900	*P. palaeochoerus*	DI1	R	8.0	5.0		
IPS113914	*P. palaeochoerus*	DP4	L	(17,0)	—	—	—
IPS113932	*Albanohyus* sp.	R i2	R	3.9	4.2		
IPS113955	*Pa. valentini*	DP3	R	—	11.1		
IPS113964	*P. palaeochoerus*	c1m	R		14.0	16.1	13.8
IPS113968	*P. palaeochoerus*	p3	L	17.6	10.8		
IPS113969	*P. palaeochoerus*	m2	L	21.6	16.9	16.1	16.9
IPS113983	*P. palaeochoerus*	i3	L	10.8	5.4		
IPS114001	*P. palaeochoerus*	dp4	L	—	11.7		

IPS114003	*P. palaeochoerus*	c1f	R	8.5	6.0		
IPS114003	*P. palaeochoerus*	dp3	R	13.4	6.7		
IPS114003	*P. palaeochoerus*	dp4	R	(24.0)	11.7		
IPS114003	*P. palaeochoerus*	m1	R	21.3	14.5	14.2	14.5
IPS114048	*Pa. valentini*	DP4	R	17.9	15.4	15.0	15.4
IPS114049	*P. palaeochoerus*	m3	L	—	>14.7	—	—
IPS114098	*P. palaeochoerus*	M1	L	20.5	17.6	17.0	17.6
IPS114102	cf. *Pa. valentini*	dp2	R	11.9	4.1		
IPS114191	*P. palaeochoerus*	DP2	R	—	5.4		
IPS114191	*P. palaeochoerus*	DP3	R	—	13.7		
IPS114191	*P. palaeochoerus*	DP4	L	18.4	14.2	14.0	14.2
IPS114191	*P. palaeochoerus*	DP4	R	18.3	15.4	15.4	15.2
IPS114191	*P. palaeochoerus*	M1	R	20.6	17.2	17.0	17.2
IPS114221	*P. palaeochoerus*	i3	R	14.1	6.8		
IPS114230	*Pa. valentini*	DP3	R	17.1	12.7		
IPS114227	*P. palaeochoerus*	M2	R	—	(20.1)	—	20.1
IPS114241	*P. palaeochoerus*	M2	L	—	>18.8	—	>18.8
IPS114242	*P. palaeochoerus*	P1	L	14.5	5.5		
IPS114251	*Pa. valentini*	M1	R	20.0	18.2	18.2	17.8
IPS114251	*Pa. valentini*	M2	R	23.5	22.0	21.3	22.0
IPS114251	*Pa. valentini*	M3	R	32.3	24.1	24.1	20.3
IPS114256	*P. palaeochoerus*	p2	R	16.6	7.3		
IPS114264	*P. palaeochoerus*	i1	R	7.9	—		
IPS114299	*P. palaeochoerus*	i3	L	13.8	6.7		

IPS114311	*P. palaeochoerus*	c1f	R	12.7	9.5		
IPS114228	*P. palaeochoerus*	DP2	L	—	7.1		
IPS114337	*Pa. valentini*	i2	R	8.3	10.7		
IPS114338	*P. palaeochoerus*	c1f	R	10.7	7.8		
IPS114339	*P. palaeochoerus*	p2	L	15.2	6.3		
IPS114342	*P. palaeochoerus*	p1	R	—	4.7		
IPS114386	*P. palaeochoerus*	p3	R	18.5	8.5		
IPS114386	*P. palaeochoerus*	p4	R	19.0	12.6		
IPS114386	*P. palaeochoerus*	m1	R	19.2	14.1	13.6	14.1
IPS114386	*P. palaeochoerus*	m2	R	23.3	17.7	17.2	17.7
IPS114386	*P. palaeochoerus*	m3	R	34.4	18.5	18.5	16.7
IPS114386	*P. palaeochoerus*	p3	L	19.2	8.5		
IPS114386	*P. palaeochoerus*	p4	L	18.8	13.3		
IPS114386	*P. palaeochoerus*	m1	L	17.4	14.3	14.0	14.3
IPS114386	*P. palaeochoerus*	m2	L	23.4	17.8	17.4	17.8
IPS114386	*P. palaeochoerus*	m3	L	35.0	18.1	18.1	16.9
IPS114387	*Pa. valentini*	c1f	R	12.2	9.6		
IPS114496	*P. palaeochoerus*	i1	R	—	>8.6		
IPS114535	*P. palaeochoerus*	di1	R	5.2	6.0		
IPS124322	*P. palaeochoerus*	i2	L	9.6	(11.8)		
IPS124323	*P. palaeochoerus*	i3	L	10.5	7.6		
IPS124324	*P. palaeochoerus*	i1	L	7.9	>9.5		
IPS124325	*P. palaeochoerus*	DP2	L	—	>5.2		
IPS124326	*P. palaeochoerus*	DI3	L	8.1	5.3		

IPS124327	*P. palaeochoerus*	i2	L	7.9	9.5		
IPS124328	*Pa. valentini*	P2	R	17.2	9.2		
IPS124329	*P. palaeochoerus*	dp4	L	—	>9.5		
IPS124330	*P. palaeochoerus*	c1f	R	12.2	8.1		
IPS124331	*Pa. valentini*	DP4	L	16.6	15.0	15.0	14.4
IPS124332	*P. palaeochoerus*	dp2	R	(9.1)	5.2		
IPS124333	*P. palaeochoerus*	di2	R	—	>7.2		
IPS124334	*Albanohyus* sp.	L i2	L	3.6	4.5		
IPS124335	*P. palaeochoerus*	di1	L	5.2	6.0		
IPS124336a	*P. palaeochoerus*	dp2	L	>7.6	(4.4)		
IPS124336a	*P. palaeochoerus*	dp3	L	13.5	6.3		
IPS124336a	*P. palaeochoerus*	dp4	L	23.9	10.5		
IPS124336a	*P. palaeochoerus*	m1	L	21.6	14.6	13.1	14.6
IPS124336b	*P. palaeochoerus*	dp3	R	13.5	6.7		
IPS124336b	*P. palaeochoerus*	dp4	R	23.4	10.7		
IPS124336b	*P. palaeochoerus*	m1	R	22.4	14.7	12.2	14.7
IPS124437	*P. palaeochoerus*	P4	L	>13.2	—		
IPS124841	*P. palaeochoerus*	dp3	R	13.3	6.0		
IPS124841	*P. palaeochoerus*	dp4	R	>14.2	>9.2		
IPS124842	*P. palaeochoerus*	dp4	R	23.7	11.1		
IPS124843	*P. palaeochoerus*	C1f	R	14.1	9.5		
IPS124844	*P. palaeochoerus*	DI1	L	9.8	5.7		
IPS124845	*P. palaeochoerus*	di1	L	4.6	6.0		
IPS125680	*P. palaeochoerus*	M1	R	—	>16.3	>16.3	—

IPS125678	*Pa. valentini*	DP4	L	>16.5	—	—	—
IPS125679	*P. palaeochoerus*	dp3	L	13.8	6.4		
IPS128038	*P. palaeochoerus*	M3	R	(33.0)[1]	22.1	22.1	19.0
IPS128039	*P. palaeochoerus*	M2	R	27.5	(23.0)	(23.0)	21.6
IPS128040	*P. palaeochoerus*	M1	R	21.0	18.5	18.5	17.7

[1] This M3 is missing the distal end of the crown (preserved MD = 29.5 mm, but by comparison with IPS28739 we estimate originat MD = 33.0 mm.

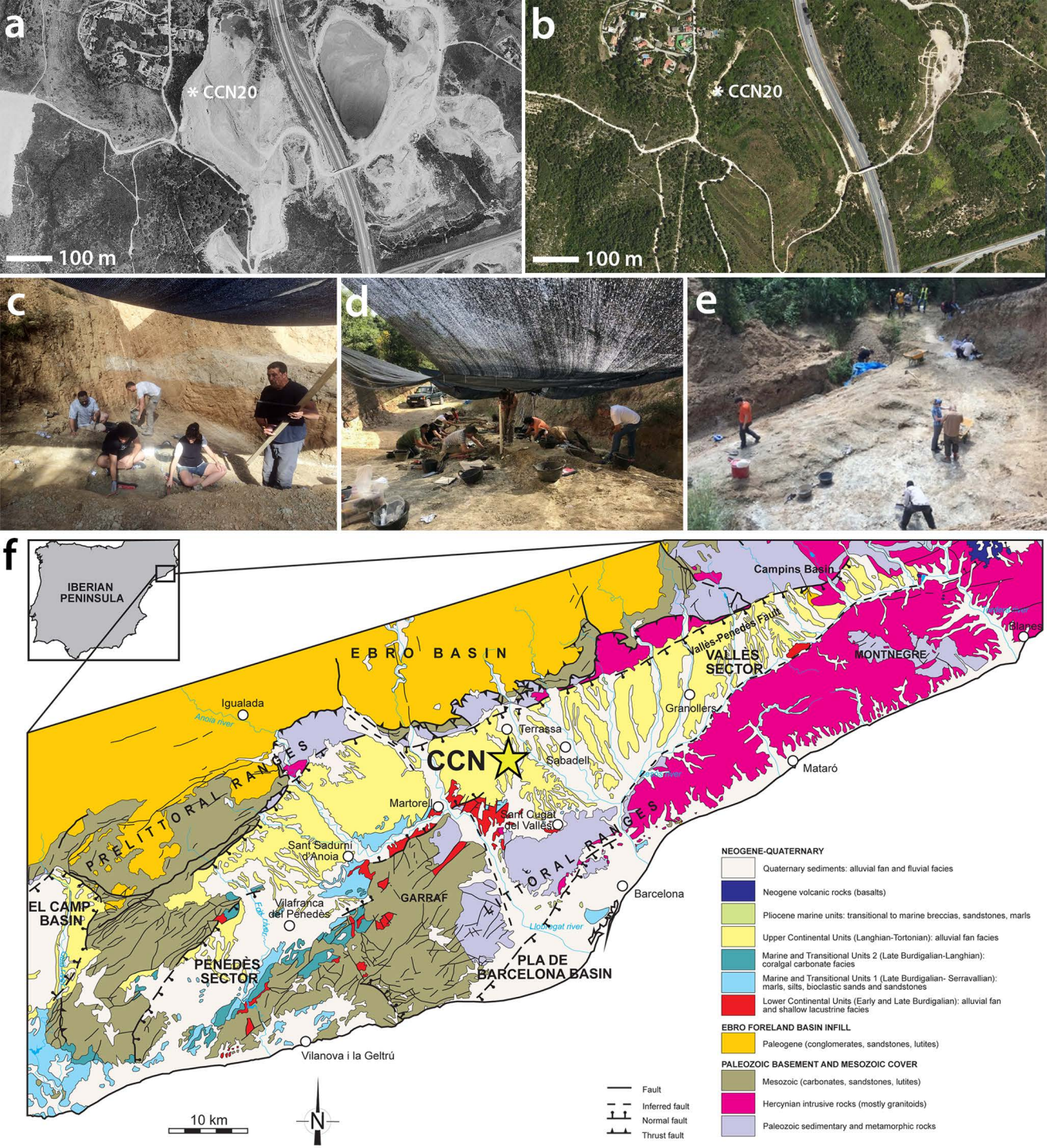
a
CCN20
100 m
b
CCN20
100 m
c
d
e
f
IBERIAN PENINSULA
EBRO BASIN
Campins Basin
Vallès-Penedès Fault
VALLÈS SECTOR
MONTNEGRE
Igualada
Anoia river
Granollers
Terrassa
CCN
Sabadell
Mataró
Martorell
Sant Cugat del Vallès
PRELITTORAL RANGES
Sant Sadurní d'Anoia
GARRAF
LITTORAL RANGES
Barcelona
EL CAMP BASIN
Vilafranca del Penedès
Foix river
Llobregat river
PENEDÈS SECTOR
PLA DE BARCELONA BASIN
Vilanova i la Geltrú
10 km
N
NEOGENE-QUATERNARY
Quaternary sediments: alluvial fan and fluvial facies
Neogene volcanic rocks (basalts)
Pliocene marine units: transitional to marine breccias, sandstones, marls
Upper Continental Units (Langhian-Tortonian): alluvial fan facies
Marine and Transitional Units 2 (Late Burdigalian-Langhian): coralgal carbonate facies
Marine and Transitional Units 1 (Late Burdigalian- Serravallian): marls, silts, bioclastic sands and sandstones
Lower Continental Units (Early and Late Burdigalian): alluvial fan and shallow lacustrine facies
EBRO FORELAND BASIN INFILL
Paleogene (conglomerates, sandstones, lutites)
PALEOZOIC BASEMENT AND MESOZOIC COVER
Mesozoic (carbonates, sandstones, lutites)
Hercynian intrusive rocks (mostly granitoids)
Paleozoic sedimentary and metamorphic rocks
Fault
Inferred fault
Normal fault
Thrust fault

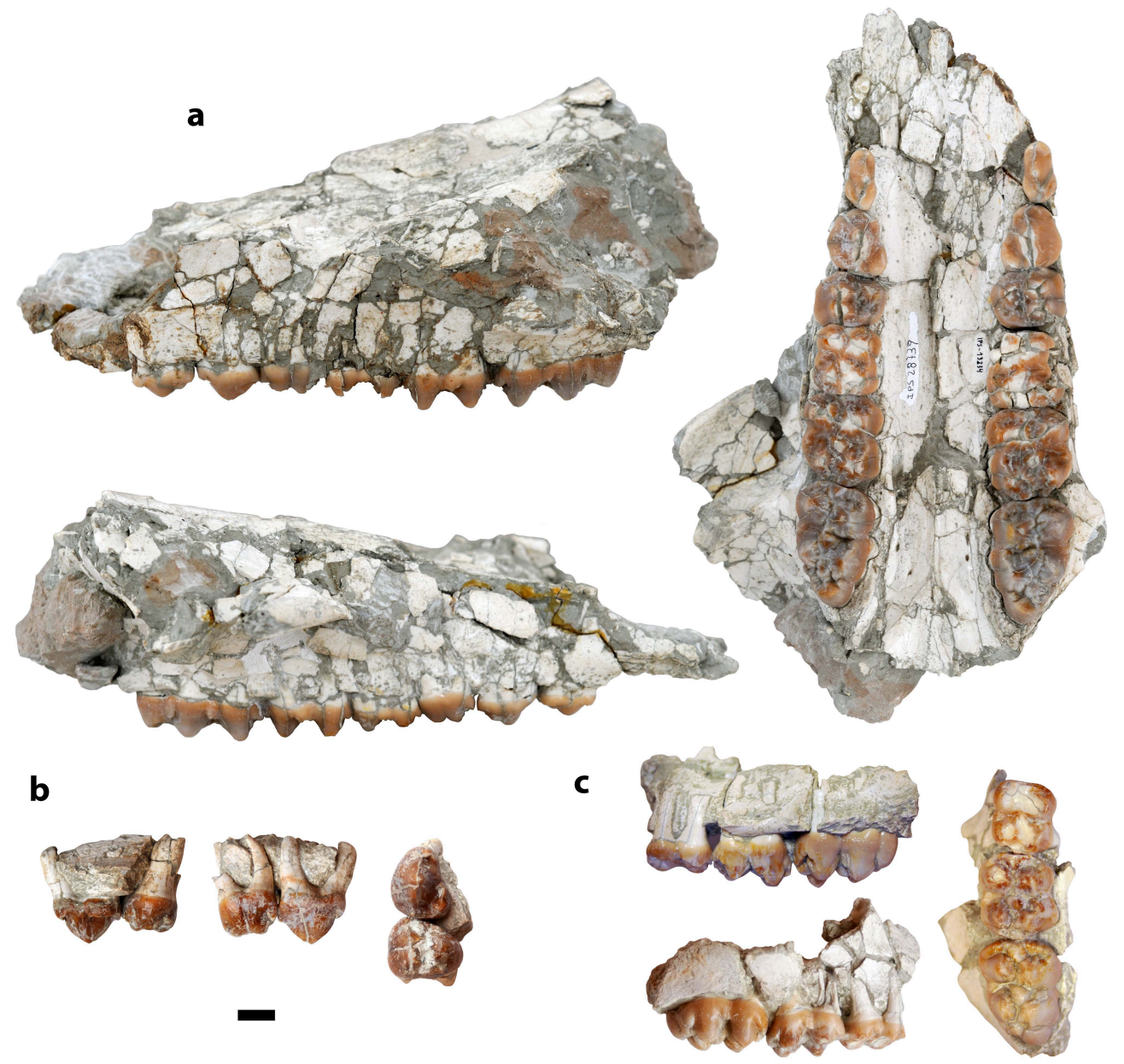
a
b
c


a
b
c
d

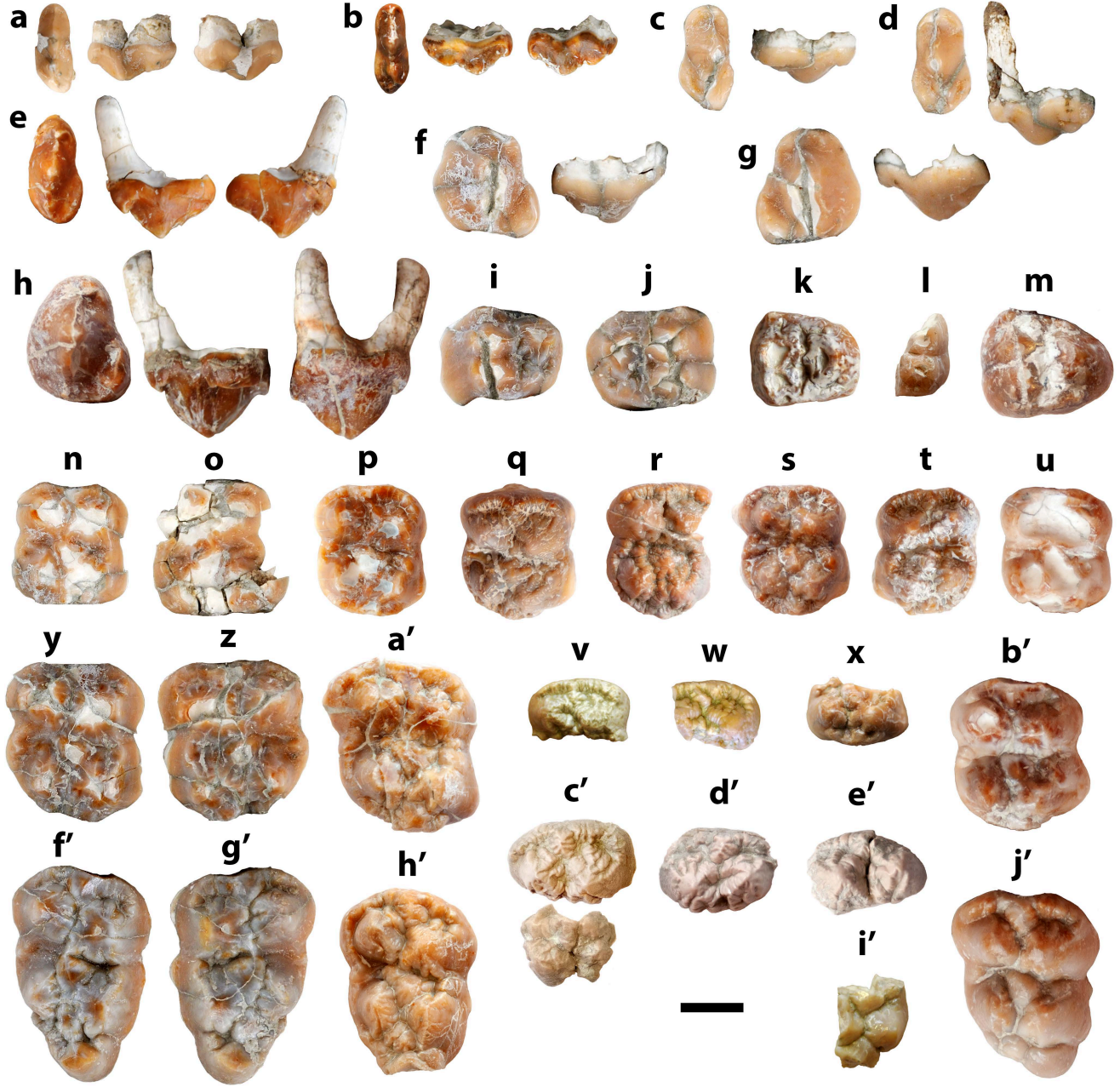
a
b
c
d
e
f
g
h
i
j
k
l
m
n
o
p
q
r
s
t
u
y
z
a′
v
w
x
b′
c′
d′
e′
f′
g′
h′
i′
j′

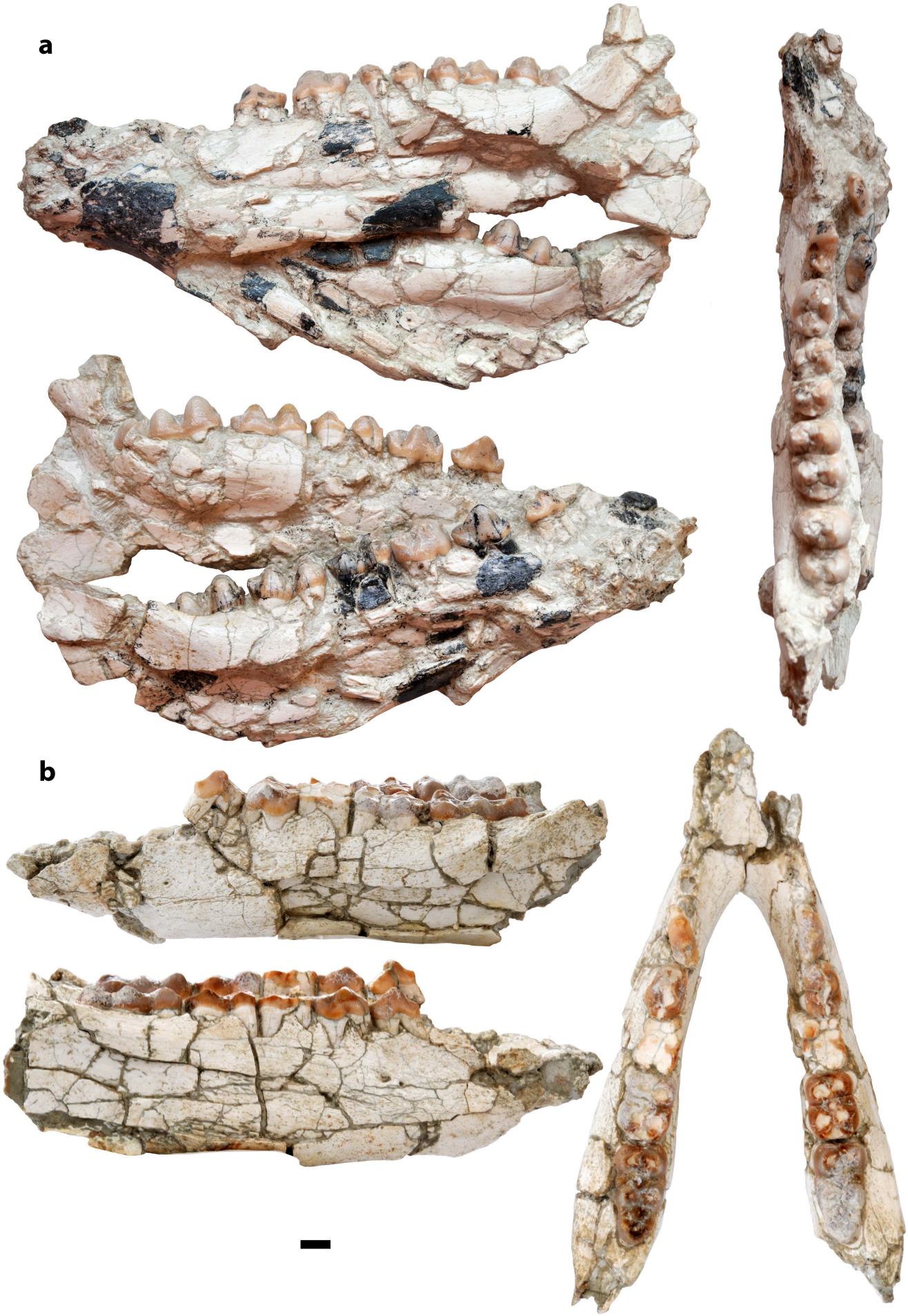
a
b

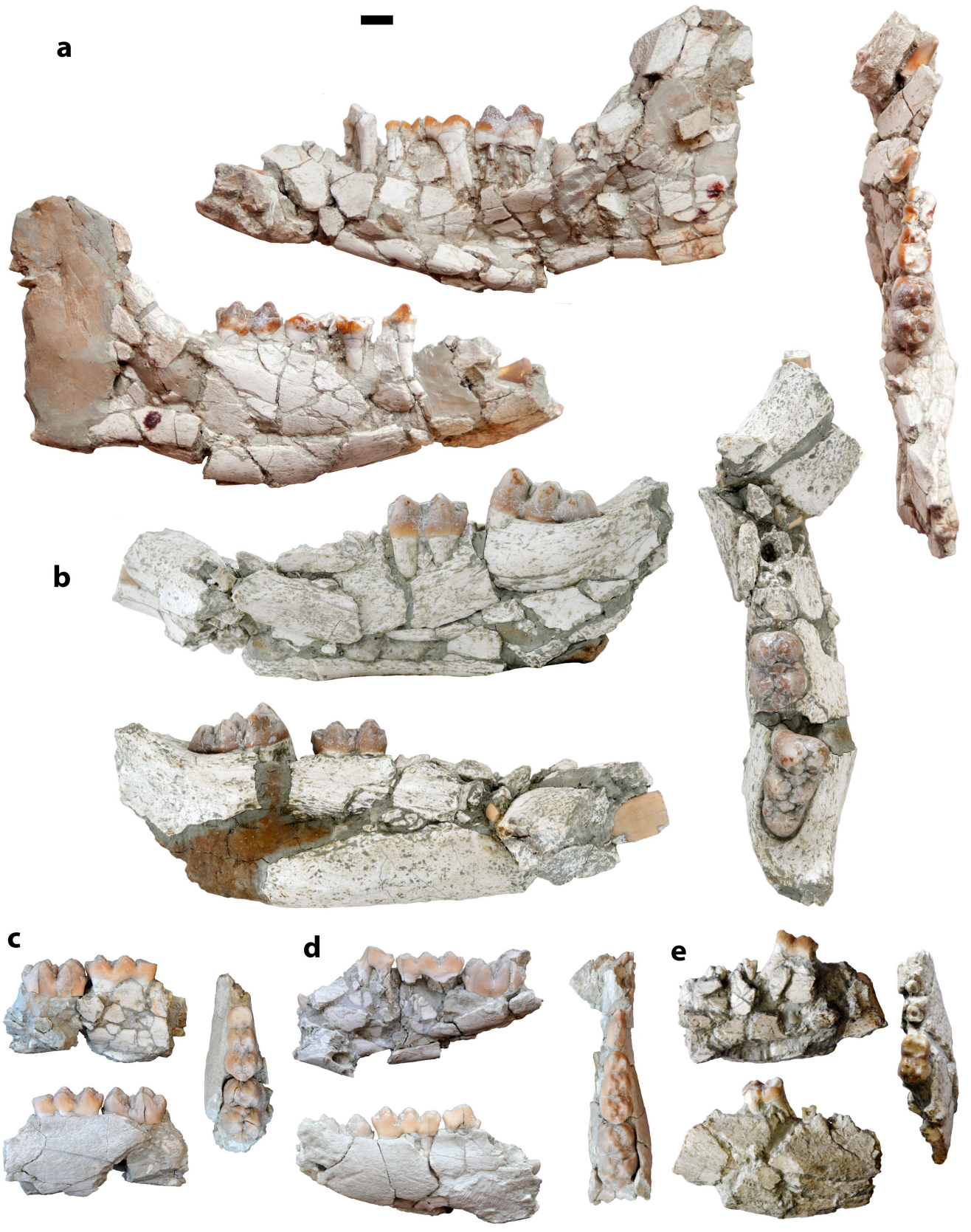
a
b
c
d
e


a
b
c
d
e
f
g
h
i
j
n
o
k
m
l
r
p
q
t
s


a
b
c
d
e
f
g
h


a
b
c
d
h
e
f
g
i
j
k
l
m
n
o
p
q
r
s
t
u
v
w
c′
d′
e′
x
y
z
a′
b′
f′
g′
h′

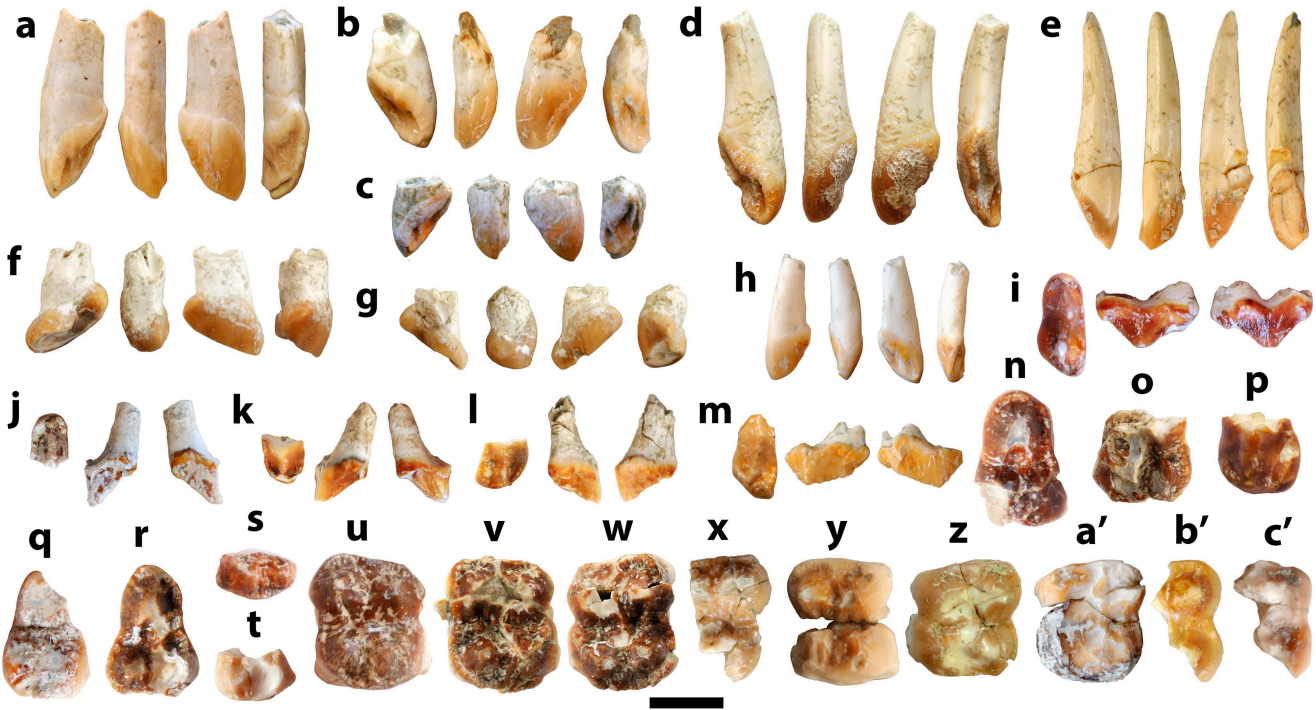
a
b
c
d
e
f
g
h
i
j
k
l
m
n
o
p
q
r
s
t
u
v
w
x
y
z
a′
b′
c′

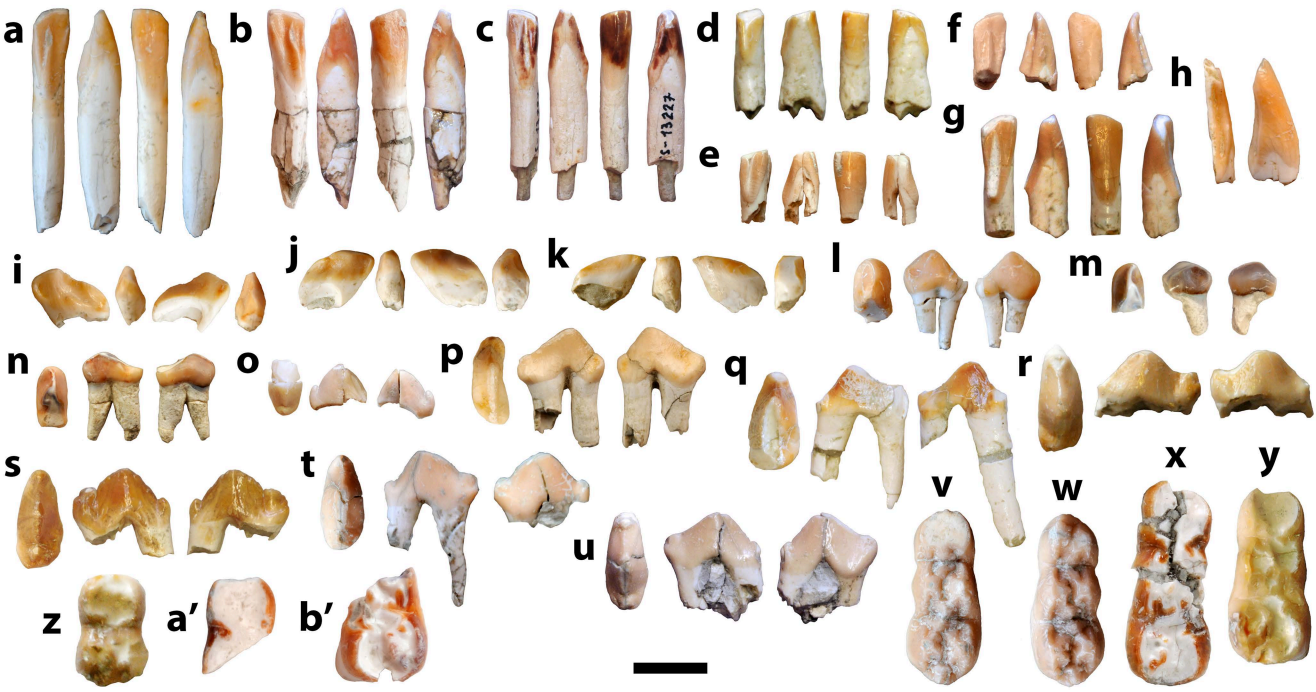
a
b
c
d
e
f
g
h
i
j
k
l
m
n
o
p
q
r
s
t
u
v
w
x
y
z
a′
b′

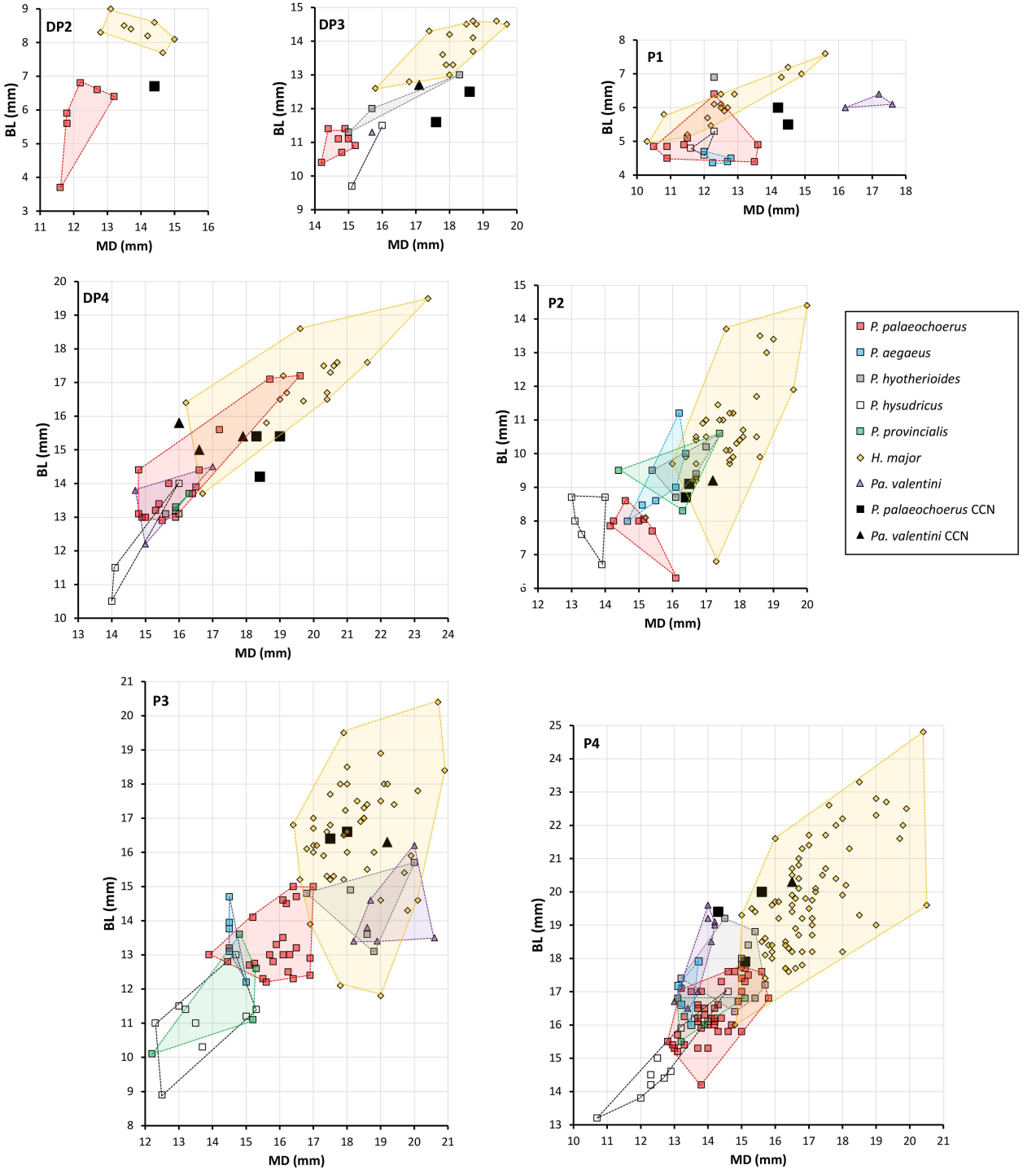
DP2
DP3
P1
DP4
P2
P3
P4
BL (mm)
MD (mm)
P. palaeochoerus
P. aegaeus
P. hyotherioides
P. hysudricus
P. provincialis
H. major
Pa. valentini
P. palaeochoerus CCN
Pa. valentini CCN

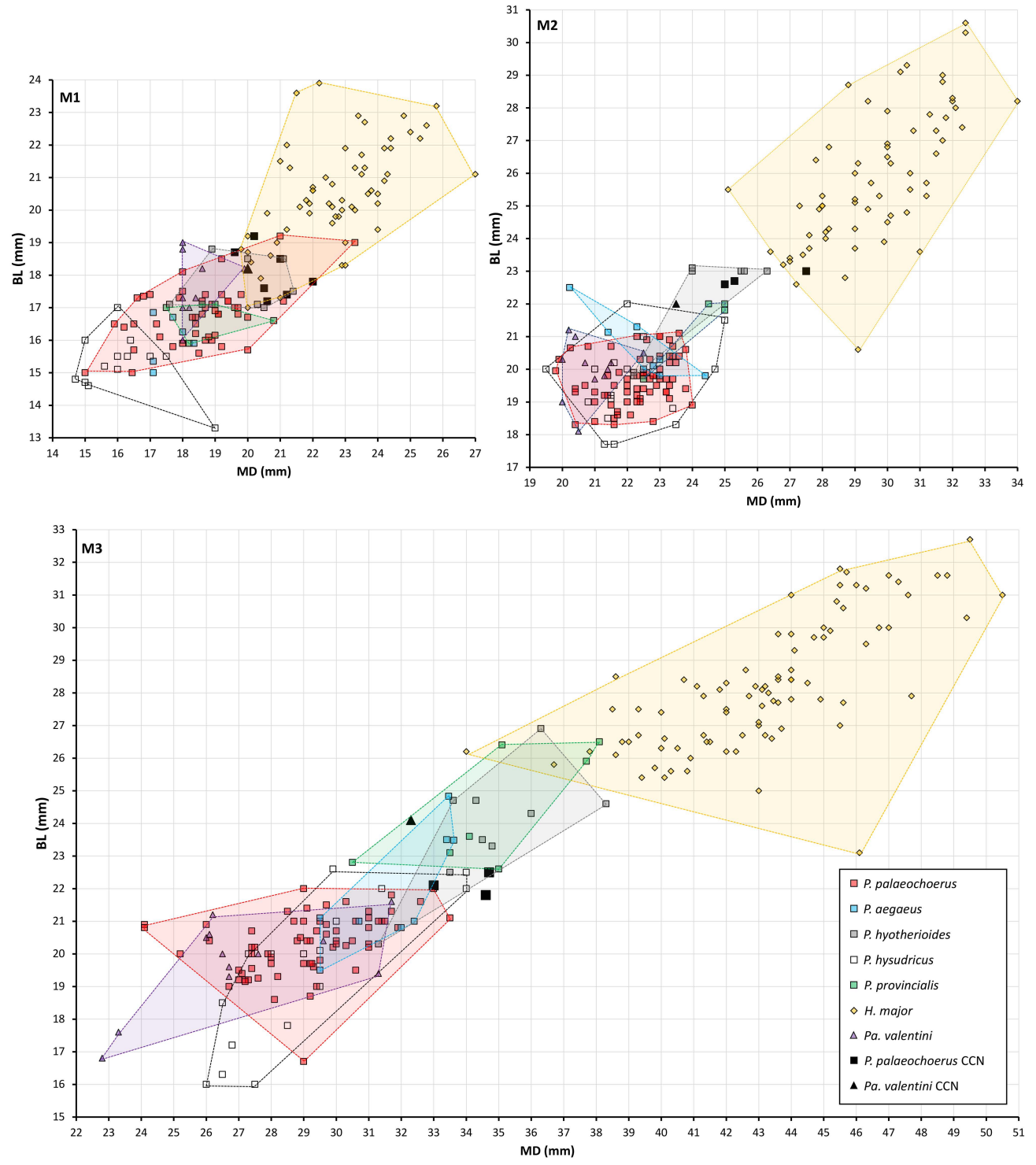
M1
BL (mm)
MD (mm)
M2
BL (mm)
MD (mm)
M3
BL (mm)
MD (mm)
P. palaeochoerus
P. aegaeus
P. hyotherioides
P. hysudricus
P. provincialis
H. major
Pa. valentini
P. palaeochoerus CCN
Pa. valentini CCN

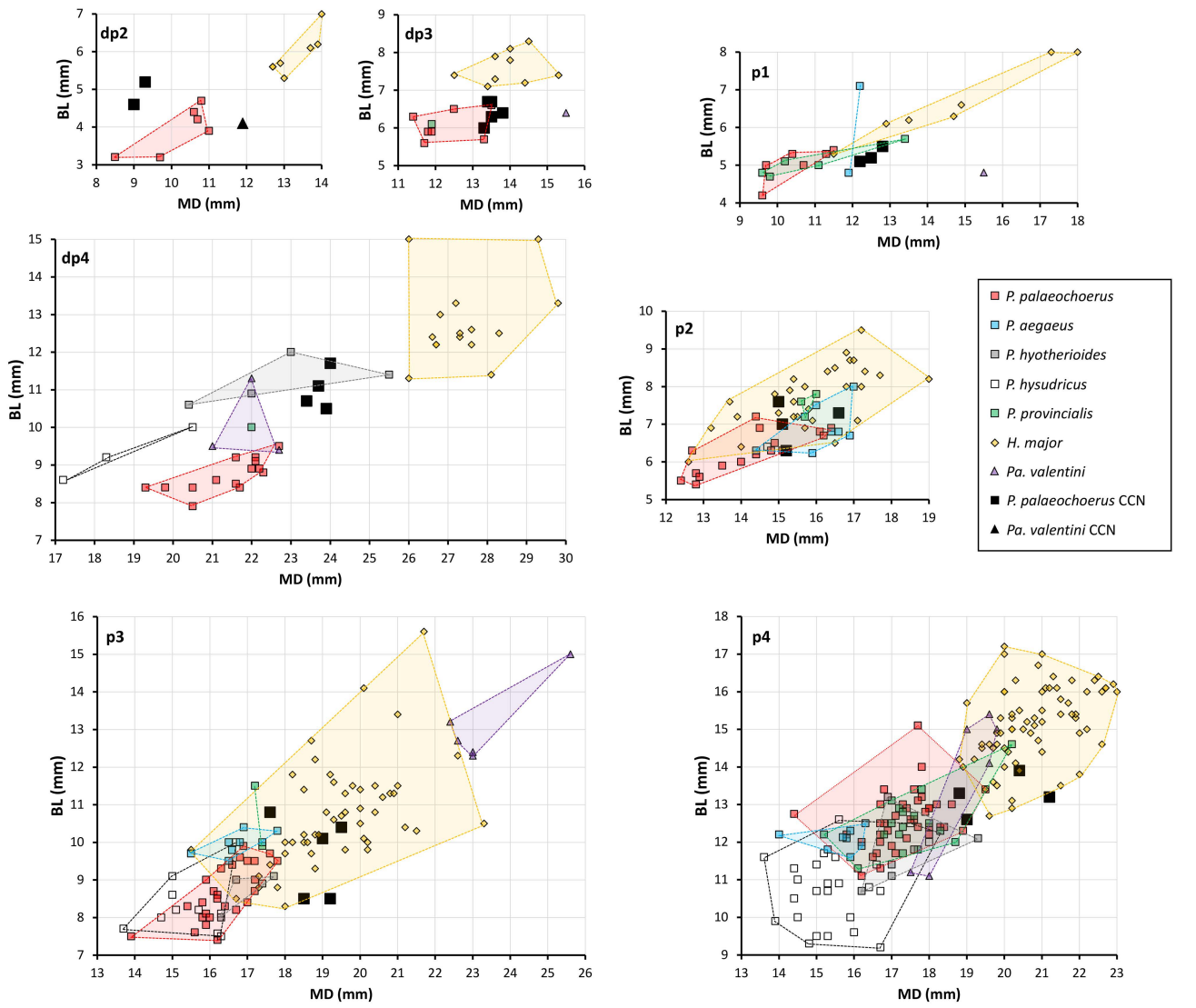
dp2
dp3
p1
dp4
p2
p3
p4
BL (mm)
MD (mm)
P. palaeochoerus
P. aegaeus
P. hyotherioides
P. hysudricus
P. provincialis
H. major
Pa. valentini
P. palaeochoerus CCN
Pa. valentini CCN

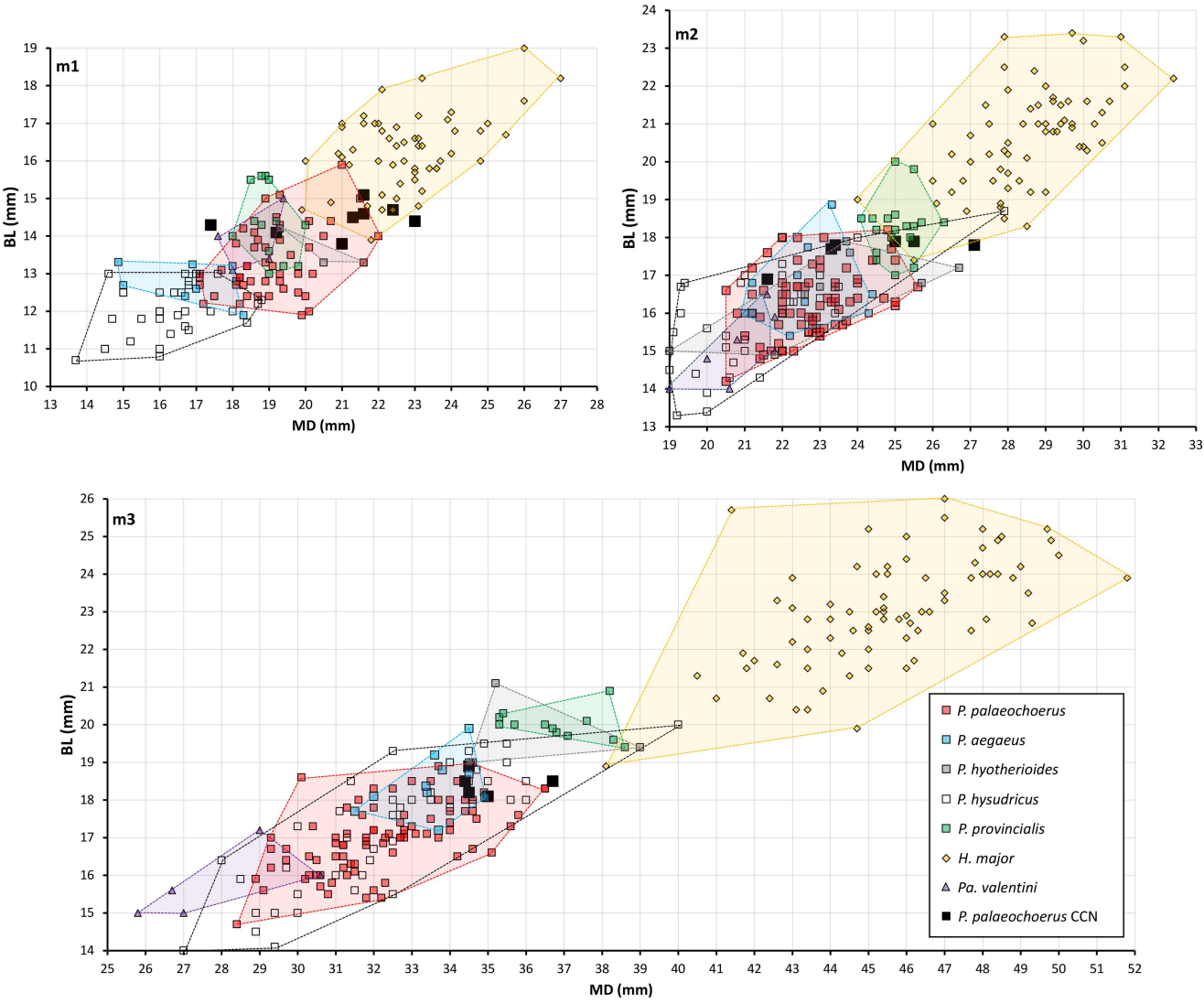
m1
BL (mm)
MD (mm)
m2
BL (mm)
MD (mm)
m3
BL (mm)
MD (mm)
P. palaeochoerus
P. aegaeus
P. hyotherioides
P. hysudricus
P. provincialis
H. major
Pa. valentini
P. palaeochoerus CCN

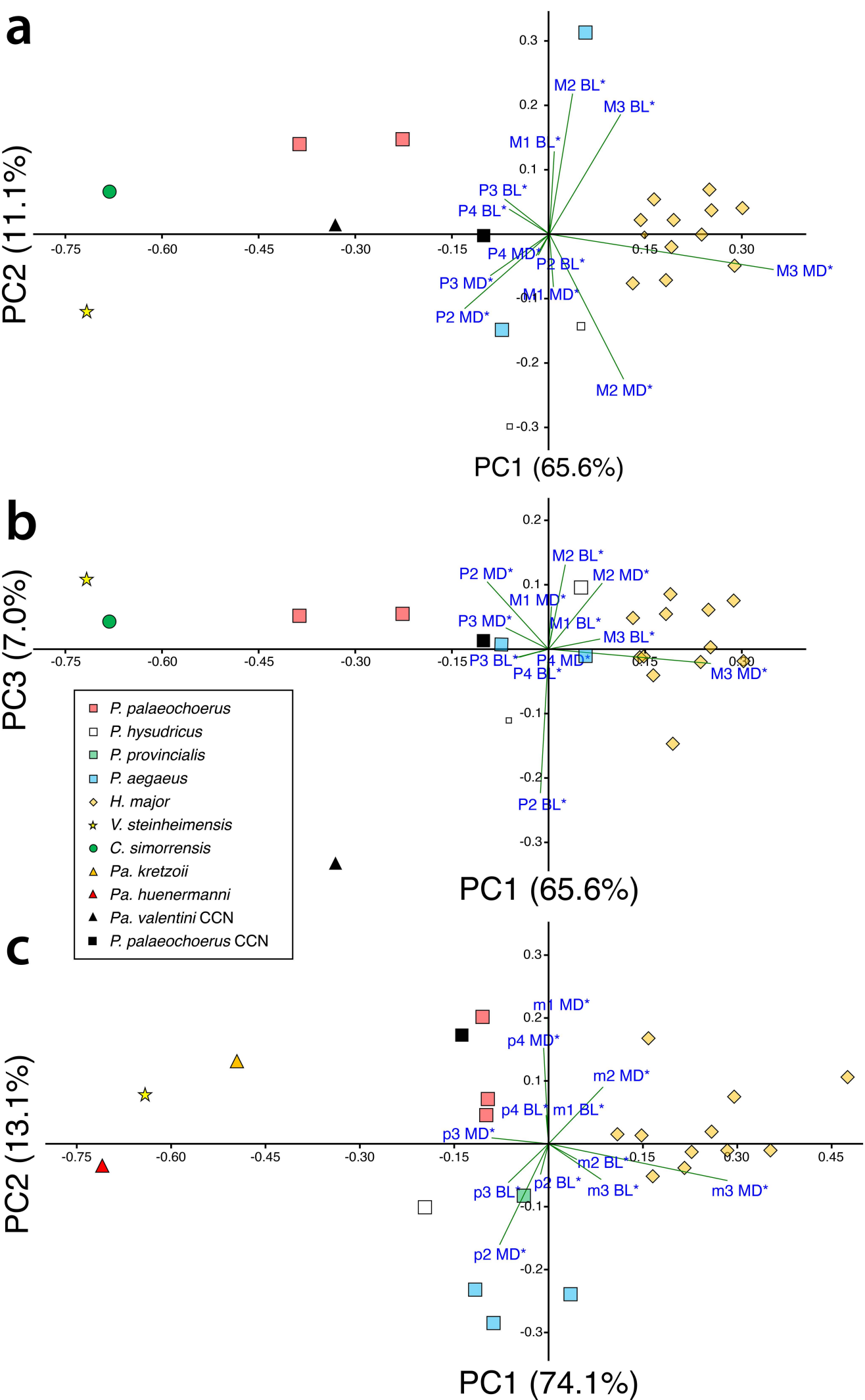
a
PC2 (11.1%)
PC1 (65.6%)
M2 BL*
M3 BL*
M1 BL*
P3 BL*
P4 BL*
P4 MD*
P2 BL*
M3 MD*
P3 MD*
M1 MD*
P2 MD*
M2 MD*
b
PC3 (7.0%)
PC1 (65.6%)
P. palaeochoerus
P. hysudricus
P. provincialis
P. aegaeus
H. major
V. steinheimensis
C. simorrensis
Pa. kretzoii
Pa. huenermanni
Pa. valentini CCN
P. palaeochoerus CCN
c
PC2 (13.1%)
PC1 (74.1%)
m1 MD*
p4 MD*
m2 MD*
p4 BL*
m1 BL*
p3 MD*
m2 BL*
p3 BL*
p2 BL*
m3 BL*
m3 MD*
p2 MD*

Online Resource 1 Raw measurements of the upper and lower cheek teeth included in the principal components analyses (PCAs). These measurements were transformed into Mosimann shape variables by dividing them by the geometric mean of each specimen before running the PCAs.

Species	Catalog No.	Site	Reference	P2 L	P3 L	P4 L	M1 L	M2 L	M3 L	P2 W	P3 W	P4 W	M1 W	M2 W	M3 W
Pa. valentini	IPS124328+IPS113819+IPS114251	CCN20	This study	17.2	19.2	16.5	20.0	23.5	32.3	16.3	16.3	20.3	18.2	22.0	24.1
P. palaeochoerus	IPS28739	CCN20	This study	16.5	17.8	15.0	19.9	25.2	34.7	8.9	16.5	19.7	19.0	22.7	22.2
P. palaeochoerus	BSP AS 103	Münchner Flinz = Isarbett	Hellmund (1995)	15.3	16.1	13.4	16.4	19.9	24.1	7.9	12.4	17.1	16.5	20.1	20.9
P. palaeochoerus	LJG 60258	Johnsdorf b. Feldbach	Hellmund (1995)	14.2	14.9	13.3	16.9	20.5	26.1	7.9	12.8	15.4	17.4	20.7	20.7
P. hysudricus	PUPC 15/28	Middle Siwaliks	Aslam et al. (2021)	13.6	12.4	11.4	15.0	21.5	27.5	7.2	10.0	13.5	14.7	17.7	16.0
P. hysudricus	PUPC 99/3	Middle Siwaliks	Aslam et al. (2021)	13.1	13.7	12.3	15.0	20.9	26.5	8.0	10.3	14.2	14.7	12.5	16.3
P. aegaeus	AMGP-MA 501	Maramena	Hellmund (1995)	17.4	16.7	13.9	17.9	24.4	32.0	9.6	12.9	15.4	16.5	19.8	20.8
P. aegaeus	KRY3820	Kryopigi	Lazaridis (2015); Lazaridis et al. (2022)	14.9	14.5	13.4	15.4	20.7	33.5	8.2	13.9	17.5	21.4	22.5	24.2
H. major	58-HAY-2/45	58-HAY-2 (Sivas)	Van der Made et al. (2013)	17.2	17.7	16.7	21.2	31.2	43.8	9.1	15.9	19.9	19.9	25.5	27.6
H. major	AMNH 20653-Q5	Q5, Limitzis, Samos	Sylvestrou and Kostopoulos (2009)	15.9	17.4	15.3	19.4	27.6	37.3	8.7	13.0	17.1	17.9	23.2	26.0
H. major	AMNH 20795-Q5	Q5, Limitzis, Samos	Sylvestrou and Kostopoulos (2009)	16.4	18.6	15.3	22.9	31.0	39.3	9.9	15.5	19.5	20.0	23.6	27.5
H. major	DT RO 2992	La Roma 2	Pickford (2015)	16.7	17.2	16.6	20.0	27.1	42.2	9.3	16.1	19.4	18.6	23.4	26.8
H. major	FM 2801	Strumyani	Pickford (2015)	18.0	19.9	15.9	24.4	30.0	45.4	10.4	15.9	19.6	22.2	27.9	30.8
H. major	[IPS9761]	Torrent de les Febulines N12	Pickford (2015)	19.6	19.2	19.2	25.7	32.0	46.7	11.9	18.0	22.8	22.9	28.3	31.4
H. major	MNCN Bat10·14·E3·46	Batallones 10	Pickford (2015)	18.0	19.6	17.2	23.0	30.1	44.1	11.0	17.9	20.1	21.1	26.4	28.4
H. major	MTLA-537	Mytilinii-1A, Samos	Sylvestrou and Kostopoulos (2009)	18.6	19.8	16.8	23.5	30.1	43.4	10.2	14.9	19.3	20.4	25.6	27.7
H. major	NHMB ML 41	Cucuron (Luberon)	Pickford (2015)	17.3	17.9	17.5	23.6	31.7	45.9	11.0	18.0	20.6	22.2	27.5	29.9
H. major	NMT 343-13(1)	Udabno	Pickford (2015)	20.0	20.7	17.6	22.2	32.1	50.5	14.4	20.4	22.6	23.9	28.0	31.0
H. major	NMT without number	Eldari	Pickford (2015)	17.6	20.9	18.5	21.2	30.8	49.4	10.1	18.4	22.0	22.0	27.3	30.3
H. major	Tbilisi	Bazaleti	Pickford (2015)	18.5	18.5	18.1	21.0	30.0	44.0	11.7	17.0	20.2	21.5	26.9	29.8
V. steinheimensis	SMNS M 20223	Steinheim	Pickford (2016a)	16.1	16.8	12.7	16.4	17.9	20.7	7.1	15.3	17.4	15.4	17.9	17.6
C. simorrensis	Without number	Käpfnach	Pickford (2016a), after Kaup (1859)	20.0	17.0	13.0	15.0	18.5	21.5	7.0	15.0	16.0	14.0	17.3	16.0
Species	Catalog No.	Site	Reference	p2 L	p3 L	p4 L	m1 L	m2 L	m3 L	p2 W	p3 W	p4 W	m1 W	m2 W	m3 W
P. palaeochoerus	IPS107069	CCN20	This study	15.1	19.3	20.8	21.6	26.3	35.6	7.0	10.3	13.6	15.1	17.9	18.7

P. palaeochoerus	22-1067	Grytsiv	Van der Made et al. (1999)	14.4	15.8	16.5	18.2	21.9	31.2	6.2	8.4	11.6	12.9	15.2	16.8
P. palaeochoerus	22-1068	Grytsiv	Van der Made et al. (1999)	14.0	16.4	16.6	18.1	22.0	31.2	6.0	8.3	11.7	12.7	15.0	16.5
P. palaeochoerus	MBFSZ V 2017.21.1.	Alsótelekes	Iannucci and Begun (2022)	12.4	13.9	15.8	18.1	21.4	28.4	5.5	7.5	12.2	12.8	15.1	14.7
P. hysudricus	GSP 2807	Middle Siwaliks loc. 105	Pickford (1988)	14.7	15.0	14.5	16.0	20.6	28.5	6.4	9.1	10.0	12.0	14.3	15.9
P. provincialis	FSL 40 072	Montpellier	Pickford (2013)	15.6	16.4	17.8	19.0	24.3	36.7	7.6	11.4	13.4	15.5	18.5	20.1
P. aegaeus	Vozarci-1544	Vozarci	Geraads et al. (2008)	16.6	16.8	15.3	15.0	21.2	33.4	6.8	10.0	11.8	12.7	16.0	18.2
P. aegaeus	RZO 330	Ravin des Zouaves nº 5	de Bonis and Bouvrain (1996)	17.0	17.6	16.1	16.9	21.8	34.1	7.4	10.2	12.1	12.5	16.2	19.6
P. aegaeus	KRY3490+1094	Kryopigi	Lazaridis (2015); Lazaridis et al. (2022)	15.9	16.6	15.7	14.9	23.3	34.9	6.2	9.8	12.1	13.3	18.9	18.1
H. major	NHMW 1911v211	Samos	Sylvestrou and Kostopoulos (2009)	15.4	18.5	19.9	20.9	30.1	46.3	7.2	10.2	15.3	16.2	21.6	22.5
H. major	NMT 343-13(3)	Udabno	Pickford (2015)	17.0	19.6	22.4	24.0	31.1	49.0	8.7	11.3	16.3	17.3	22.5	24.2
H. major	PER-360	Perivolaki	Sylvestrou and Kostopoulos (2006)	12.6	17.6	19.7	19.9	25.5	38.1	6.0	9.4	13.6	14.7	17.4	18.9
H. major	MNHN LUB 656	Cucuron (Luberon)	Pickford (2015)	17.3	19.8	20.5	22.7	29.9	46.0	8.4	10.8	17.0	18.1	23.3	25.4
H. major	MNHN LUB 658	Cucuron (Luberon))	Pickford (2015)	15.0	18.3	21.3	22.5	29.0	45.4	7.3	10.0	15.7	16.4	20.9	23.2
H. major	MTLA-479	Mytilinii-1A, Samos	Sylvestrou and Kostopoulos (2009)	14.0	18.0	21.5	21.2	29.9	45.5	6.4	8.3	13.5	15.9	20.4	24.2
H. major	K-5276	Kalimantsi	Kostopoulos et al. (2001)	15.6	20.1	21.6	21.8	29.0	44.8	8.1	11.5	15.8	17.0	21.3	23.4
H. major	MNCN BAT·10·09 G2·B3	Batallones 10	Pickford (2015)	18.4	21.4	22.3	23.1	30.1	45.3	8.3	10.4	14.8	16.5	20.4	22.9
H. major	IPAS Dz 133	Dzedzvtachevi	Pickford (2015)	16.8	19.3	22.5	23.1	29.5	48.0	8.9	11.6	16.4	16.6	21.1	24.7
H. major	DTK 286	Dytiko	de Bonis and Bouvrain (1996)	15.4	18.8	19.8	21.7	28.4	45.3	7.6	10.0	15.5	16.4	20.9	23.6
H. major	58-HAY-05	58-HAY-19 (Sivas)	Van der Made et al. (2013)	14.9	17.3	19.4	20.4	23.6	41.7	7.8	9.0	14.6	14.6	19.4	21.9
V. steinheimensis	GPIT MA 1178-39	Steinheim	Pickford (2016a)	14.6	19.6	17.6	17.5	19.0	25.0	5.7	11.0	12.6	12.0	14.0	14.9
C. simorrensis	MNCN 08.17.7180 6-148	Carpetana	Pickford (2013a)	17.9	22.3	17.2	16.9	18.9	26.1	8.2	15.3	14.9	13.9	15.4	16.4
Pa. kretzoii	MAFI1993/107	Rudabánya	Fortelius et al. (2005)	11.1	13.8	13.8	14.7	16.4	20.4	4.9	7.6	9.8	10.9	12.7	13.3
Pa. huenermanni	HPM-GP 10767	Lučane	Bernor et al. (2004)	14.9	17.8	16.0	15.5	18.0	22.9	6.8	10.1	11.8	12.7	14.6	14.0

Online Resource 2 Scores of each individual for the principal components (PCs) explaining more than 5% variance in the principal components analyses based on Mosimann shape variables computed from upper and lower cheek teeth measurements. Percentage of variance explained by each PC is reported within parentheses.

PCA based on upper cheek teeth (P2–M3)					PCA based on lower cheek teeth (p2–m3)			
Species	Catalog No.	PC1 (60.8%)	PC2 (13.5%)	PC3 (8.6%)	Species	Catalog No.	PC1 (65.5%)	PC2 (18.1)
Pa. valentini	IPS124328+IPS113819+IPS114251	-0.331	0.015	-0.333	*P. palaeochoerus*	IPS107069	-0.138	0.173
P. palaeochoerus	IPS28739	-0.101	-0.002	0.012	*P. palaeochoerus*	22-1067	-0.099	0.046
P. palaeochoerus	BSP AS 103	-0.387	0.140	0.052	*P. palaeochoerus*	22-1068	-0.096	0.071
P. palaeochoerus	LJG 60258	-0.227	0.147	0.055	*P. palaeochoerus*	MBFSZ V 2017.21.1.	-0.105	0.202
P. hysudricus	PUPC 15/28	0.050	-0.143	0.096	*P. hysudricus*	GSP 2807	-0.197	-0.101
P. hysudricus	PUPC 99/3	-0.062	-0.298	-0.111	*P. provincialis*	FSL 40 072	-0.039	-0.083
P. aegaeus	AMGP-MA 501	-0.073	-0.148	0.007	*P. aegaeus*	Vozarci-1544	-0.087	-0.285
P. aegaeus	KRY3820	0.057	0.313	-0.011	*P. aegaeus*	RZO 330	-0.117	-0.232
H. major	58-HAY-2/45	0.287	-0.049	0.076	*P. aegaeus*	KRY1094	0.035	-0.239
H. major	AMNH 20653-Q5	0.189	-0.020	0.085	*H. major*	NHMW 1911v211	0.353	-0.010
H. major	AMNH 20795-Q5	0.131	-0.076	0.049	*H. major*	NMT 343-13(3)	0.259	0.019
H. major	DT RO 2992	0.236	-0.001	-0.020	*H. major*	PER-360	0.159	0.168
H. major	FM 2801	0.248	0.069	0.061	*H. major*	MNHN LUB 656	0.166	-0.052
H. major	[IPS9761]	0.142	0.022	-0.013	*H. major*	MNHN LUB 658	0.295	0.075
H. major	MNCN Bat10·14·E3·46	0.148	-0.001	-0.011	*H. major*	MTLA-479	0.475	0.106
H. major	MTLA-537	0.182	-0.071	0.055	*H. major*	K-5276	0.147	0.013
H. major	NHMB ML 41	0.251	0.037	0.003	*H. major*	MNCN BAT·10·09 G2·B3	0.109	0.015
H. major	NMT 343-13(1)	0.193	0.022	-0.147	*H. major*	IPAS Dz 133	0.227	-0.013
H. major	NMT without number	0.301	0.040	-0.019	*H. major*	DTK 286	0.284	-0.010
H. major	Tbilisi	0.163	0.054	-0.041	*H. major*	58-HAY-05	0.216	-0.038
V. steinheimensis	SMNS M 20223	-0.682	0.068	0.043	*V. steinheimensis*	GPIT MA 1178-39	-0.642	0.079
C. simorrensis	Without number	-0.717	-0.118	0.110	*C. simorrensis*	MNCN 08.17.7180 6-148	-0.496	0.132
					Pa. kretzoii	MAFI1993/107	-0.710	-0.035

Pa. huenermanni	HPM-GP 10767	-0.138	0.173

Online Resource 3 Variable loadings for the principal components (PCs) explaining more than 5% variance in the principal components analyses based on Mosimann shape variables computed from upper and lower cheek teeth measurements. Percentage of variance explained by each PC is reported within parentheses. The asterisks denote that the variables do not correspond to the raw measurements reported in Table S1, but to the shape variables computed by dividing them by the geometric mean of each individual.

PCA based on upper cheek teeth (P2–M3)				PCA based on lower cheek teeth (p2–m3)		
Variable	PC1 (65.6%)	PC2 (11.1%)	PC3 (7.0%)	Variable	PC1 (74.1%)	PC2 (13.1)
P2 L*	-0,308	-0,270	0,338	p2 L*	-0,228	-0,471
P3 L*	-0,214	-0,150	0,107	p3 L*	-0,266	0,028
P4 L*	-0,048	-0,078	-0,015	p4 L*	-0,023	0,448
M1 L*	0,015	-0,191	0,214	m1 L*	-0,003	0,594
M2 L*	0,269	-0,526	0,331	m2 L*	0,255	0,265
M3 L*	0,813	-0,128	-0,072	m3 L*	0,835	-0,172
P2 W*	-0,041	-0,076	-0,721	p2 W*	-0,038	-0,143
P3 W*	-0,163	0,127	-0,042	p3 W*	-0,188	-0,181
P4 W*	-0,146	0,091	-0,040	p4 W*	-0,011	0,134
M1 W*	0,018	0,300	0,095	m1 W*	0,001	0,139
M2 W*	0,084	0,510	0,423	m2 W*	0,132	-0,074
M3 W*	0,258	0,434	0,051	m3 W*	0,246	-0,167